DOWNDRAFT GASIFICATION OF BIOMASS: EXPERIMENTAL INVESTIGATION AND ASPEN PLUS SIMULATION

ANTONIO GERALDO DE PAULA OLIVEIRA

Doctor of Philosophy

ASTON UNIVERSITY
June 2013

© Antonio Geraldo de Paula Oliveira, 2013

Antonio Geraldo de Paula Oliveira asserts his moral right to be identified as the author of this thesis

This copy of the thesis has been supplied on condition hat anyone who consults it is understood to recognise that its copyright rests with its author and that no quotation from the thesis and no information derived from it may be published without proper acknowledgement.

DOWNDRAFT GASIFICATION OF BIOMASS: EXPERIMENTAL INVESTIGATION AND ASPEN PLUS SIMULATION

ANTONIO GERALDO DE PAULA OLIVEIRA

Doctor of Philosophy, 2013

THESIS SUMMARY

Biomass gasification is considered today as a promising route for energy production, including electricity, natural gas or synthetic biofuels. Mechanisms involved in such processes are very complex and need further understanding. In downdraft gasification processes, the gasification dynamics is fundamental to the energy efficiency and the quality of gas produced.

The focus of this work is to provide necessary data for development and validation of 2D CFD codes to investigate the behaviour of the gasification zone of a downdraft gasifier. For this, two major set of experiments were performed:

Char Gasification in A Continuous Fixed Bed Reactor – CfiBR: The experiments were performed in a cylindrical reacting char bed and measurements of pressure drop, gas composition (longitudinal direction) and temperature (radial and longitudinal directions) were made. The char bed height was kept to 65 cm and the product gas was extracted through the bottom of the reactor and taken to a combustion chamber for final oxidation, after passing through a cyclone which separates the fine particles. Profiles of gas composition and temperature are presented for two different inlet gas compositions.

Gasification in a 25kw Throated Fixed Bed Biomass Gasifier: a commercially available 25kg/h throated reactor was modified to be able to measure pressure drop, gas composition (longitudinal direction) and temperature (radial and longitudinal directions). The device consists of a metallic reactor (280mm id, 76.2mm throat) surrounded by refractory insulation. An auger enables the feeding of biomass to the top of the reactor. The biomass flow rate is controlled by the consumption of the reactor. Air inlet and gas outlet are both measured using orifice plates installed in the device. The gas is extracted through the bottom of the reactor and taken to a flare for final oxidation, after passing through a cyclone which separates the fine particles and a biomass filter that trap condensables in aerosol phase.

The final stage of the work consist of the development and validation of a ASPEN PLUS model to simulate biomass gasification.

Keywords: Gasification, downdraft gasifier, biomass, modelling, Aspen Plus

To my family

ACKNOWLEDGMENTS

This research was supported by the Coordination for the Improvement of Higher Education Personnel (CAPES) under the process BEX 4922/06-9. The author is grateful this institutions for its support.

My unending thanks go to Dr. John Brammer for his supervision and support.

Through his fruitful guidance, patience, and contributions I have experienced a debt that cannot be repaid. My thanks are only outweighed only by a debt of gratitude.

I must also thanks Professor A.V Bridgwater and Professor Andreas Hornung for their constructive comments and advice, as well as for providing financial support in the acquisition of the GEK gasifier and training period at CIRAD, without which this research would not have reached completion.

I must also thank all my colleagues in CIRAD for all their support. Dr. Laurent Van de steene and Dr. Jean-Philippe Tagutchou for advising me on the principles of operation of the CFiBR; Jeremy Valette and Jean Baptiste for their assistance on the operation of the reactor and help in realizing the gas and biomass analysis; and all of them for their friendship that made my time in Montpellier very pleasant.

To my colleagues from BERG and EBRI Antzela Fivga, Panos Doss, Zsuzsa (zs) Mayer, Yianna Dimitriou, Yang Yang, Alan Harms and Asad Mahmood, I say a big thank you for creating a friendly research atmosphere and for all the good times we have had together.

To my friend and tutor Professor Manoel Fernandes Martins Nogueira, I save a big thank for leading me to a research career, and for all the guidance he provide me since my years as a undergrad student in Brazil.

Thanks also to all my Brazilian friends that created a bit of Brazil in Birmingham and made my time there more interesting. A big thank to Breno (ninja) Nunes, Rodrigo & Sana, Beto & Lu, Carmen and Ana.

Last but not least, I leave my final thanks to Thaís for the many times she crossed the Atlantic to visit me, and the most important thing, for being loving, caring and giving me many reasons to progress.

TABLE OF CONTENTS

THESIS SUMMARY	2
ACKNOWLEDGMENTS	<u>4</u>
TABLE OF CONTENTS	<u>6</u>
LIST OF FIGURES	12
LIST OF TABLES	4.5
LIST OF TABLES	16
CHAPTER 1	19
GENERAL INTRODUCTION	19
1.1 BIOMASS DEFINITIONS AND SPECIFICATION	19
1.1.1 DIFFERENT FORMS OF BIOMASS RESOURCES	20
1.1.2 CHEMICAL CHARACTERISTICS AND COMPOSITION OF BIOMASS	21
1.1.3 MAIN DISPARITIES BETWEEN BIOMASS AND OTHER FUELS	26
1.2 BIOMASS UTILIZATION	30
CHAPTER 2	32
BIOMASS GASIFICATION	32
2.1 Types of Gasification	33
2.2 GASIFICATION THERMODYNAMICS (PROCESS REACTIONS)	34
2.2.1 Drying Zone	35
2.2.2 PYROLYSIS ZONE	36
2.2.3 COMBUSTION (OXIDATION) ZONE	37
2.2.4 REDUCTION (GASIFICATION) ZONE	38

2.3 Types of Gasifier	39
2.3.1 Fixed Bed Gasifiers	39
2.3.2 FLUIDIZED BED GASIFIERS	45
2.4 TAR IN PRODUCER GAS	50
2.4.1 TAR DEFINITION	50
2.4.2 TAR QUANTITY ACCORDING TO THE PROCESS APPLIED	50
2.4.3 TAR PRODUCTION AND REMOVAL TECHNIQUES	51
2.5 SIMULATION OF GASIFICATION PROCESSES	53
2.5.1 EQUILIBRIUM BASED MODELS	54
2.5.2 KINETICS-BASED MODELS	55
2.5.3 COMPUTATION FLUID DYNAMICS (CFD)	55
2.5.4 ASPEN PLUS GASIFICATION MODELS	56
2.5.5 NEURAL NETWORK	59
CHAPTER 3	60
PREVIOUS WORK	60
3.1 GASIFICATION EXPERIMENTS WITH CHARACTERIZATION OF TEMPERATURE AND/OR GAS PROFILE	60
3.1.1 Experimental study on 75 kW _{th} downdraft (biomass) gasifier system <i>(Sharma 2009)</i> .	60
3.1.2 Experimental investigation of a downdraft biomass gasi er (Zainal et al. 2002)	62
3.1.3 GASIFICATION OF CHARCOAL WOOD CHIPS: ISOLATED PARTICLE AND FIXED BED (TAGUTCHOU 200	18) 63
3.2 THERMODYNAMIC EQUILIBRIUM MODELS	65
3.2.1 THERMOCHEMICAL EQUILIBRIUM MODELLING OF A GASIFYING PROCESS (MELGAR ET AL. 2007)	65
3.2.2 Modelling of a downdraft gasifier fed by agricultural residues (Antonopoulos et Ai	L. 2012)
	67
$3.2.3$ Thermodynamic equilibrium model and second law analysis of a downdraft waste G_{ℓ}	ASIFIER
(IADUNGTHAMMACHOTE & DUTTA 2007)	69

3.2.4 MATHEMATICAL MODELING OF A FLUIDIZED BED RICE HUSK GASIFIER: PART III – MODEL VERIFICA	TION
(K G MANSARAY A E GHALY A M 2000)	70
3.2.5 PERFORMANCE ANALYSIS OF A BIOMASS GASIFIER (MATHIEU & DUBUISSON 2002)	73
3.3 KINETIC AND COMPUTATIONAL FLUID DYNAMICS (CFD) MODELS	75
3.3.1 Pressurized Downdraft Combustion of Woodchips (Purnomo et al. 1990)	75
3.3.2 Numerical Modelling of a Deep, Fixed Bed Combustor (Bryden & Ragland 1996)	76
3.3.3 DYNAMIC BEHAVIOUR OF STRATIFIED DOWNDRAFT GASIFIERS (DI BLASI 2000)	78
3.3.4 PERFORMANCE ANALYSIS OF A FIXED-BED BIOMASS GASIFIER USING HIGH-TEMPERATURE AIR (W.	YANG
ET AL. 2006)	80
3.3.5 THE 2D EULERIAN APPROACH OF ENTRAINED FLOW AND TEMPERATURE IN A BIOMASS STRATIFIED	
Downdraft Gasifier (Rogel & Aguillon 2006)	81
CHAPTER 4	82
WORK PROGRAM	82
4.1 LITERATURE REVIEW	82
4.2 OBJECTIVES	83
4.3 Work Plan	84
4.3.1 Experimental work	84
4.3.2 MODELLING WORK	85
CHAPTER 5	86
CHAR GASIFICATION IN A CONTINUOUS FIXED BED REACTOR - CFIBR	86
5.1 Experimental Apparatus (Continuous Fixed Bed Reactor – CFiBR)	86
5.1.1 REACTIVE ATMOSPHERE	89
5.1.2 CONTINUOUS FIXED BED OPERATION	92
5.1.3 ASH AND RESIDUES REMOVAL SYSTEM	93

5.2 Production and characterization of the Biomass used	95
5.2.1 GRANULOMETRIC ANALYSIS AND PARTICLES SIZE DISTRIBUTION	96
5.2.2 Physicochemical characterization	99
5.2.3 MORPHOLOGICAL AND STRUCTURAL CHARACTERIZATION OF THE CHAR PARTICLES	101
5.3 Instrumentation, measurements and calculations	102
5.3.1 TEMPERATURE	102
5.3.2 Pressure	103
5.3.3 Gas composition	103
5.3.4 SOLID RESIDUES MEASUREMENTS AND CHARACTERIZATION	108
5.3.5 Mass and energy balances	111
5.4 OPERATIONAL PARAMETERS	113
5.4.1 CHAR FLOW	113
5.4.2 REACTIVE ATMOSPHERE	114
5.5 EXPERIMENTAL PROCEDURES AND PARAMETERS	116
5.5.1 Preliminary verification tests	116
5.5.2 GASIFICATION EXPERIMENTS	117
5.5.3 Data collection and processing	118
5.5.4 ESTABLISHMENT OF STEADY STATE	118
5.6 EXPERIMENTAL RESULTS	121
5.6.1 REACHING STEADY STATE	121
5.6.2 STEADY STATE: VARIATION OF PROPERTIES ACROSS THE REACTOR	123
5.6.3 Mass and energy balances	133
5.7 Conclusions	136
CHAPTER 6	138
GASIFICATION IN A 25KW THROATED FIXED BED BIOMASS GASIFIER	138

6.1 EXPERIMENTAL APPARATUS (GEK – GASIFIER EXPERIMENTERS KIT)	138
6.1.1 REACTOR	140
6.1.2 CYCLONE	141
6.1.3 AUGER FEED AND DRYING BUCKET	142
6.1.4 FILTER	143
6.1.5 PyroCoil:	144
6.2 Instrumentation and Measurements	145
6.2.1 TEMPERATURE:	145
6.2.2 Pressure	147
6.2.3 MASS FLOW RATE	147
6.2.4 GAS COMPOSITION	149
6.2.5 Data collection:	152
6.3 PRODUCTION AND CHARACTERIZATION OF THE BIOMASS USED	153
6.4 EXPERIMENTAL PROCEDURES AND PARAMETERS	154
6.4.1 COMMISSIONING	154
6.4.2 Preliminary verification tests and setup of the Grid	155
6.4.3 OPERATIONAL PARAMETERS	156
6.5 Gasification runs	157
6.5.1 Run 1: 100% MIXED WOOD PELLETS	157
6.5.2 Run 2: 75% MIXED WOOD PELLETS AND 25% MISCANTHUS PELLETS	159
6.5.3 Run 3: 50% mixed wood pellets and 50% Miscanthus pellets	160
6.5.4 Run 4: 25% MIXED WOOD PELLETS AND 75% MISCANTHUS PELLETS	162
6.5.5 Run 5: 100% wheat straw pellets	164
6.5.6 Run 6: 50% mixed wood pellets and 50% wheat straw pellets	165
6.5.7 SUMMARY OF THE GASIFICATION RUNS	167
6.6 CONCLUSION	169

<u>CHAPTER 7</u>
SIMULATION OF CHAR GASIFICATION PROCESS IN A CONTINUOUS FIXED BED REACTOR
USING ASPEN PLUS
7.1 Principles of RGibbs and Gasification modelling 170
7.1.1 Non-stoichiometric equilibrium method (minimization of the Gibbs free energy)
7.1.2 STOICHIOMETRIC METHOD (REACTIONS ENABLED)
7.2 ASPEN PLUS GASIFICATION MODEL 175
7.2.1 Physical property method
7.2.2 MODEL DESCRIPTION (BREAKING DOWN THE GASIFICATION PROCESS)
7.2.3 STOICHIOMETRIC METHOD (REACTIONS ENABLED)
7.3 VALIDATION OF THE SIMULATION RESULTS 193
7.4 CONCLUSIONS
CHAPTER 8
CHAPTER 8
GENERAL CONCLUSIONS
8.1 CHAR GASIFICATION IN A CONTINUOUS FIXED BED REACTOR - CFIBR 198
8.2 GASIFICATION IN A 25KW THROATED FIXED BED BIOMASS GASIFIER 199
8.3 SIMULATION OF CHAR GASIFICATION PROCESS IN A CONTINUOUS FIXED BED REACTOR USING ASPEN PLUS
200
SUGESTIONS FOR FURTHER WORK
REFERENCES
LIST OF PUBLICATIONS 211

LIST OF FIGURES

Figure 1.1: Example of the variety of biomass types	20
Figure 1.2: Conversion routes to bioenergy.	31
Figure 2.1: Heat flow and chemical reactions in gasification processes. (Knoef 2005)	35
Figure 2.2: Scheme of an updraft gasifier (All Power Labs n.d.).	40
Figure 2.3: Scheme of a downdraft gasifier (All Power Labs n.d.).	42
Figure 2.4: Scheme of a cross draft gasifier (All Power Labs n.d.).	43
Figure 2.5: Scheme of a two-stage gasifier (Henriksen et al. 2006)	44
Figure 2.6: Fluidized bed regimes (Higman & Van Der Burgt 2008)	46
Figure 2.7: Bubbling bed gasifier scheme (Knoef 2005).	47
Figure 2.8: Scheme of a circulating bed gasifier (Knoef 2005)	48
Figure 2.9: Scheme of a typical transport fluidized-bed gasifier (Basu 2010a)	49
Figure 2.10: Aspen Plus flow sheet example of coal combustion.	57
Figure 2.11: Aspen Plus example of window for defining a stream specification	58
Figure 3.1: Schematic diagram of the 75kW _{th} downdraft biomass gasifier (Sharma 2009).	61
Figure 3.2: Schematic of the fixed bed downdraft reactor (Zainal et al. 2002).	62
Figure 3.3: Schematic of the Continuous Fixed Bed Reactor (CFiBR) (Tagutchou 2008).	63
Figure 3.4: Comparison of the predicted and experimentally obtained producer gas	
composition (left) and low heating value for pine wood with 18% moisture.	66
Figure 3.5: Experimental vs. calculated data comparison of hydrogen and carbon	
monoxide concentrations on syngas from biomass feedstock in relation to	
feedstock moisture content. (Antonopoulos et al. 2012)	67
Figure 3.6: Effect of temperature on syngas species concentration: (a) miscanthus,	
(b) cardoon and (c) olive wood.	68

Figure 3.7: Gasifier diagram showing the continuous exchange of gases and solid particles	70
Figure 3.8: ASPEN PLUS simulation flow diagram developed to model the fluidized bed	
gasifier based on the two-compartment approach.	71
Figure 3.9: Comparison of predicted and measured exit temperatures at various	
equivalence ratios, fluidization velocities and bed heights.	72
Figure 3.10: Comparison of predicted and measured mole fractions of carbon monoxide,	
hydrogen and methane at various equivalence ratios, fluidization velocities and bed	
heights.	72
Figure 3.11: Gasifier model	73
Figure 5.1: Continuous Fixed Bed Reactor – CFiBR	88
Figure 5.2: Position of the burners in the combustion chamber	90
Figure 5.3: Front view of the conveyor belt	93
Figure 5.4: Ash removal system	94
Figure 5.5: (A) raw wood chips, (B) charcoal after wood chip pyrolysis	95
Figure 5.6: Illustration of the cone and quartering sampling method	97
Figure 5.7: Particle size distribution of char - lenght	98
Figure 5.8: Particle size distribution of char - thickness	98
Figure 5.9: Diagram of the producer gas sampling line	105
Figure 5.10: Solid residues collection device	108
Figure 5.11: The phases to reach steady state.	119
Figure 5.12: Bed level monitored by T4	120
Figure 5.13: Conversion profile of Experiment A/B using direct method.	122
Figure 5.14: Conversion profile of Experiment C using direct method.	123
Figure 5.15: Temperature profiles for CFiBR Experiment A/B and C (right).	125
Figure 5.16: Longitudinal profiles of concentration and species mass flow in	
Experiment A.	128

Figure 5.17: Longitudinal profiles of	of concentration and	l species mass f	flow in Experiment C.
---------------------------------------	----------------------	------------------	-----------------------

	129
Figure 5.18: Comparison of concentration on the radial and longitudinal profile of	
Experiment A/B. Lines represent samples in the centre of the reactor and larger	
symbols represent samples extracted by the wall.	131
Figure 5.19: Bulk density and conversion rate across the bed for Experiment A/B	132
Figure 5.20: Control volume over which mass and energy balances are applied	133
Figure 5.21: Mass and energy balance for Experiment A/B	135
Figure 5.22: Mass and energy balance for Experiment C	135
Figure 6.1: GEK with full thermal integration	139
Figure 6.2: Imbert reactor. All units are in centimetres.	140
Figure 6.3: Disassembled reactor showing air tubes on the left and top view of	
the reactor on the right	141
Figure 6.4: Diagram of cyclone attached to the reactor.	142
Figure 6.5: Auger and drying bucket	143
Figure 6.6: PyroCoil	144
Figure 6.7: Base of the k-type multipoint thermocouple probe showing its wiring, and	
3.17mm probe.	145
Figure 6.8: Thermocouple positioning inside the reactor. (The dash lines represent TCs).	146
Figure 6.9: Diagram of the inflow OP.	148
Figure 6.10: Diagram of the outflow OP.	148
Figure 6.11: Diagram of the hopper.	149
Figure 6.12: Diagram of the producer gas sampling line	150
Figure 6.13: Temperature profile - Run 1	158
Figure 6.14: Temperature profile – Run 2	160
Figure 6.15: Temperature profile – Run 3	161

Figure 6.16: Temperature profile – Run 4	163
Figure 6.17: Temperature profile – Run 5	165
Figure 6.18: Temperature profile – Run 6	166
Figure 6.19: Equivalence ratio diagram (Reed 1985)	168
Figure 7.1: ASPEN Plus flow sheet of charcoal gasification in the CFiBR	178
Figure 7.2: Temperature approach sensitivity analysis of Nonstoichiometric equilibrium	
modelof Experiment A and B.	183
Figure 7.3: Temperature approach sensitivity analysis of Nonstoichiometric equilibrium	
model of Experiment C.	183
Figure 7.4: Temperature approach sensitivity analysis of Eq. 5.6 for Experiment A and B.	186
Figure 7.5: Temperature approach sensitivity analysis of Eq. 5.6 for Experiment C.	187
Figure 7.6: Temperature approach sensitivity analysis of Eq. 5.4 for Experiment A and B.	188
Figure 7.7: Temperature approach sensitivity analysis of Eq. 5.4 for Experiment C.	188
Figure 7.8: Temperature approach sensitivity analysis of Eq. 7.19 for Experiment A.	189
Figure 7.9: Temperature approach sensitivity analysis of Eq. 7.19 for Experiment C.	190
Figure 7.10: Temperature approach sensitivity analysis of Eq. 7.20 for Experiment A.	191
Figure 7.11: Temperature approach sensitivity analysis of Eq. 7.20 for Experiment C.	191

LIST OF TABLES

Table 1.1: Characteristics of selected fuels—proximate analysis (Cuiping et al. 2004).	22
Table 1.2: Characteristics of selected fuels—ultimate analysis. (Cuiping et al. 2004)	24
Table 1.3: Composition of Selected Biomasses (Boundy et al. 2011)	25
Table 1.4: Bulk density of selected fuel	27
Table 1.5: Chemical Characteristics of Selected Feedstock Source: (Boundy et al. 2011)	29
Table 1.6: Comparisons of biomass compositions from different countries.	30
Table 2.1: Energy content of the producer gases obtained from different types of	
gasification: (Reed 1985)	34
Table 2.2: Maturation scheme for tars (Elliott 1988)	51
Table 3.1: Comparison between experimental and model predicted compositions for the	
producer gas of rubber wood with 14.7% moisture content	66
Table 3.2: Comparison between the predicted and measured composition of the produce	·r
gas	79
Table 5.1: Proximate and ultimate analysis of maritime pine char and woodchips	99
Table 5.2: Composition of mineral materials in the charcoal samples	100
Table 5.3: morphological properties of charcoal samples	101
Table 5.4: Micro-GC columns operational parameters	106
Table 5.5: Operating conditions of the CFiBR gasification experiments	115
Table 5.6: Comparison of concentration on the radial and longitudinal profile of	
Experiment A/B.	130
Table 6.1: Calibration report provided by ILC – Idaho Laboratories Corporation	147
Table 6.2: Input and output signals of the GCU	153
Table 6.3: Feedstock characteristics.	154
Table 6.4: Gasification runs series	157

Table 6.5: Mass balance for the Run 1	157
Table 6.6: Gas concentrations – Run 1	159
Table 6.7: Mass balance for the Run 2	159
Table 6.8: Gas concentrations – Run 2	160
Table 6.9: Mass balance for the Run 3	161
Table 6.10: Gas concentrations – Run 3	162
Table 6.11: Mass balance for the Run 4	162
Table 6.12: Gas concentrations – Run 4	163
Table 6.13: Mass balance for the Run 5	164
Table 6.14: Gas concentrations – Run 5	165
Table 6.15: Mass balance for the Run 6	166
Table 6.16: Gas concentrations – Run 6	167
Table 6.17: Summary of the experimental results	167
Table 7.1: Description of ASPEN Plus flowsheet unit operation blocks presented in	
Figure 7.1	178
Table 7.2: Description of ASPEN Plus flowsheet streams presented in Figure 7.1	179
Table 7.3: Feedstock Proximate and Ultimate analysis	180
Table 7.4: Simulation initial properties	181
Table 7.5: Experimental results versus model predictions by Nonstoichiometric	
equilibrium for Experiment A and B.	182
Table 7.6: Experimental results versus model predictions by Nonstoichiometric	
equilibrium for Experiment C	182
Table 7.7: Experimental results versus model predictions by Nonstoichiometric	
equilibrium with temperature approach for Experiment A.	184
Table 7.8: Experimental results versus model predictions by Nonstoichiometric	
equilibrium with temperature approach for Experiment C.	184

Table 7.9: Experimental results versus model predictions by Stoichiometric method for	
Experiment A.	192
Table 7.10: Experimental results versus model predictions by Stoichiometric method for	
Experiment C.	192
Table 7.11: Summary of input data of the validation experiment.	193
Table 7.12: Experimental results versus model predictions by Non-stoichiometric	
equilibrium for Van de Steene (2010)	194
Table 7.13: Experimental results versus model predictions by Non-stoichiometric	
equilibrium with temperature approach for Van de Steene (2010)	194
Table 7.14: Experimental results versus model predictions by Stoichiometric	
method for Van de Steene (2010)	195

CHAPTER 1

GENERAL INTRODUCTION

The environmental pollution, greenhouse gas emissions and global climate change, depletion of fossil fuel reserves, energy security, with the potential of biomass as an energy source with reduced environmental impacts puts biomass as one of the most promising renewable energy sources. Among all biomass conversion technologies, this thesis focuses on biomass gasification that is considered today as a promising route for energy production, including electricity, natural gas, or synthetic biofuels. This chapter includes a brief description of biomass characteristics and energy potential, in addition to an overview of the main for biomass conversion processes into energy.

1.1 Biomass definitions and specification

A general definition of biomass is the total mass of organic substances occurring in a habitat. It includes plant and animal based material. However, as this work focuses on energy generation a more suitable definition of biomass is: plant material, vegetation, or agricultural waste used as a fuel or energy source. All future references to biomass will imply this latter definition. As the definition implies, the forms of biomass are many and varied as shown in Figure 1.1.

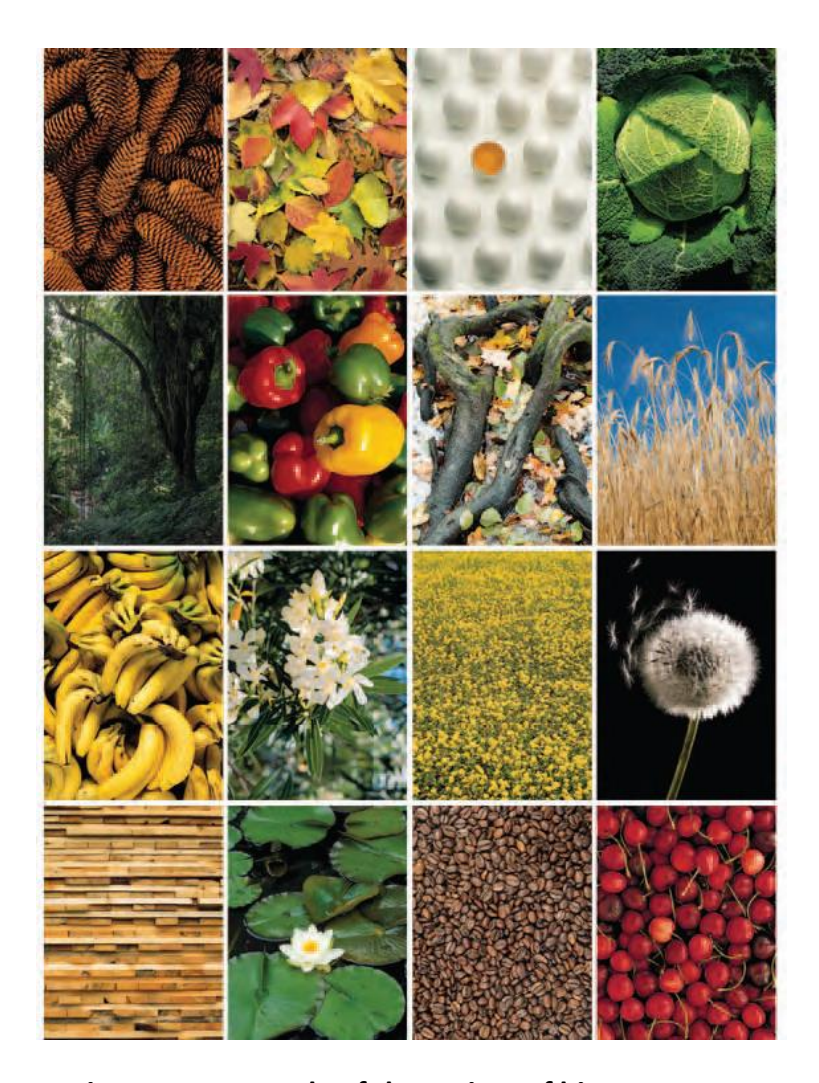


Figure 1.1: Example of the variety of biomass types

1.1.1 Different forms of biomass resources

Biomass can be divided into four categories according to its origin:

- Energy crops: Energy crops are plants like sunflower, rape and any other plant that grows as a low maintenance and low cost resource, which can be used to generate energy, either directly or via biofuels production. They work similarly to a solar cell, capturing solar radiation and carbon and then storing it in their biomass for an energetic use. Additional examples of energy crops are *Miscanthus sinensis*, maize and Short Rotation Coppice (SRC) such as poplar and willow (Common Osier, Basket Willow).
- Post-harvest residues: These are the residues that occur in the harvesting of cereals, such as straw from corn, and the residues from wood forestry. They are natural wastes that have a limited use. This group of "by-products from nature" is especially suitable for energy

recovery because it results in a lowering of production costs for the main products.

- Organic by-products: The processing of biomass to create products forms a further group of by-products. These by-products include manure and liquid manure from animal husbandry and residues from the industrial processing of wood and vegetable fibres. Using these byproducts for energy generation can lead to increased profitability and ensure that parts of the production process are environmentally sustainable.
- Organic waste: Organic waste is a major component of municipal solid waste and comprises the products that are used by consumers and producers and their residues. This includes kitchen waste (e.g. potato and fruit peelings), waste food (e.g. leftovers in restaurants, spoiled fruit and vegetables from markets), garden waste (e.g. grass clippings and hedge trimmings) and industrial waste (e.g. from food processing factories).

1.1.2 Chemical characteristics and composition of Biomass

The composition and molecular structures of any lignocellulose and carbonaceous fuel, such as coal and biomass, are very complex and varied. They encompass a considerable diversity of inorganic and organic compounds, with the latter being the major fraction. These organic compounds are structured in hydrocarbon chains where, apart from C, H, O, and N, several other atoms are present such as S, Fe, Ca, Al, Si, Zn, Na, K, Mg, Cl, heavy metals, etc. (de Souza-Santos, 2004). Here, chemical characteristics and composition will be described for selected biomass fuels in terms of *Proximate*, *Ultimate* and *Summative Analysis*, *Heating Value* and *Other Thermo physical Properties*.

1.1.2.1 Proximate Analysis

The "proximate" analysis (Table 1.1) gives the composition of biomass in terms of moisture content, volatile content, the free carbon remaining after volatiles have been driven off, and ash (mineral) content.

Table 1.1: Characteristics of selected fuels—proximate analysis (Cuiping et al., 2004).

	Moisture (wt%) ¹	Ash (wt% db) ²	Volatile matter (%)	Fixed carbon (%)	LHV ³ (MJ/kg)
Rice straw	08.11 ± 01.51	15.25 ± 2.64	61.10 ± 2.51	15.54 ± 1.36	14.66 ± 0.71
Wheat straw	0.377083 ± 02.03	12.45 ± 9.02	63.96 ± 7.29	14.96 ± 1.49	16.56 ± 1.05
Corn straw	09.31 ± 02.05	13.12 ± 8.79	62.74 ± 6.15	14.83 ± 2.13	16.64 ± 0.38
Soybean	09.34 ± 0.102778	6.08 ± 1.10	68.95 ± 1.74	15.62 ± 0.17	16.96 ± 0.62
Corn cob	06.41 ± 0.139583	7.55 ± 6.91	70.24 ± 6.43	15.8 ± 1.85	16.98 ± 0.64
Cotton stalk	0.3375 ± 0.101389	6.41 ± 3.08	67.36 ± 3.49	18.57 ± 1.14	17.91 ± 0.47
Cotton shuck	10.23	6.88	62.16	20.74	17.88
Peanut shuck	09.36 ± 00.41	12.15 ± 3.02	61.64 ± 1.9	916.85 ± 0.71	18.62 ± 0.21
Peanut stalk	8.56	9.12	66.67	15.66	15.75
Sesame stalk	7.66	6.11	68.93	17.3	15.92
Broad bean stalk	7.62	5.03	68.44	18.9	16.31
Rape stalk	6.15	3.6	72.99	17.26	16.65
Foliole eucalyptus	06.05 ± 01.02	25.55 ± 2.44	67.75 ± 5.01	20.19 ± 2.77	19.33 ± 1.60
Rubber plant	0.394444 ± 02.27	9.9 ± 3.31	62.92 ± 5.59	18.3 ± 1.44	18.14 ± 1.30
Willow tree	09.08 ± 01.45	6.17 ± 3.7	76.9 ± 5.08	15.55 ± 1.99	18.79 ± 0.40
Poplar	0.354861 ± 0.086806	2.63 ± 0.87	74.04 ± 0.36	15.42 ± 1.14	18.57 ± 0.17
Pine tree	0.375694 ± 0.104861	0.89 ± 0.13	76.50 ± 2.45	14.45 ± 0.41	19.38 ± 0.35
Spruce	09.21 ± 00.05	55.36 ± 2.33	71.04 ± 3.26	14.39 ± 5.09	18.93 ± 0.71
Phoenix tree	7.74	5.28	68.68	18.29	17.96
Birch tree	9.06	2.36	74.91	13.68	19.34
Metasequoia	7.38	2.2	74.3	16.11	19.62
Bituminous coal	0.140972 ± 0.045833	20.08 ± 3.49	28.33 ± 1.89	49.08 ± 2.12	34

^{1 (}wt %) = percentage of weight.
2 (wt % db) = percentage of weight in dry basis
3 Low Heating Value. See the section 1.1.2.4.

The proximate analysis is very simple to determine and is extremely important in deciding whether the biomass is suitable or not for a particular thermal conversion process. Moisture content, as an example, is of considerable importance in the selection of energy conversion process technology. Biomass fuels with low moisture content are more suitable for thermal conversion technologies; biomass fuels with high moisture content are more suitable for biochemical process such as fermentation (McKendry, 2002a). As another example, the ash content will determine whether a biomass can be used in a thermal process that reaches temperatures above the ash melting point. Melting ashes are very problematic as they cause blockages and reduce heat transfer rates.

1.1.2.2 Ultimate Analysis

The "ultimate" analysis (Table 1.2) gives the composition of the biomass in wt% of carbon, hydrogen and oxygen (the major components) as well as sulphur and nitrogen (if any) on a dry and ash free basis. The content of Chlorine would also normally be presented, although it was not measured by the authors of Table 1.2. The work of Nordin (1994) found that the Cl content has a wide range of variation from 0.008–0.74% dry basis. According to Faaij (1997), the Chlorine content is in the range of 0–1.1% dry basis, and the chlorine concentration can vary widely between samples. Higher chlorine concentration can also be found from samples obtained close to the sea.

Table 1.2: Characteristics of selected fuels—ultimate analysis in dry basis. (Cuiping et al., 2004)

	N	С	S	Н	0
Rice straw	0.69 ± 0.21	38.52 ± 1.03	0.29 ± 0.17	6.13 ± 0.49	39.28 ± 2.14
Wheat straw	0.58 ± 0.28	42.11 ± 2.12	0.32 ± 0.10	6.53 ± 0.46	40.51 ± 2.67
Corn straw	0.99 ± 0.20	42.69 ± 1.47	0.21 ± 0.13	6.16 ± 0.81	42.69 ± 2.11
Soybean	0.95 ± 0.28	43.16 ± 1.13	0.20 ± 0.04	6.9 ± 0.13	44.76 ± 2.42
Corn cob	0.49 ± 0.12	44.53 ± 0.50	0.11 ± 0.05	6.89 ± 0.10	45.97 ± 1.51
Cotton stalk	1.09 ± 0.10	46.10 ± 0.49	0.26 ± 0.09	6.85 ± 0.39	43.35 ± 2.63
Cotton shuck	1.23	44.54	0.39	6.66	46.66
Peanut shuck	1.17 ± 0.09	45.90 ± 0.54	0.18 ± 0.05	6.74 ± 0.27	42.79 ± 0.05
Peanut stalk	2.06	40.28	0.28	7.18	42.47
Sesame stalk	0.81	41.34	0.29	6.57	45.16
Broad bean	0.97	42.16	0.24	6.13	45.28
Rape stalk	0.23	42.42	0.27	7.06	46.1
Foliole eucalyptu	0.50 ± 0.47	50.15 ± 2.55	0.02 ± 0.03	7.45 ± 0.46	39.64 ± 3.88
Rubber plant	0.97 ± 1.04	48.69 ± 1.69	0.11 ± 0.09	7.29 ± 0.60	39.03 ± 3.25
Willow tree	0.77 ± 0.79	46.79 ± 1.14	0.30 ± 0.17	7.10 ± 0.44	40.60 ± 3.75
Poplar	0.17 ± 0.06	47.46 ± 0.45	0.10 ± 0.09	6.74 ± 0.02	44.50 ± 1.36
Pine tree	0.10 ± 0.02	49.41 ± 0.24	0.05 ± 0.04	7.67 ± 0.42	42.19 ± 0.61
Spruce	0.20 ± 0.10	48.56 ± 0.25	0.18 ± 0.17	6.53 ± 0.52	43.55 ± 1.55
Phoenix tree	0.7	48.14	0.04	7.88	39.84
Birch tree	0.16	48.32	0.2	8.36	40.6
Metasequoia	0.11	47.98	0.08	6.82	43.98
Bituminous coal	1.13 ± 0.01	63.78 ± 2.33	0.97 ± 0.19	3.97 ± 0.38	10.08 ± 4.66

The ultimate analysis is more involved than the proximate analysis, but the results provided by this analysis enable the calculation of the combustion, pyrolysis and gasification reactions.

1.1.2.3 Summative Analysis

The summative analysis, showed in Table 1.3, gives the proportions of the three major polymer constituents of biomass: cellulose, hemi-cellulose and lignin. Other minor components are not taken into account due the fact they have no energy content (Klautau, 2008; Boundy et al., 2011).

Table 1.3: Composition of Selected Biomasses in dry basis (Boundy et al., 2011)

	Cellulose (%)	Hemi-cellulose (%)	Lignin (%)
corn stove	35	28	16-21
sweet corn	27	25	11
sugarcane	32-48	19-24	23-32
hardwood	45	30	20
softwood	42	21	26
hybrid	42-56	18-25	21-23
bamboo	41-49	24-28	24-26
switchgrass	44-51	42-50?	13-20
miscanthus	44	24	17
Arundo donax	31	30	21

1.1.2.4 Heating Value

The heating value (HV) of a material is an expression of the energy content released when it is burnt in air, and it represents a theoretical value of available energy that can be used for energy generation through direct combustion. The HV is usually measured in terms of the energy content per unit mass or volume; MJ/kg for solids, MJ/I for liquids, or MJ/Nm³ for gases. The HV of a fuel can be expressed in the forms of higher heating value (HHV) and lower heating value (LHV). The HHV is the total energy content released when the fuel is burnt in air including the latent heat contained in the water vapour, and therefore represents the maximum amount of energy potentially usable from a given biomass; this value is also important to calculate the Adiabatic Flame Temperature of a combustion process. The actual quantity of energy used will fluctuate according to the conversion technology (combustion, gasification, and pyrolysis and their respective efficiencies). In practical terms, the latent heat of vaporization contained in the water vapour cannot be used effectively and consequently, the LHV (which does not contain the latent heat of vaporisation) is the

appropriate value to use for the energy available for subsequent utilization. The Table 1.1 and Table 1.5 list respectively LHV and HHV of a range of biomass materials.

1.1.3 Main disparities between biomass and other fuels

There are a great variety of fuels. They can be classified in very general terms such as fossil or renewable; gas, liquid or solid; etc., they also differ in terms of composition, chemical/physical characteristics and applications. Some categories show a wider range of usage than others, e.g. liquid fossil fuels are used worldwide for power generations and, principally, transportation as most of the vehicles are designed to operate on liquid fuel.

Biomass feedstocks, even with their wide range of possible sources, are surprisingly uniform in many of their fuel properties. Despite different forms and appearances they present similar characteristics in terms of elemental composition, compared with fossil feedstocks such as coal or petroleum. In the following paragraphs the properties of heating value, moisture content, ash content and bulk density will be discussed.

In terms of heating value, there are many kinds of coal with a range of HHV of 20-30 MJ/kg. Nevertheless, practically all kinds of biomass feedstock destined for combustion fall in the range 15-19 MJ/kg (dry basis). For most agricultural residues, the heating values are even more uniform – about 15-17 MJ/kg; the values for most woody materials are 18-19 MJ/kg (Nordin, 1994; Sander, 1997; Lee, 2005).

In contrast, the biomass moisture content varies widely depending on the type and history of the biomass. Typically forced circulation air-dried biomass has

about 15-20% moisture, while the moisture content for oven-dried biomass is around 0% (ECN, 2011).

A negative characteristic of biomass feedstock compared to liquid fossil fuels is the bulk density, and consequently the energy density. Most biomass feedstocks have a generally low bulk density; even after densification it is about 10-40% less dense than liquid fossil fuels see Table 1.4 for bulk density of selected solid and liquid fuels. The relatively low energy density of biomass, when compared to liquid fossil fuels, restricts the utilisation of most biomass feedstocks to close to the place of production, as the costs with transportation can be higher than the income of the energy produced.

Table 1.4: Bulk density of selected fuel (Francescato et al., 2009)

Fuel	Moisture content (%db)	Bulk density (kg/m³)
Beech wood chips	30	328
Saw dust	15	160
Pellets	8	620 - 650
Diesel		820 - 950
Gasoline		737
Aviation fuel		820

Considering that ash content is not desirable for thermal processing, as ash sintering can promote damage to the equipment (Rezaiyan & Cheremisinoff, 2005; Warnatz et al., 2006; Glassman & Yetter, 2008; Higman & Van Der Burgt, 2003), biomass has an advantage over most coals, which have higher ash content. In terms of sulphur content, biomass also has a much lower level compared to many fossil fuels (see the comparison in Table 1.5) (Lee, 2005; Boundy et al., 2011; ECN, 2011; Netto et al., 2006). Due to the absence of toxic metals and other trace contaminants common

in coal ash, biomass ashes can often be used as a soil conditioner to help replenish nutrients removed by harvest. A few biomass feedstocks stand out for their peculiar properties, such as high silicon or alkali metal contents – these may require special precautions for harvesting, processing and combustion equipment. Note also that mineral content can vary as a function of soil type and the timing of feedstock harvest (see Table 1.6 for a comparison of biomass of the same species grown in different regions)(Nordin, 1994; Sander, 1997; Cuiping et al., 2004).

Another advantage of biomass over fossil fuels is that most biomass materials are easier to gasify than coal because they are more reactive due to their higher ignition stability. Consequently it is more suitable and easier to process biomass thermochemically into higher-value fuels such as methanol or hydrogen (Lee, 2005).

Table 1.5: Chemical Characteristics of Selected Feedstock Source: (Boundy et al., 2011)

	HHV ⁴ MJ/kg)	Ash (%)	Sulphur (%)	Potassium (%)	Temperature ⁵ (°C)
Corn stove	17.6	5.6			
Sweet	15.4	5.5			
Sorghum					
Sugarcane	18.1	3.2-5.5	0.10-	0.73-0.97	
Bagasse			0.15		
Sugarcane	17.4	7.7			
Leaves					
Hardwood	20.5	0.45	0.009	0.04	[900]
Softwood	19.6	0.3	0.01		
Hybrid	19	0.5-1.5	0.03	0.3	1350
Poplar					
Bamboo	18.5-19.4	0.8-2.5	0.03-0.05	0.15-0.50	
Switch grass	18.3	4.5-5.8	0.12		1016
Miscanthus	17.1-19.4	1.5-4.5	0.1	0.37-1.12	1090 [600]
Giant cane	17.1	5.0-6.0	0.07		
Coal ⁶	15-19	5.0-20.0	1.0-3.0	0.02-0.3	~1300
Coal ⁷	27-30	1.0-10.0	0.5-1.5	0.06-0.15	~1300

⁴ High heating value (gross, unless specified)

⁵ Some ash sintering observed

⁶ Low rank; lignite/sub-bituminous

⁷ High rank bituminous/anthracite

Table 1.6: Comparisons of biomass compositions from different countries.

Element	China	Sweden	Denmark
	(Cuiping et al., 2004)	(Nordin, 1994)	(Sander, 1997)
N (wt%)	0.11-2.06	0.12-3.1	0.1-1.5
C (wt%)	38.52-50.15	44.0-58.8	47–52
S (wt%)	0.02-0.39	0.009-0.26	0.1-0.2
H (wt%)	6.13-8.36	5.7-6.3	5.2–6.4
O (wt%)	39.03-46.66	32-46.2	
Al (ppm)	120-5001	19-2200	50-150
Si (ppm)	1.6-351 (soluble)	28-46000	1000-8000
Ca (ppm)	1757–23301	650-16000	2000–4000
Fe (ppm)	382–4867	26–1600	150–1000
K (ppm)	826-21969	400-25000	1000-10000
Mg (ppm)	260-7613(10855)	160-1800	400–700
Na (ppm)	24-3497(10051)	110-2000	150-500
P (ppm)	91–1849	75–2900	200-800
Cu (ppm)	6.4–128	1.8-62	
Zn (ppm)	11–162	22–120	
Pb (ppm)	0.75-63	1.5-86	
Cd (ppm)	0.05-0.92	0.01-0.02	

1.2 Biomass utilization

Not only are the forms of biomass on our planet varied; there is also a wide range of primary uses of biomass by humans. In addition to its use as an energy source, biomass is widely used by the food industry; it can also be used in the manufacturing of clothing or construction materials, or even in the pharmaceutical industries. After these primary uses of biomass, the residues can also be used as fuel for energy generation, or alternatively material for handicraft, fertilizer production, etc.

In energy production, the chemical energy available in biomass may be utilised either directly as in combustion, or by initial upgrading into more valuable and versatile fuels such as charcoal, liquid fuels, producer gas or biogas. Thus, biomass conversion technologies can be separated into four basic categories: direct combustion, thermo-chemical conversion processes (pyrolysis, gasification), bio-

chemical processes (anaerobic digestion, fermentation) and physicochemical processes (the route to biodiesel). Direct combustion provides heat and electricity via steam power plants (Rankine cycle). Gasification provides a fuel gas that can be combusted to generate heat or used in an engine, turbine or fuel cell for electricity generation. The produced fuel gas can be also processed towards liquid hydrocarbons through Fischer-Tropsch synthesis, or towards synthetic methanol, ammonia, or methane among others (S. P. Babu, 1995; Rezaiyan & Cheremisinoff, 2005; Basu, 2010a). See Figure 1.2 for the routes of biomass conversion.

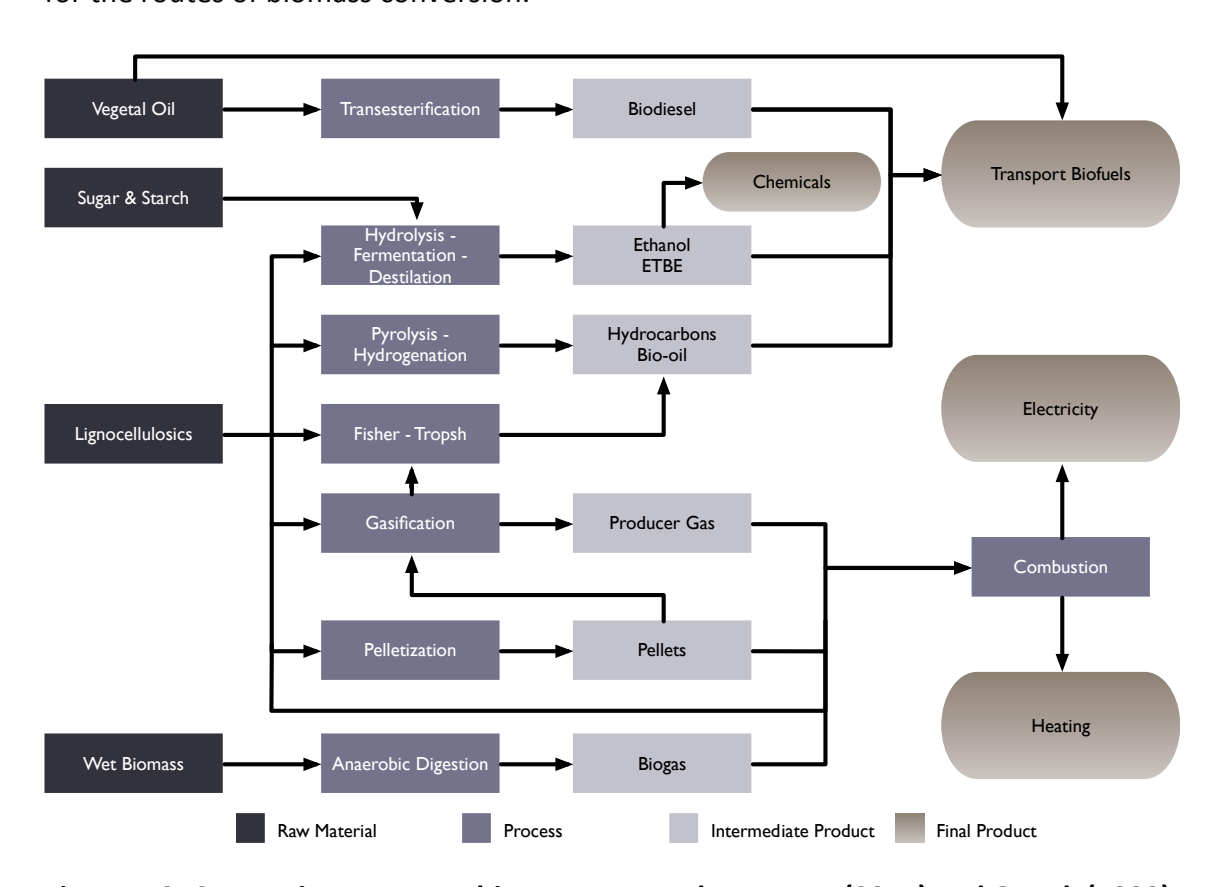


Figure 1.2: Conversion routes to bioenergy. Based on Luque (2011) and Quaak (1999).

This work focuses on the process of gasification. In the following chapters, several processes of biomass gasification will be described including the physics and chemistry of the process, as well as gas cleaning and conditioning techniques.

CHAPTER 2

BIOMASS GASIFICATION

Gasification is a thermochemical process in which partial oxidation of organic matter at high temperatures results in a mixture of products, but mainly consisting of a gaseous fuel (producer gas) that can be utilized for energy applications. The gas generated is more suitable than the organic feedstock material for generation of heat and power (Priyadarsan et al., 2005). Various oxidizing agents can be utilized for gasification; air, oxygen or a mixture of these gases; in some cases, steam is also used. For economic reasons, air remains the most commonly utilized oxidizing agent. With excess air, combustion produces CO₂ and H₂O, but in the sub-stoichiometric conditions used in gasification, products such as CO and H₂ appear (Quaak et al., 1999). The producer gases released from air-blown gasification generally contain CO (18-20%), H₂ (18-20%), CH_4 (1-2%), H_2O (11-12%) and N_2 . Gasification of biomass can generate gases with a calorific value in the order of 3.9 to 11.8 MJ/m³ using air, and 11.8 to 27.5MJ/m³ with the use of oxygen. With a greater degree of control leading to higher production of methane and other light hydrocarbons, the value can reach 27.5 to 39.3MJ/m³. The values mentioned for air and oxygen-induced gasification correspond to approximately 20-50% the energy content of natural gas on a volume basis (Reed & Das, 1988).

For over 180 years, organic feed has been used to produce fuel from the gasification process in blast furnaces. The prospect of making use of this gas for heat and power led in Europe to the industry of producer gas systems. At the time, charcoal and peat were used as the feedstock. As petroleum gained greater usage as a fuel due

to its advantages over producer gas, gasification became less popular and an uncompetitive technology. Nevertheless, with the shortage of petroleum during both world wars, gasification became a widespread technology again. In 1945, approximate 9,000,000 vehicles were running on producer gas (Goswami, 1986). With the end of World War II, all the countries with access to cheap petroleum abandoned gasification; therefore the technology was out of the spotlight once more.

The current interest in gasifier R&D mostly dates from the oil crises of the 1970s, and has been spurred since the 1990s by concerns over climate change. But now, instead of coal, biomass is the primary feedstock.

2.1 Types of Gasification

Conversion of biomass into gases containing the highest energy content possible is the major challenge with gasification. The thermochemical conversion from biomass to gases can be realized in a few ways: air gasification, oxygen gasification, hydrogasification, pyrolytic gasification, and by the new prospect of biomass gasification in near- and super-critical water (Matsumura et al., 2005). Air and oxygen gasification are the more common and studied methods.

Air gasification is a simple process, which usually takes place in fixed bed updraft, fixed bed downdraft and fluidized bed gasification systems (see the sections 2.3.1 and 2.3.2). Air gasifiers, in addition to having a simple configuration, are affordable and reliable. Gasification by partial oxidation is most efficient at the lowest equivalence ratio⁸ at which all of the solid carbon is just consumed, which for air is about 0.25, representing 1.6g of airflow per gram of biomass dry ash free. However,

⁸ ratio of the actual oxygen (air) to fuel ratio divided by the stoichiometric oxygen (air) to fuel ratio required for complete combustion.

the gas generated with air gasification has a low energy content (Table 2.1), which makes it uneconomical for some applications such as pipeline transportation.

Table 2.1: Energy content of the producer gases obtained from different types of gasification. : (Reed, 1985)

Gasification Type	Gas Energy Content (MJ/Nm³)	
Air Gasification	5.6 - 7.5	
Oxygen Gasification	11.2 - 18.6	

Oxygen gasification can be performed in the same systems as those designed for air gasification; however, the gases obtained during oxygen gasification have a calorific value 2 to 3 times higher. The higher calorific value could make it economical to carry the gases in pipelines, unlike the gases obtained from air gasification. In addition, the gases can be used to synthesize methanol, ammonia, gasoline, or methane. The reactions occurring with oxygen gasification have the advantage of occurring faster and requiring lower gas flow, as there is no nitrogen to dilute the mixture. The limitation of oxygen gasification resides in the cost of oxygen compared to air which is free (Reed, 1985).

2.2 Gasification Thermodynamics (Process Reactions)

In fixed bed gasifier types (see the section 2.3.1) such as downdraft, updraft and cross-draft, gasification processes occur over four main zones. The chemical reactions happening in these zones must be controlled in order to obtain maximum efficiency of gas production (Goswami, 1986), nevertheless, controlling these reactions cannot be done in most of the fixed bed reactors that do not have ways to control air flow and pressure drop. These zones are the drying, pyrolysis, oxidation (combustion)

and reduction zones. The biomass also passes through the same four processes in a fluidized bed gasifier, but the four zones are not separated as in fixed bed gasifiers. The general behaviour of a fixed bed gasification processes can be viewed in the diagram below.

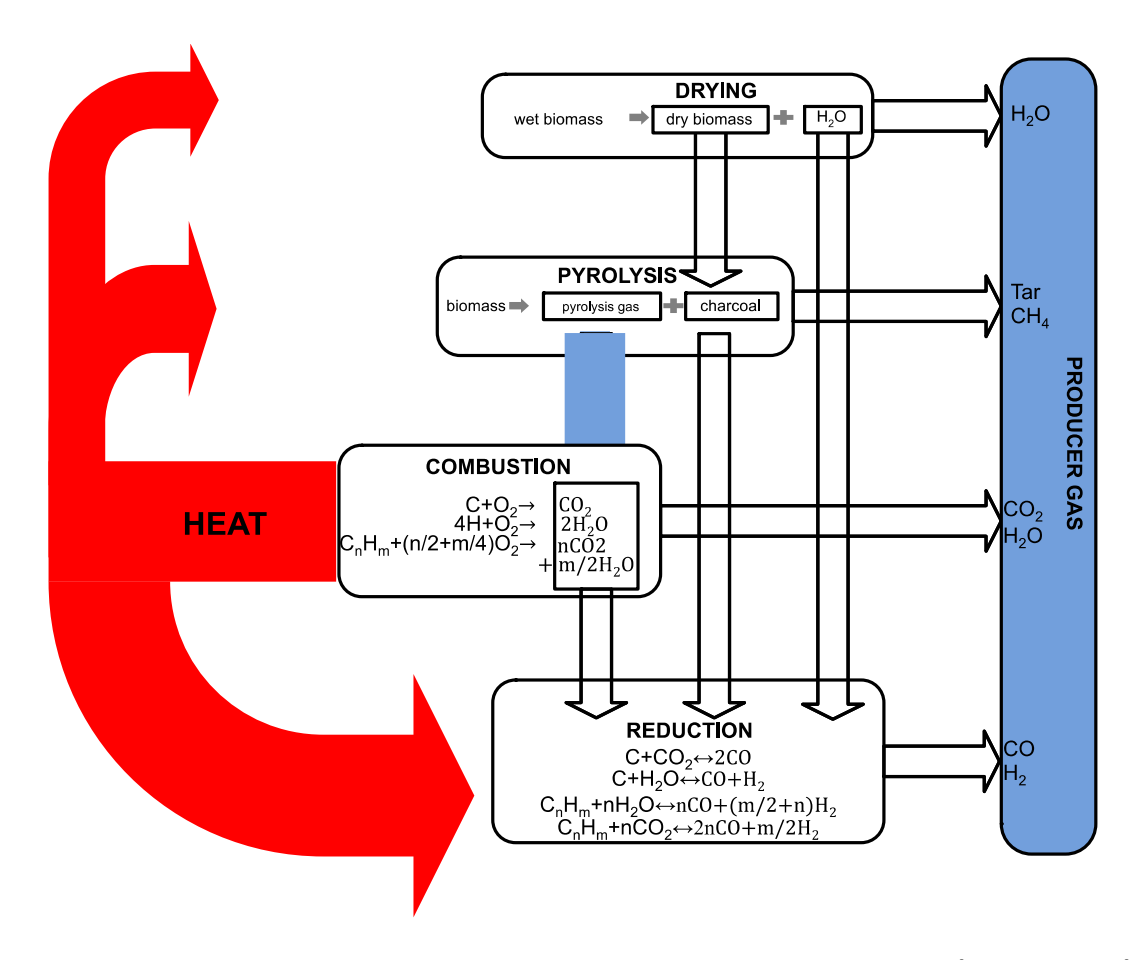


Figure 2.1: Heat flow and chemical reactions in gasification processes. (Knoef, 2005)

2.2.1 Drying Zone

Water is removed from the feedstock in the drying zone. During the drying process, the mass transfer from the feedstock to the surroundings depends on: the feedstock temperature, the rate of heat transfers from the surroundings to the biomass and the relative humidity of the surrounding gas layer. It has been observed that the ions present in the surrounding gas layer will affect the partial pressure and

water concentrations around the feedstock (de Souza-Santos, 2004). At atmospheric pressure, drying is considered to occur at a wide range of temperatures - from ambient up to 200°C (Goswami, 1986).

2.2.2 Pyrolysis Zone

Also known as devolatilization, pyrolysis is the process by which a mixture of organic and inorganic gases and vapours are released to the surroundings as a result of heating.

Pyrolysis products are affected by the initial carbon structure and composition, pyrolysis temperature, pressure, residence time in the reactor, heat losses, feedstock consumption and heating rate. Generally, the following transformations are found to occur during these temperatures:

- Moisture evaporation 100°C and higher
- Decomposition of extractives (hot water (HW) extractives, ethanol/cyclohexane (E/C) extractives) - 100-250°C
- Decomposition of hemicelluloses 250-350^oC
- Decomposition of lignin 500ºC

In addition, from 200 to 280°C, carbon dioxide, acetic acid and water are released, while between 280 and 500°C, tars, methyl alcohol, and other gases are produced. From 500 to 700°C, the gas production is low, but may contain H₂ (Goswami, 1986). The devolatilization process as a function of temperature is fairly similar for coal and biomass (de Souza-Santos, 2004). Pyrolysis occurs at different heating rates; categorized as slow, moderate, and fast. The heating rate of slow pyrolysis is about 10 K/s, while fast pyrolysis occurs generally at rates above 10³ K/s. The type of reactor influences the heating rate; as a result, pyrolysis is dependent on

the design of the reactor. In moving and fixed bed combustion or gasification, moderate to slow pyrolysis happens. In fluidized beds, heating rates of $10^2 - 10^4$ K/s are obtained (de Souza-Santos, 2004), i.e. moderate to fast pyrolysis. An increase in pyrolysis pressure results in a reduction of the yield of volatiles, an increase of H/C ratio in volatiles and a decrease of char gasification reactivity (de Souza-Santos, 2004; Cetin et al., 2005). Methane is desired for its high calorific value. Increasing operating pressure can enhance methane formation. The atmosphere surrounding the process also affects the volatile yield. Pyrolysis is an anaerobic process; however, enhancement of hydrogen atmosphere increases the volatile yield. The lack of hydrogen leads to pyrolysis products with longer chains and lower mobility (de Souza-Santos, 2004).

2.2.3 Combustion (Oxidation) Zone

If complete combustion takes place, all carbon in the fuel is transformed into carbon dioxide and all hydrogen is transformed into water; the theoretical adiabatic flame temperature obtained is about 1450°C. Nevertheless, complete combustion does not take place and adiabatic flame temperature cannot be reached. The temperature in the oxidation zone depends on local factors, on the design of the gasifier, besides the composition of the biomass. The main combustion reactions occurring in the oxidation zone are:

$$C + O_2 \rightarrow CO_2$$
 2.1

$$2H_2 + O_2 \rightarrow 2H_2O$$
 2.2

2.2.4 Reduction (Gasification) Zone

In a fixed bed gasifier, a significant solid content remains in the form of charcoal after leaving the oxidation zone, which passes down to the charcoal bed to form the reduction zone. The processes in the reduction zone are mainly endothermic reactions and hence there is a drop in temperature. The temperature of the reduction zone varies between 600 and 700°C. The common reactions are (Goswami, 1986; Knoef, 2005):

2.2.4.1 Solid-Gas Heterogeneous Reaction

Carbon oxidation

$$C + \frac{1}{2}O_2 \to CO \tag{2.3}$$

• Boudouard Reaction

$$C + CO_2 \rightarrow 2CO$$
 2.4

• Water-Gas Shift Reaction

$$C + H_2O \rightarrow CO + H_2$$
 2.5

Methane Formation Reaction

$$C + 2H_2 \rightarrow CH_4 \qquad 2.6$$

2.2.4.2 Gas-Gas Homogeneous Reactions

• Water-Gas Reactions

$$CO + H_2O \rightarrow CO_2 + H_2$$
 2.7

$$CH_4 + H_2O \rightarrow CO + 3H_2$$
 2.8

2.3 Types of Gasifier

There are several ways to categorize gasifiers; the most used one classifies them according to the reactor design. In this classification, there are 4 different types of gasification. They are fixed bed, fluidized bed, entrained flow and twin-bed; the first two mentioned are more relevant to this work and will be described in the following sections.

2.3.1 Fixed Bed Gasifiers

Fixed bed (sometimes called moving bed) gasifiers use a bed of solid fuel particles through which air and gas pass either up or down. They are the simplest type of gasifiers and the only ones suitable for small-scale application (Reed & Das, 1988; Reed, 1985). Fixed bed gasifiers are often utilized for drying, extraction, boiling and calcination (Reed, 1985). The three most common and studied types are the updraft, downdraft and cross-draft designs.

2.3.1.1 Updraft Gasifier

The updraft gasifier (Figure 2.2) is a counter-flow design where biomass fuel moves downward while the air and producer gas move upward. Gases follow a natural upward movement as the increasing temperature reduces their density. With this configuration, the air or oxidizing agent entering contacts the chars creating the combustion zone. The gases coming out of the combustion zone have to go through the layer of chars above them created by the heat of the combustion zone. Here, CO₂ and H₂O are reduced into CO and H₂. The reduced gases still contain enough energy to pyrolyse the descending biomass in a range 200 to 500°C, thus creating the chars that feed the combustion zone. The pyrolysis gases evolved have sufficient temperature to

dry the wet biomass entering above them. However, during pyrolysis, chemicals, condensable organics (tars) and oils are released and become part of the producer gas.

This drawback restricts the application of the updraft gasifier, because these products released from pyrolysis would be detrimental to a heat engine or a fuel cell, as they can condense and form deposits at key location. Engines can encounter serious problems if they operate with an amount exceeding 100 mg/Nm³ of tar for more than 250h (The German Solar Energy SocietyEcofys 2005, 2005) and Molten Carbonate Fuel Cell can only admit 4000ppm of tar (EG G Technical Services Inc, 2006). However, it could be used for heating applications where the producer gas is combusted without cooling, since for these uses tar is not an inconvenience. Another major obstacle in updraft gasifiers is the high temperature at the grate that can melt the ashes (Reed, 1985).

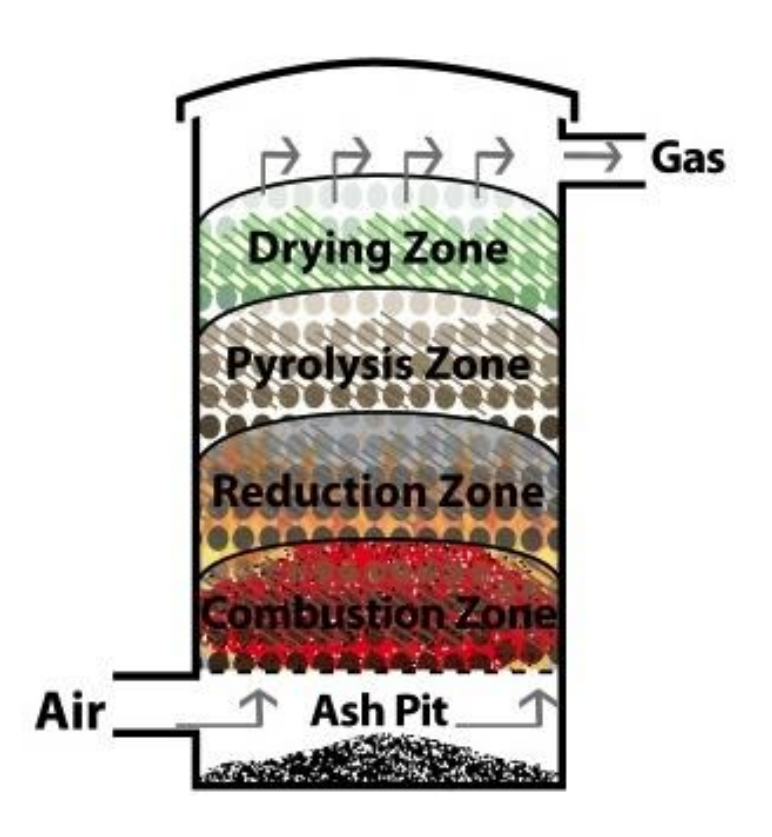


Figure 2.2: Scheme of an updraft gasifier (All Power Labs, 2008).

2.3.1.2 Downdraft Gasifier

The downdraft gasifier is a co-current flow design; thus, both the biomass and the air and producer gas follow a downward movement. In this system air first enters the combustion zone from the side and then passes downwards through the reduction zone made of the charcoal bed as shown in Figure 2.3. Above the combustion zone, despite the gases flowing downwards, heat from the combustion zone initiates pyrolysis of the biomass feed. The oils and steam formed due to pyrolysis have to pass together with the products of oxidation through the charcoal bed below, where the vapours are cracked and the predominantly endothermic gasification reactions take place, so that the temperature is maintained at 800 – 1000°C. This environment is very conducive to the cracking of tars, such that as much as a 90% reduction in the producer gas tar content seen in the updraft gasifier is observed. Some designs incorporate a paddle to mix material in the combustion zone, avoiding preferential zones where tar could pass without getting cracked (de Souza-Santos, 2004). With a filtration step, these gases can be used in fuel spark and diesel engines (Reed, 1985).

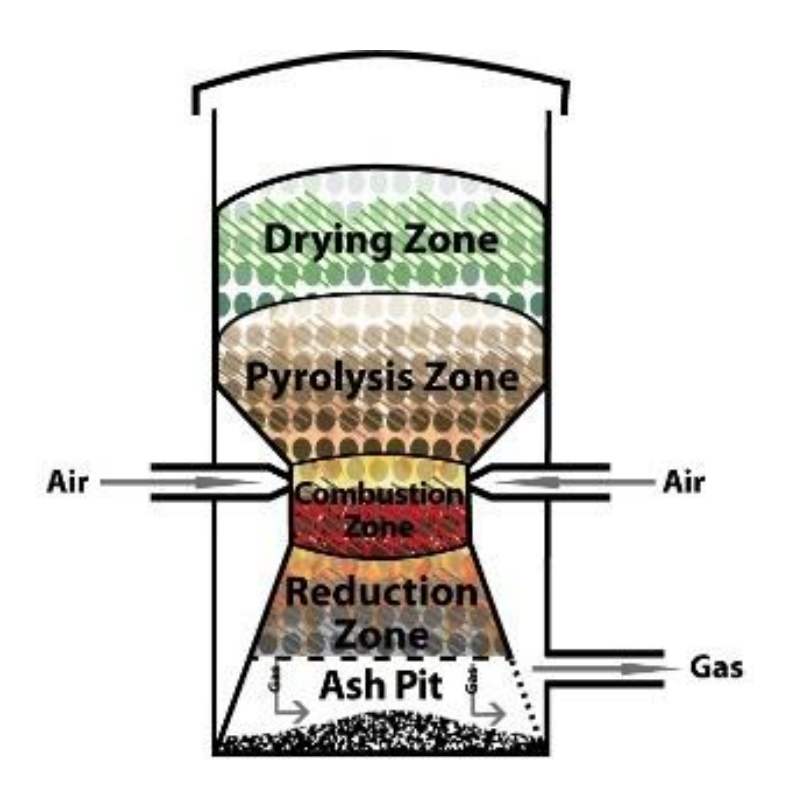


Figure 2.3: Scheme of a downdraft gasifier (All Power Labs, 2008).

2.3.1.3 Cross-draft Gasifier

The cross-draft gasifier (Figure 2.4) is similar in design to the downdraft. Air or oxygen entry is again from the side, but the outlet is situated on the opposite side of the gasifier, usually at the same height (Rajvanshi, 1986).

A high temperature combustion/reduction zone is located near the air inlet; consequently, the pyrolysis and drying zones are higher up in the reactor. The producer gas leaves the reactor at temperatures around 800-900 C. The design is not particularly effective at directing the vapours and gases through the reduction zone; hence a low overall energy efficiency is achieved and a high tar content in the producer gas (McKendry, 2002b). Nevertheless, this scheme allows the reactor to be relatively small (<10kWe), ands the walls are protected from high temperature by layers of fuel and ash (Higman & Van Der Burgt, 2003; Basu, 2010c).

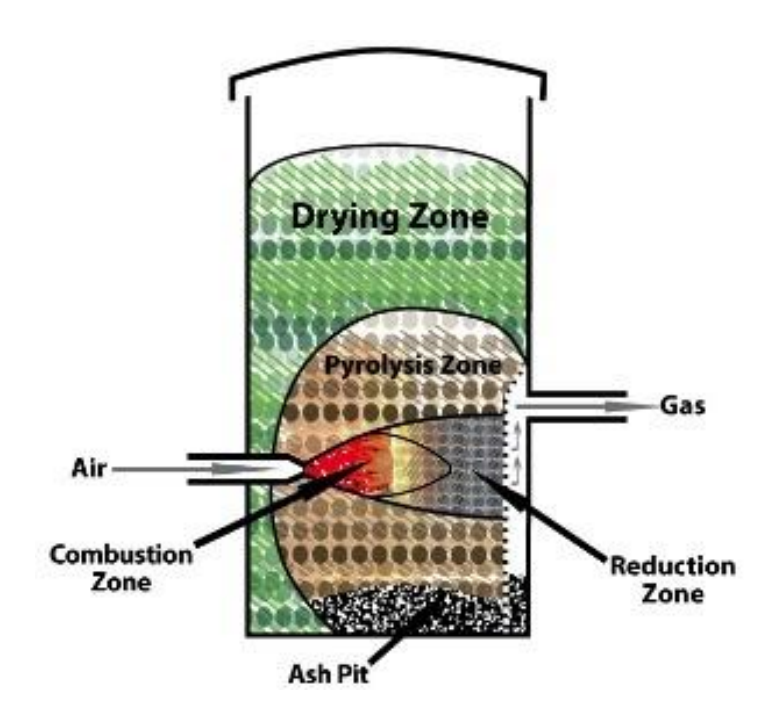


Figure 2.4: Scheme of a cross draft gasifier (All Power Labs, 2008).

2.3.1.4 Two-stage Gasifier

The two-stage gasifier (Figure 2.5) is essentially a downdraft gasifier (biomass and producer gas follow a downward movement). However, in this design, the pyrolysis and char reduction zones have been separated into two reactors by an intermediate high temperature oxidation zone (Henriksen et al., 2006). Here the pyrolysis products are partially oxidized by preheated air addition; and temperatures over 1100°C are reached. This enables the tar content in the pyrolysis products to be reduced by a factor of 100, and thermal energy for the endothermic char gasification is produced. The tar content in the final producer gas is less than 15mg/Nm³ before entering the cleaning systems (Brandt et al., 2000).

This is a sophisticated system and requires very precise control of each step, as it is not a "self controlled" system like a downdraft or updraft gasifier. This gasification system more expensive than conventional fixed bed gasifiers, as it requires

additional temperature and pressure controls systems as well as precise airflow monitoring equipment.

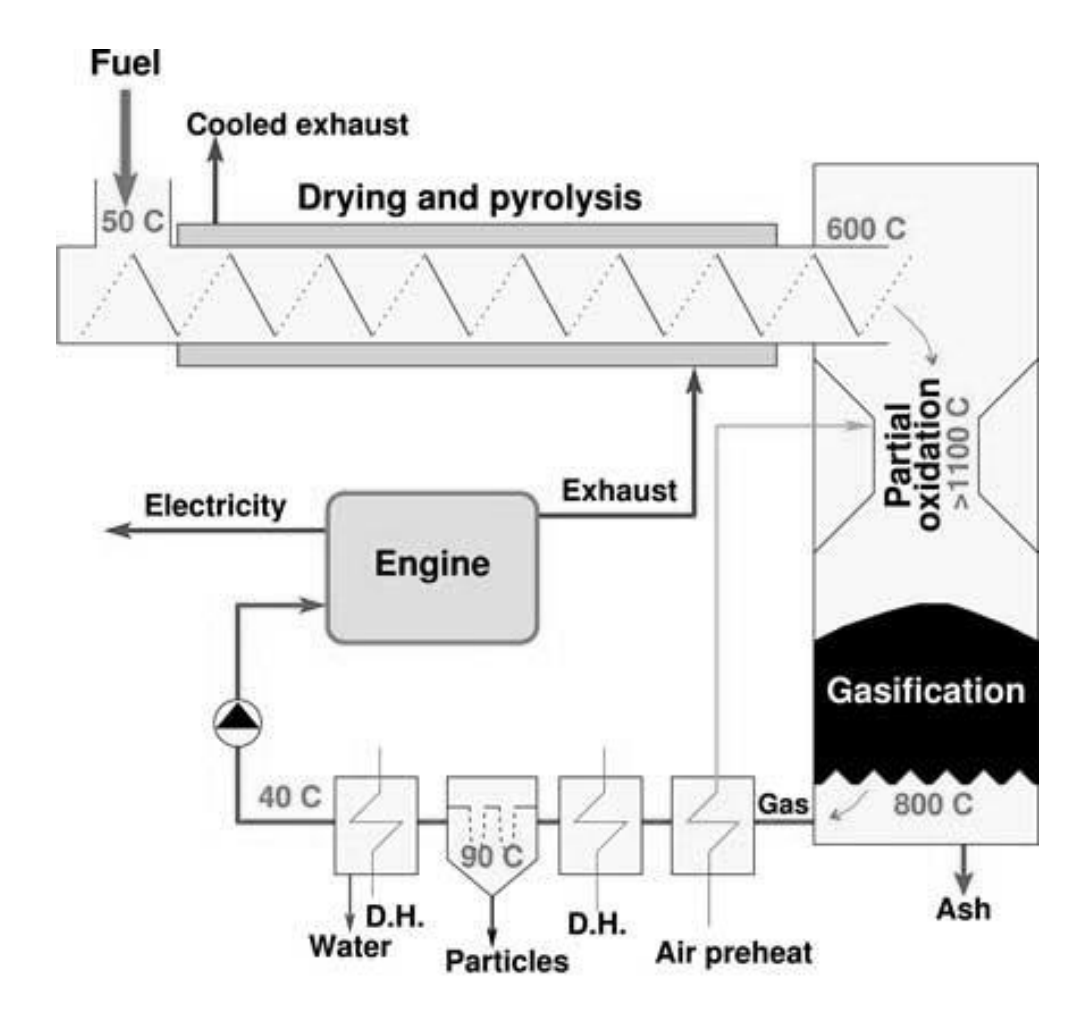


Figure 2.5: Scheme of a two-stage gasifier (Henriksen et al., 2006)

2.3.2 Fluidized Bed Gasifiers

Fluidized bed gasifiers are given this name because the gaseous oxidising agent is injected upwards at high velocity through the bed material so as to create a suspended and well-mixed bed. These gasifiers are quite commonly used for larger (> 10MWth) power applications because of their compact nature, due to high heat exchange and reaction rates resulting from intensive mixing in the bed, and are also favoured for low ash melting point fuels due to the relatively low reaction temperature of about 900°C (Quaak et al., 1999).

These designs provide a uniform contact temperature between gases and solids (Reed, 1985). The bed is comprised of inert material such as sand, which acts as a heating medium. The bed is heated to the desired temperature, and feedstock is then injected to it. The oxidant gas is blown upward through the bed (as in an updraft) but at sufficient velocity to bring the bed into movement ("fluidization"). This significantly enhances heat and mass transfer, and promotes homogeneous conditions throughout the reactor vessel. Thus, there are no distinct oxidation or reduction zones such as in fixed bed gasifiers.

There are three main types of fluidized bed and they are classified according to the flow behaviour as described below. A graphical representation of the three different regimes in terms of gas velocity is showed in Figure 2.6.

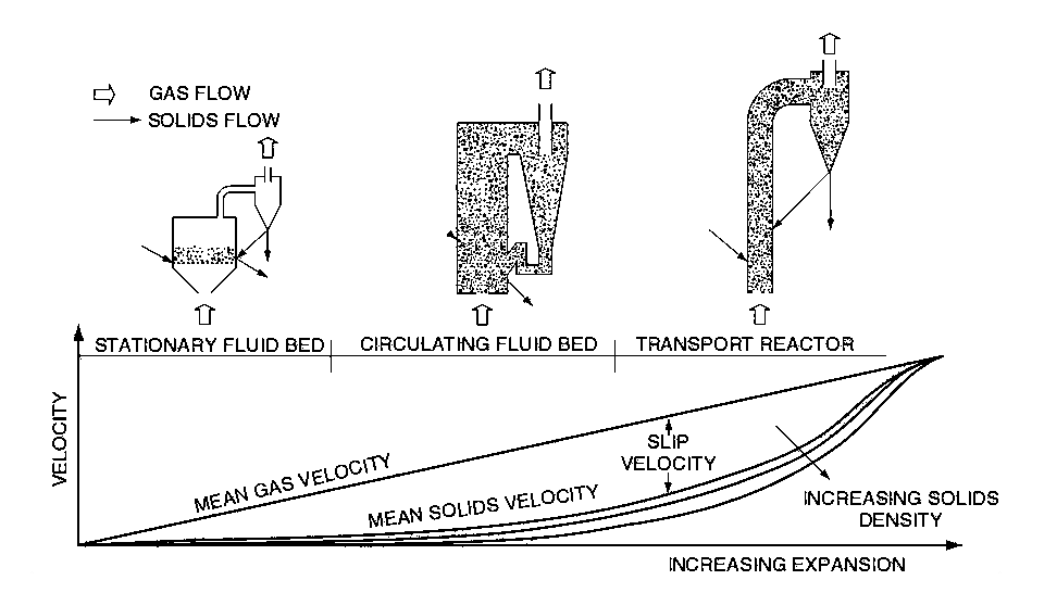


Figure 2.6: Fluidized bed regimes (Higman & Van Der Burgt, 2008)

2.3.2.1 Stationary fluid bed (bubbling bed)

In a bubbling bed gasifier (Figure 2.7), the fluidization regime has a relatively low gas velocity (2–3 m/s), enough to keep the bed suspended in a bubbling state but insufficient to transport solids from the reactor. There is a well-defined division between the dense phase and the freeboard where the solid particles uncouple from the gas.

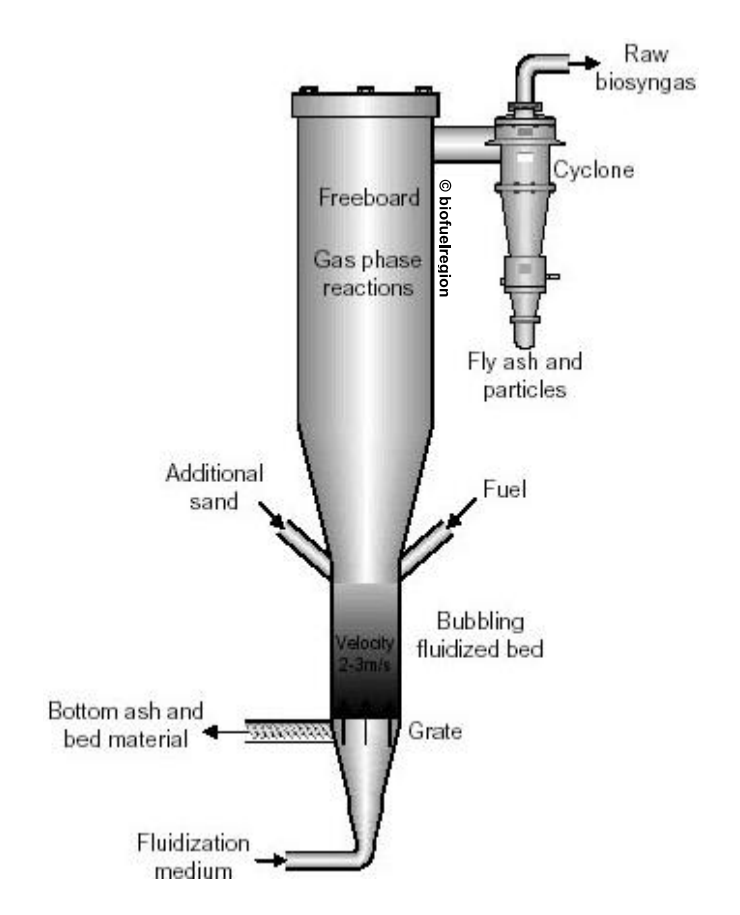


Figure 2.7: Bubbling bed air gasifier scheme (Knoef, 2005).

2.3.2.2 Circulating fluidized- bed (CFB)

The fluidization velocity (3.5–5.5 m/s) in a CFB is much higher than that in a bubbling bed. At these gas velocities, the differential velocity between gas and solids reaches a level where particles are carried out of the reactor. The solids (or a desired size fraction) are then captured by a cyclone separator and return to the bed. A CFB gasifier (see Figure 2.8) has a distinctive appeal for biomass gasification due to the longer residence time it provides to the gas, when compared to the other types of fluidized bed reactor. It is especially suitable for fuels with high volatile content (lignocellulose). A CFB typically comprises a riser, a cyclone, and a solid recycle device.

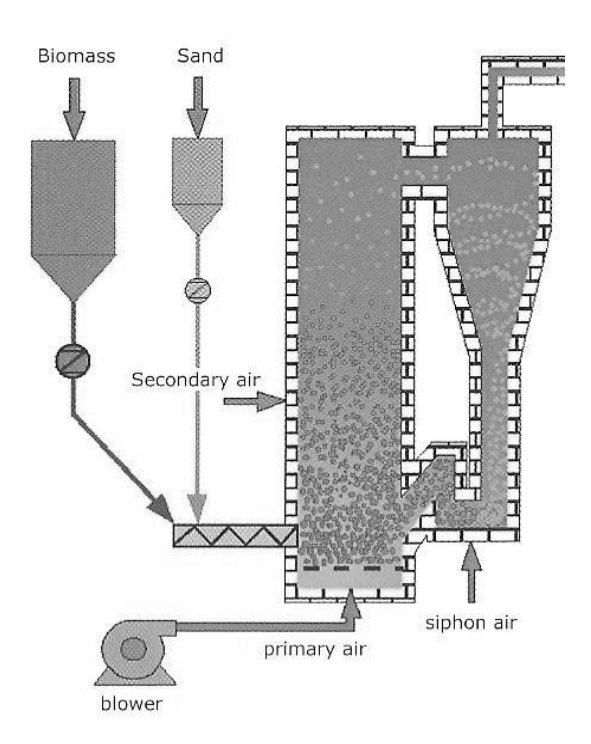


Figure 2.8: Scheme of a circulating bed gasifier (Knoef, 2005)

2.3.2.3 Transport Reactor

The transport gasifier can use either air or oxygen as the gasification medium. The reactor contains a mixing zone, a riser, a disengager, a cyclone, a standpipe, and a J-leg (Figure 2.9). Feedstock, sorbent and air are injected into the reactor's mixing zone. The disengager removes larger carried-over particles, and the removed solids return to the mixing section through the J-valve⁹ placed at the bottom of the standpipe. The majority of the remaining finer particles are removed by a cyclone located downstream, from which the gas exits the reactor.

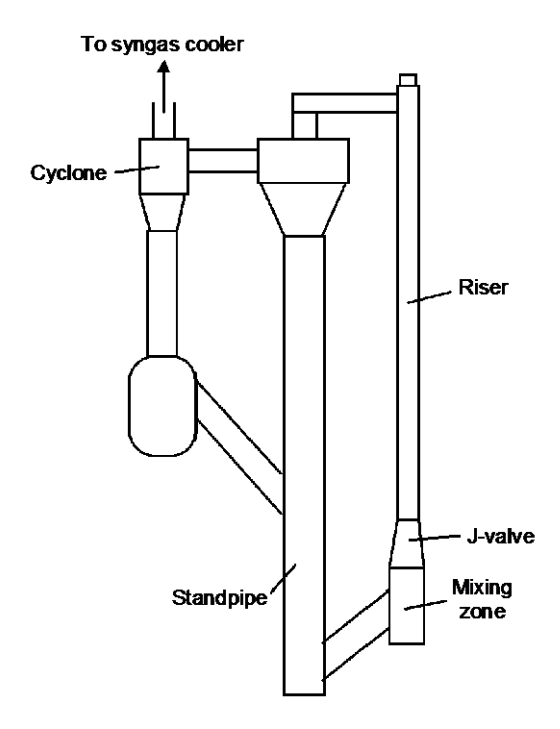


Figure 2.9: Scheme of a typical transport fluidized-bed gasifier (Basu, 2010a)

.

 $^{^{9}}$ Common type of returning system for recirculating solids (Scala, 2013).

2.4 Tar in Producer Gas

Tar remaining in the producer gas is the most awkward and problematic parameter in any gasification commercialization effort for any type of gasifier. In this section, a general discussion about tar in producer gas and its removal processes are presented.

2.4.1 Tar Definition

Tar has been defined in different ways by researchers. But recently a protocol was developed for standardization of tar sampling and analysis (Good et al., 2005; Neeft, 2005). The Tar Protocol defines Tar as: "A generic (unspecific) term comprising all organic compounds present in the producer gas excluding gaseous hydrocarbons (C1-C6) and benzene".

In the present work, tar will be defined into four categories as classified by (Evans & Milne, 1987). The four categories are primary products, secondary products, alkyls as tertiary products, and condensed tertiary products. Primary products generally consist of organic compounds derived from cellulose, hemicellulose and lignin. Secondary products are characterised as phenolics (which are alcohols with the hydroxyl group bonded directly to benzene ring or olefins). Alkyl tertiary products contain mainly methyl derivatives of aromatics. Condensed tertiary products include benzene, naphthalene, acenaphthylene, anthracene, phenanthrene and pyrene.

2.4.2 Tar Quantity According to the Process Applied

As described before, gasifiers can be divided into four principal categories according to the design applied: namely, fixed bed (downdraft and updraft), fluidized bed, twin-flow and entrained flow. The same categories can be applied for classifying

gasifiers according their tar production. There is a general agreement about the relative order of magnitude of tar production, with updraft being the "dirtiest, downdraft the "cleanest"; and fluidized bed, entrained flow and twin bed being "intermediate". A generalization would place the producer gas tar content of updraft gasifiers at 100g/Nm³, fluidized bed gasifiers at 10g/Nm³ and downdraft gasifiers at 1g/Nm³ (Milne et al., 1998).

2.4.3 Tar Production and Removal Techniques

The types of tars produced are a function of both the time and temperature over which reaction occurs, sometimes known as "reaction severity" (Evans & Milne, 1987).

The higher temperatures and the longer the residence times, the higher the reaction severity. Increased reaction severity favours the production of secondary and tertiary tars. Primary and tertiary tars are generally not found together, indicating that primary tars are destroyed before the formation of tertiary products due the high (Evans & Milne, 1987). The presence of both primary and tertiary products indicates process disarrays. Tar composition as a function of reactor operating temperature is shown in Table 2.2 (Elliott, 1988).

Table 2.2: Maturation scheme for tars (Elliott, 1988)

Temperature (ºC)	Products
400	Mixed oxygenates
500	Phenolic ethers
600	Alkyl phenolics
700	Heterocyclic ethers
800	Polynucleic aromatic hydrocarbons (PAH)
900	Larger PAH

Different approaches for tar reduction or elimination have been reported in the literature. All the methods available can be categorized into two groups depending on where tar reduction is carried out; either inside the gasifier itself (primary methods) or outside the gasifier (secondary methods) (Devi et al., 2003).

A general definition of primary methods is that they are applied to the gasification step itself to avoid or convert tar formed in the gasifier. They include: suitable selection of operating conditions, the use of appropriate bed additives (e.g. a catalyst) during gasification, and gasifier design modifications.

Secondary methods are the most conventional and already in commercial use in the treatment of the hot product gas from gasifiers. These methods can be either chemical, such as tar cracking downstream the gasifier either thermally or catalytically, or more commonly physical methods such as use of cyclones, baffle filters, ceramic filters, fabric filters, rotating particle separators, electrostatic precipitators or scrubbers.

Secondary methods, such as downstream tar cracking keep the energy in the process, but physical process (cyclone, scrubbers, etc.) separates the tar from the gas creating a disposal problem, besides taking the tar energy out of the cycle (although some processes aim to recycle the separated tars back to the gasifier).

2.5 Simulation of Gasification Processes

"Essentially, all models are wrong, but some models are useful"

(Box & Draper, 1987)

Mathematical modelling applied to thermochemical process is commonly used worldwide; despite its extensive practice, it is still not developed sufficiently to give accurate predictions of performance in most applications, including gasification. Nevertheless, mathematical models of gasifiers can provide qualitative assistance with respect to the following objectives:

- Determining optimal operating conditions,
- · Creating the most appropriate reactor design,
- Providing information on hazardous process environments, such as high temperature, high pressure, risk of explosion, where experiments are impractical and/or expensive to perform,
- Studying a wider range of conditions that cannot be obtained experimentally,
- Understanding experimental results and analysing improper performance of a gasifier,
- Choosing an appropriate feedstock and evaluating its yield,
- Scaling-up a reactor.

There are several numerical models of gasifiers being used and developed.

They can be grouped as follows:

- Thermodynamic equilibrium
- Kinetics-based
- Computational fluid dynamics (CFD)
- Aspen Plus gasification models
- Artificial neural network

2.5.1 Equilibrium based models

Thermodynamic equilibrium calculation is relatively simple compared to kinetics-based and CFD modelling, and does not take account of gasifier dimensions. Therefore, calculations do not require powerful computers, and results can be delivered quickly. This makes this approach suitable for studying the influence of feedstocks and process parameters. Equilibrium models are more accurate at high temperatures (>1500 K), where chemical reactions are quicker and the reaction time likely to be much less than the residence time of the producer gases (Altafini et al., 2003)

Chemical equilibrium may not be reached in the gasifier, as the temperature of producer gases in the outlet is usually in the range from 750 to 1000°C (Bridgwater, 1995; Reed & Das, 1988; Puig-Arnavat et al., 2010). In reality, a limited residence time is offered for the reaction process in a gasifier or any thermochemical process. Consequently, a thermodynamic equilibrium model may fail to predict the exact yield. Nevertheless, the solution will provide the operator a reasonable prediction of the maximum achievable yield of the producer gas. For applications where the disparities between thermodynamic equilibrium time and residence time are too great, a kinetics-based model is required.

Chemical equilibrium can be resolved by either of the following:

- The equilibrium constant (stoichiometric) method
- Minimization of the Gibbs free energy

Prior to 1958, all equilibrium calculations were performed by the application of the equilibrium constant of the governing equations (Zeleznik & Gordon, 1968).

Later, calculation of equilibrium by the Gibbs free energy minimization technique became a recognized alternative.

2.5.2 Kinetics-based models

Kinetics-based models are more accurate and provide more detailed information about the gasification process (Di Blasi, 2000; Sharma, 2008). The models can be time dependent, which allows the understanding of the fuel conversion during the process, as well as thermal and chemical behaviour, which is fundamental for designing and improving gasifier reactors. In contrast to equilibrium models, kinetics-based models are not limited by residence time or operation at low temperatures (<800 °C) (Altafini et al., 2003), as they do not require the gasifier to reach equilibrium.

The drawback of these types of models is the amount of parameters involved, such as reaction mechanisms and rates, residence time of particles, gasifier hydrodynamics among others. Furthermore, it is computationally intensive and hard to implement when compared to equilibrium models.

With the improvement of computer capabilities, kinetics-based models for gasification processes have been applied numerous times for prediction of performance (Sharma, 2008; W. Yang et al., 2006), dynamic behaviour of the gasification process (Di Blasi, 2000), reactor design (Henriksen et al., 2006), as well as other applications (Cetin et al., 2005; Kirubakaran et al., 2009; Perkins & Sahajwalla, 2008; Puig-Arnavat et al., 2010).

2.5.3 Computation fluid dynamics (CFD)

CFD models (Eulerian type), are 2D or 3D kinetics-based models, where equations for conservation of mass, energy, momentum and species are solved

simultaneously over a discrete region of the reactor. Computers are used to perform the millions of calculations required to simulate the interaction of liquids, gases and solids (particles and/or equipment surfaces) in the defined geometry. Even with simplified equations and high-speed supercomputers, only approximate solutions can be achieved in many cases. Those models are always approximations of reality since they do not have an analytical solution.

The CFD technique permits the calculation of parameters including velocity, pressure, temperature, species and turbulence properties, based on the conservation principles of mass, energy and momentum. The solutions can either be time dependent or not.

CFD gasification codes are generally made through the combination of a series of sub-models, which describe the progress of the biomass decomposition process, such as drying, devolatilization, partial combustion of pyrolysis products, and the char reduction (B. V. Babu & Chaurasia, 2003; Di Blasi, 2008)

Several models have been developed which involve sophisticated reaction kinetics mechanisms and complex particle—particle and particle-gas interactions. However, the majority of the models require the use of sub-models, and the drawing of major assumptions about processes where enough data is not yet accessible and/or generated.

2.5.4 Aspen Plus gasification models

Aspen Plus is a problem-oriented input program that is used to calculate chemical, physical, and biological processes. It can be applied in the simulation of processes that involve solids, vapour and liquid streams. Models can be easily built,

where the user places the operation blocks in a flow sheet as shown in Figure 2.10. The software uses a sequential modular approach, where it solves the process flow sheet block by block using the inlet stream of a block to calculate the outlet stream. Models are also easily updated in Aspen Plus, where small sections of simple or complex systems can be created and tested as separate modules, in advance of being integrated.

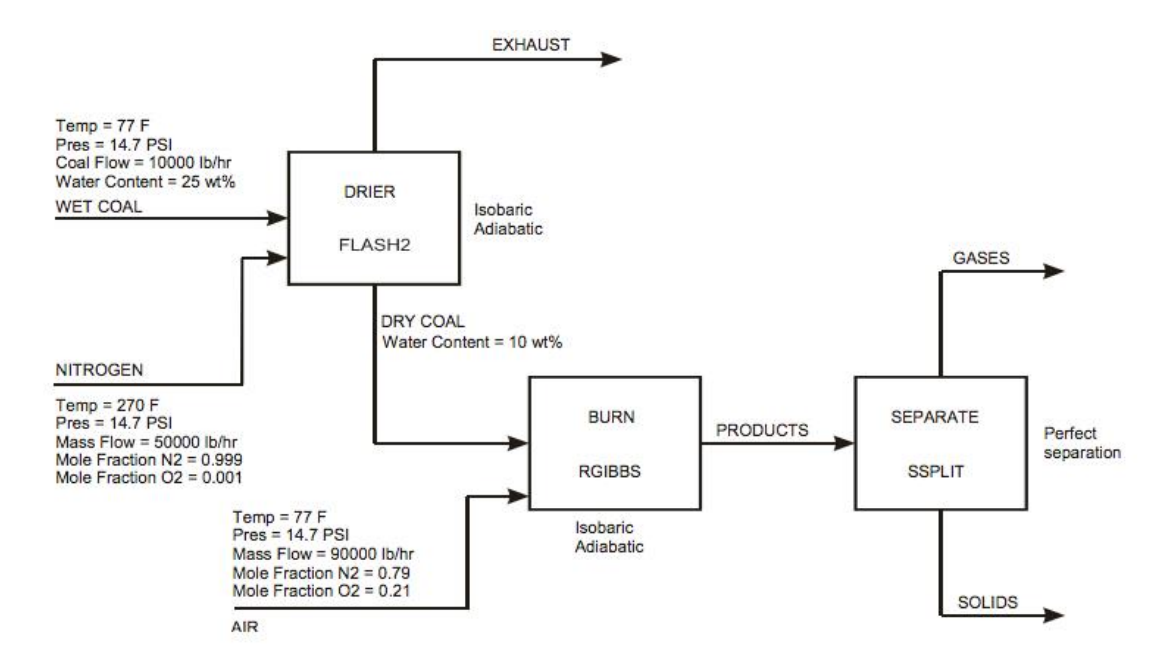


Figure 2.10: Aspen Plus flow sheet example of coal combustion.

By selecting any of the blocks or stream a window (Figure 2.11) opens and the conditions of the selected block or stream cam be specified.

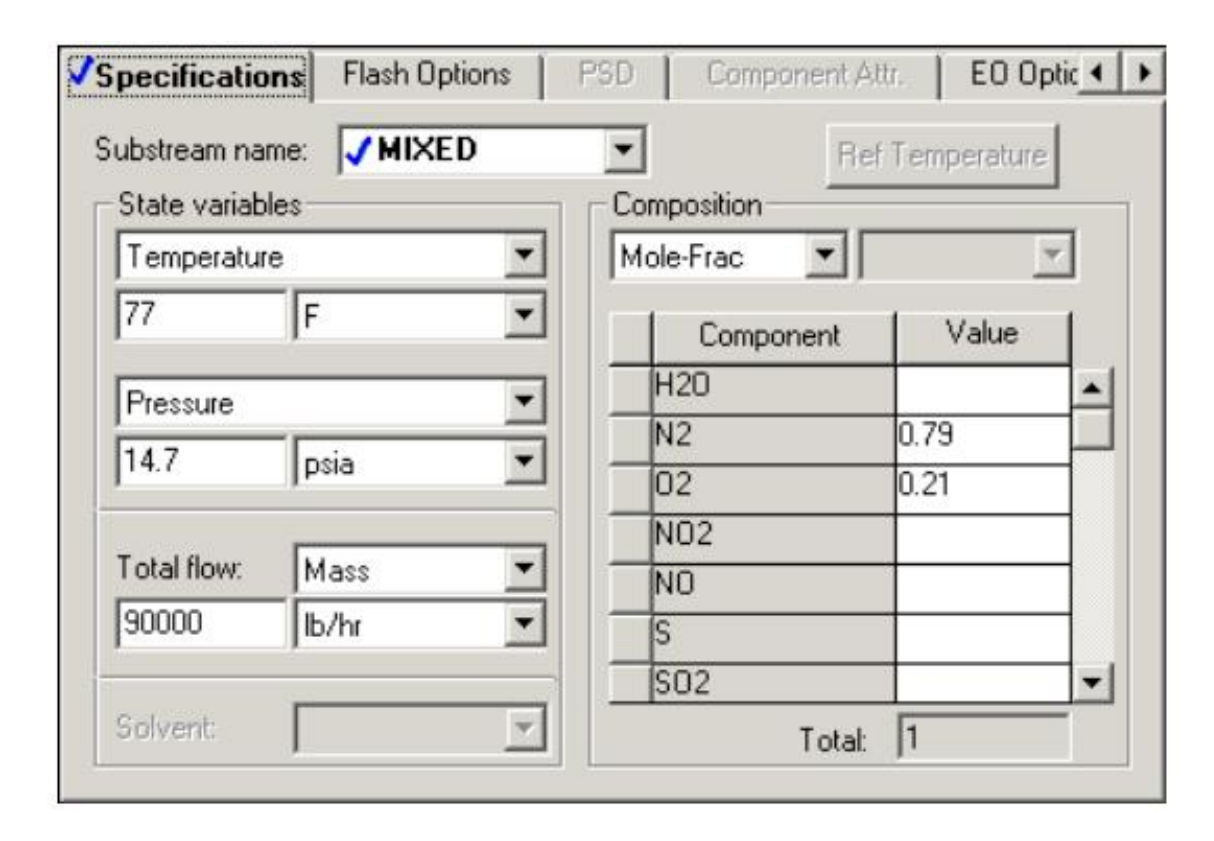


Figure 2.11: Aspen Plus example of window for defining a stream specification

Aspen Plus has a large property data bank containing numerous material properties required to model the streams of a gasification plant, with the possibility of adding in-house property data.

These characteristics permit that Aspen Plus to develop the simplest chemical equilibrium gasification model, as well as complex gasification systems using kinetic-based 1D models.

Aspen has two reactors that can be used to develop equilibrium based gasification models, REQUIL and RGIBBS.

For kinetic-based gasification models there are three reactors available, RCSTR, RPlug and RBatch. More sophisticated block capabilities are required to complete the models, but they can be developed as FORTRAN subroutines.

2.5.5 Neural network

Neural network analysis is a new modelling tool for simulating gasifiers. Its implementation requires previous knowledge of the gasification process, as it works, to a certain extent, in a similar way to an experienced operator (Puig-Arnavat et al., 2010). This model learns from experimental data in the same way as experienced users gain knowledge over time, and then apply this knowledge to forecast how the gasifier will perform under certain operational conditions.

CHAPTER 3

PREVIOUS WORK

The most relevant previous work in the field of fixed bed gasification is reviewed in this chapter. This work involves both experimental and numerical simulation studies that are presented in chronological order divided into the following sections: gasification experiments with characterization of temperature and/or gas profile; thermodynamic equilibrium models, and kinetic-based and computational fluid dynamics (CFD) models.

3.1 Gasification experiments with characterization of temperature and/or gas profile

This section presents a series of reference papers on downdraft biomass gasification that explore the interior of the reactor. The three publications that are discussed cover experiments performed on fixed bed downdraft gasifiers, where longitudinal profiles of temperature were measured throughout the experiments. An experiment that achieved a longitudinal profile of gas and temperature is also discussed.

3.1.1 Experimental study on 75 kW_{th} downdraft (biomass) gasifier system (Sharma, 2009)

This work reports experiments on a 75 kW $_{th}$ downdraft gasifier operating with biomass. The test rig was set up to measure temperature profile in the longitudinal direction, outlet gas composition and calorific value, as well as, the pressure variation

across the bed. Figure 3.1 presents a schematic drawing of the apparatus used and its instrumentation.

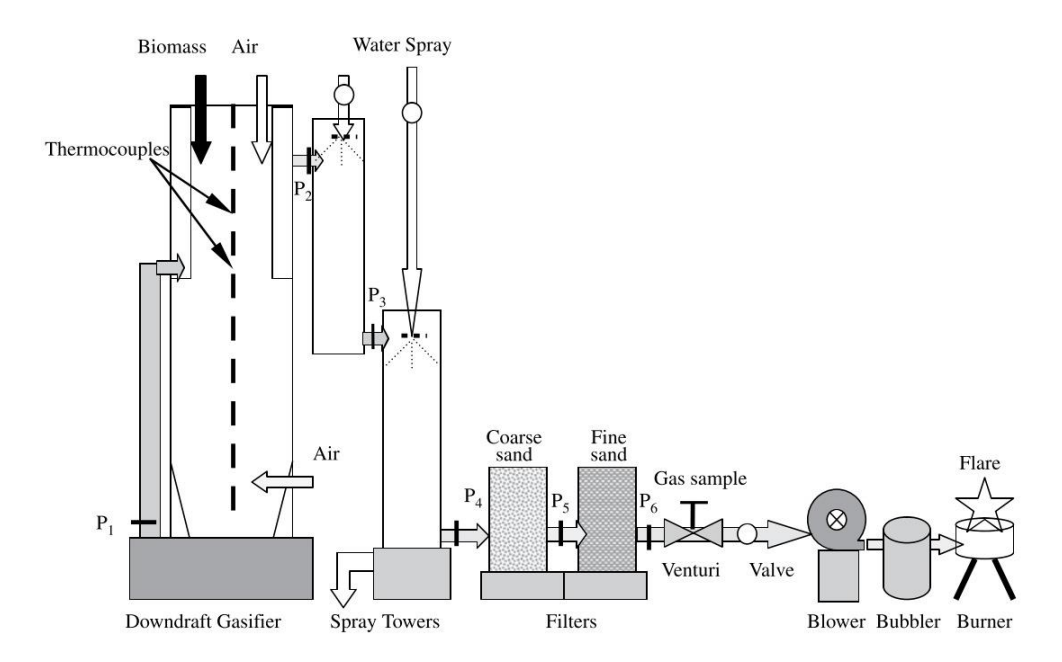


Figure 3.1: Schematic diagram of the 75kW_{th} downdraft biomass gasifier (Sharma, 2009).

During a reacting run of the gasifier, measurements of pressure drop and temperature profile across the fixed bed, and likewise gas composition and calorific values, showed a sensitive response to gas flow rate variations.

Non-reacting flow experiments were performed in the reactor extinguished bed and the results showed an increase in pressure drop when compared to a newly started bed. A newly started bed has a more uniform particle size, whereas an extinguished gasified bed shows a reduction in particle size and an increase in particle density from top to bottom.

The experimental data produced and analysed in this paper may be valuable for the development and validation of numerical codes for gasifiers, for both equilibrium and kinetics-based models.

3.1.2 Experimental investigation of a downdraft biomass gasi er (Zainal et al., 2002)

This paper presents the work carried out in a 2kg/h biomass gasifier. The fuels used for the experiment were wood furniture chunks and wood chips. The experiments were performed for several equivalence ratios, where the variation of calorific value of the producer gas peaked at an equivalence ratio of 0.38.

Temperature measurements were performed across the longitudinal section of the bed, with data being recorded every 30s in order to trace the thermochemical conversion stages of moisture evaporation, pyrolysis, combustion and gasification from top to bottom. To acquire the longitudinal temperature data 5 type-K thermocouples were used. The outlet producer gas temperature was measured by another thermocouple installed at the gas outlet. The main body is built from a pipe of 600mm diameter and 2500mm height. Figure 3.2 presents the schematic drawing of the reactor and thermocouple locations.

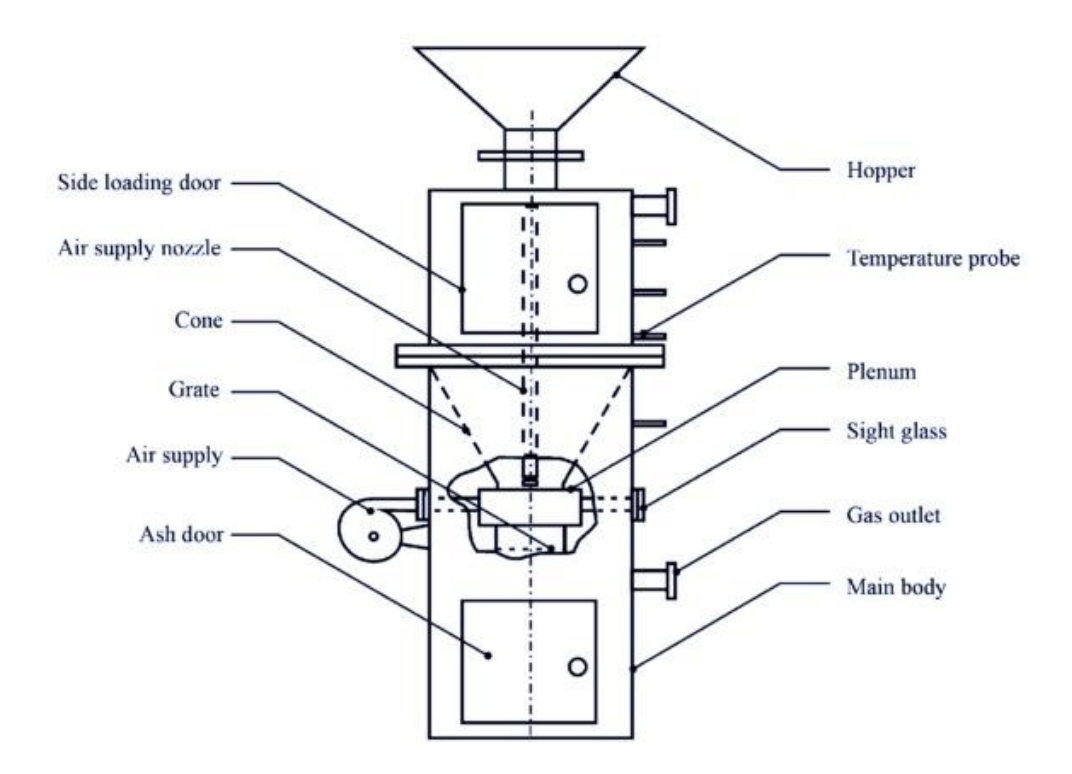


Figure 3.2: Schematic of the fixed bed downdraft reactor (Zainal et al., 2002).

3.1.3 Gasification of charcoal wood chips: Isolated particle and fixed bed (Tagutchou, 2008)

This thesis focuses on understanding the behaviour of the reduction zone of a two-stage gasifier – a.k.a Viking (Henriksen et al., 2006; Brandt et al., 2000) – fed with charcoal wood chips. Temperature profiles and gas composition profiles were acquired across the longitudinal section of the reactor. A schematic drawing of the Continuous Fixed Bed Reactor (CFiBR) is presented in Figure 3.3.

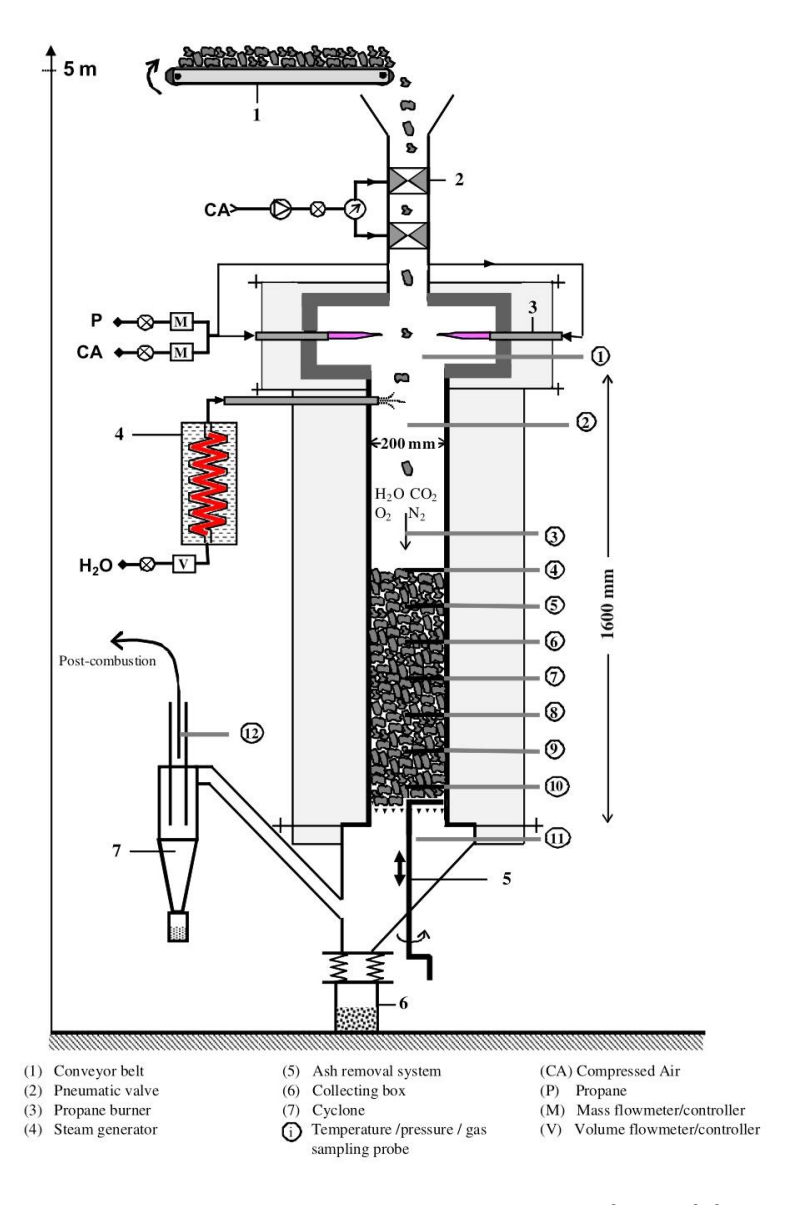


Figure 3.3: Schematic of the Continuous Fixed Bed Reactor (CFiBR) (Tagutchou, 2008).

The atmosphere of the reactor, i.e. inlet gas temperature and composition (a mixture of H_2O , CO_2 , O_2 and N_2) is generated by the exhausts of two propane burners

(3). A conveyer (1) enables the feeding of char to the top of the reactor. The char flow rate can be varied between 0 and 3 kg/h. A known mass of char is distributed on the belt, and knowledge of the belt speed enables a precise control of the char flow rate. A system of two pneumatic valves (2) ensures that no air can enter the reactor when the char is introduced.

The reactor consists of a refractory stainless steel tube (4) of 20 cm in diameter and 160 cm in height. Eight probes are arranged in a helicoidal form along the reactor for gas sampling, and measurement of temperature and pressure. The thermal insulation (5) of the reactor consists of a 20 cm thick layer of ceramic wool, which entirely covers its lateral surface. The wool layer is protected on the outside by an aluminium sheet.

Compared to the reactors presented previously, the CFiBR is the most sophisticated in terms of instrumentation, as it not only permits longitudinal measurements of temperature, but also gas sampling. The helicoidal probe installation allows a better flow of the biomass avoiding bridging. The design of the probes permits gas sampling and temperature measurement at the same time, allowing for better understanding of the thermochemical reactions across the bed.

The experimental data produced and analysed in this thesis may be valuable for the development and validation of numerical codes for gasifiers, both equilibrium and kinetics-based models. The existence of both temperature and gas profile allow for a more accurate validation of 1D kinetics-based and CFD models.

3.2 Thermodynamic equilibrium models

This section presents a series of reference papers on equilibrium modelling of downdraft biomass gasifiers, both using the equilibrium constant technique and Gibbs free energy minimization. The five studies discussed here represent the variety of equilibrium models developed so far; either implemented in commercial packages or programmed in open source computer languages.

All the presented models present fair agreement with the experimental results for hydrogen, carbon monoxide, carbon dioxide, water and nitrogen. Nevertheless the majority of the models that apply chemical equilibrium and use the classical method of Gibbs free energy minimization underestimate methane concentrations. Methane is also formed during the pyrolysis process and it formation does not reach equilibrium.

3.2.1 Thermochemical equilibrium modelling of a gasifying process (Melgar et al., 2007)

This work discusses the development of an equilibrium model for charcoal and biomass gasification. It uses the approach of the equilibrium constant together with thermodynamic equilibrium of the global reaction. In this model, the temperature of reaction is not provided by the user as commonly practised; it is taken as the adiabatic flame temperature, which is calculated from the thermodynamic equilibrium of the global gasification reaction.

The model was validated by comparison with the results of (Jayah et al., 2003) as shown in Table 3.1, and it was developed to predict producer gas composition and high heating value, shown in Figure 3.4. Among all the species measured, methane presented the highest deviation.

Table 3.1: Comparison between experimental and model predicted compositions for the producer gas of rubber wood with 14.7% moisture content

Gas composition (vol%)	Model (Jayah et al., 2003)	Experimental (Jayah et al., 2003)	Model (Melgar et al., 2007)	Experimental (Melgar et al., 2007)
СО	18.3	19.1	19.2	19.3
H ₂	16.4	15.5	16.6	17.6
CO ₂	11.1	11.4	11	11.1
CH ₄	1.1 ¹⁰	1.1	0.2	0.4
N ₂	53.2	52.9	53	51.6

A parametric study was also performed to evaluate the impact of the equivalence ratio and moisture content on the producer gas composition, as well as the influence on the overall gasifier efficiency as shown in the Figure 3.4.

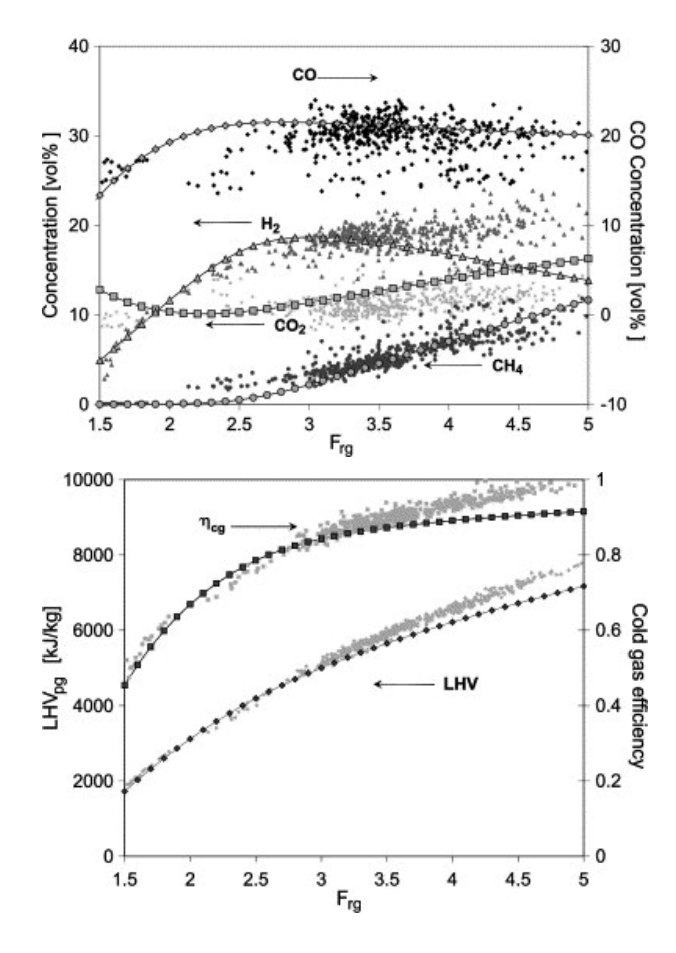


Figure 3.4: Comparison of the predicted and experimentally obtained producer gas composition (top) and low heating value for pine wood with 18% moisture (bottom).

 $^{^{\}rm 10}$ Value inserted by the user, not calculated in the model.

3.2.2 Modelling of a downdraft gasifier fed by agricultural residues (Antonopoulos et al., 2012)

This model uses a non-stoichiometric (Gibbs free energy minimization) approach to predict producer gas composition and performance of a 0.5 MW downdraft gasifier. The system of equations was solved by the software Engineering Equation Solver – EES.

The main input parameters required are the chemical composition of the biomass, moisture content, temperature of reaction and expected elements in the producer gases. The model simulated the gasification of Olive wood, miscanthus and cardoon at a temperature range of 800 – 1200 °C and equivalence ratio of 0.45, and it was validated by comparison with results of (Kurkela & Ståhlberg, 1992; Martinez et al., 2012), as shown in the Figure 3.5. Hydrogen estimation presented good agreement, but carbon monoxide was over calculated.

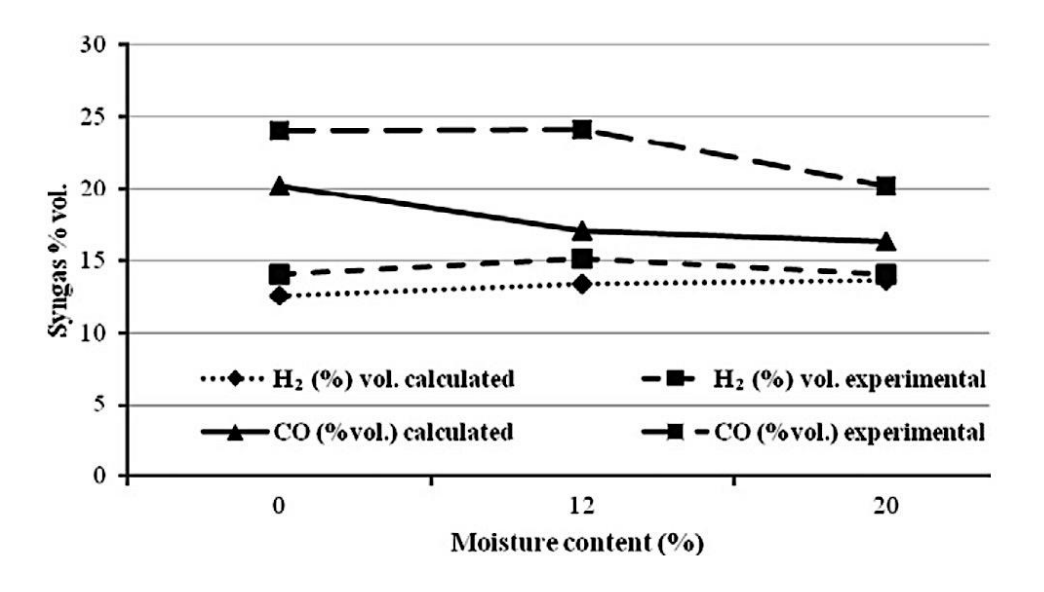


Figure 3.5: Experimental vs. calculated data comparison of hydrogen and carbon monoxide concentrations on syngas from biomass feedstock in relation to feedstock moisture content. (Antonopoulos et al., 2012)

The results were used to design an olive wood gasification reactor, as well as to perform sensitivity analysis of the influence of moisture content and temperature. The concentration of N_2 was reported to remain constant for all fuels, whereas H_2 and CO_2 concentrations presented a decreasing trend as the temperature increased as shown in Figure 3.6.

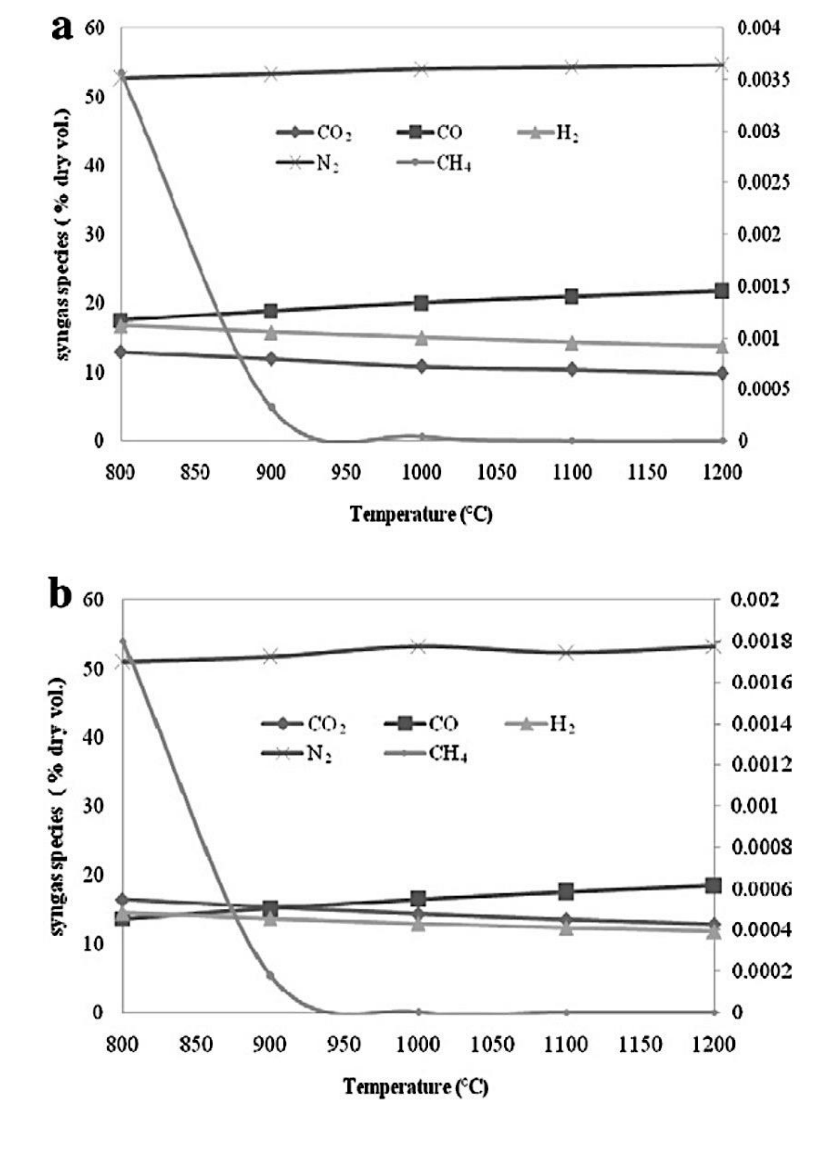


Figure 3.6: Effect of temperature on syngas species concentration: (a) miscanthus and (b) cardoon . (Antonopoulos et al., 2012)

Additionally, CH_4 presented negligible concentrations at temperatures above 900 °C.

3.2.3 Thermodynamic equilibrium model and second law analysis of a downdraft waste gasifier (Jarungthammachote & Dutta, 2007)

In this paper, a stoichiometric method is applied to predict the producer gas composition of a fixed bed downdraft gasifier fed with municipal solid waste. To overcome the under-estimation of methane and hydrogen concentrations, as well the over-estimation of carbon monoxide concentration, empirical correction coefficients¹¹ were multiplied to the equilibrium constants of methane reaction and water-shift reaction.

The correction coefficients were empirically calculated using 11 cases of experimental results from literature (Altafini et al., 2003; Zainal et al., 2001; Jayah et al., 2003). A coefficient of 11.28 was used to multiply the equilibrium constant of the methane reaction to improve accuracy of the model. To correct the slight under calculation of CO and barely higher calculated values for CO2, a correction coefficient of 0.91 was used to multiply the equilibrium constant of the water-gas shift reaction.

The results for the modified method showed an increase on the mole fraction of H_2 , CO_2 and principally CH_4 ; on the other hand, CO and N_2 slightly decrease. The modified model (uses correction coefficients) presents better results than the traditional thermodynamic equilibrium method.

The model was validated by comparison with the results of (Jayah et al., 2003), and it was developed to evaluate the impact of moisture content in the gasification of Thailand municipal solid waste (MSW).

¹¹ Coefficients determined from the comparison of the predicted results with experimental results from literature. They are used to approximate numerical results to experimental calculations.

3.2.4 Mathematical Modeling of a Fluidized Bed Rice Husk Gasifier: Part III – Model Verification (K G Mansaray A E Ghaly A M, 2000)

In this paper is presented the validation of a two-compartment model developed for fluidized bed gasification of biomass for the system shown in Figure 3.7. The model was validated using experimental data from a dual-distributor-type fluidized bed gasifier. The fluidized bed gasifier runs on rice husks at various equivalence ratios (0.25, 0.30, and 0.35), bed heights (19.5, 25.5, and 31.5 cm), and fluidization velocities (0.22, 0.28, and 0.33 m/s).

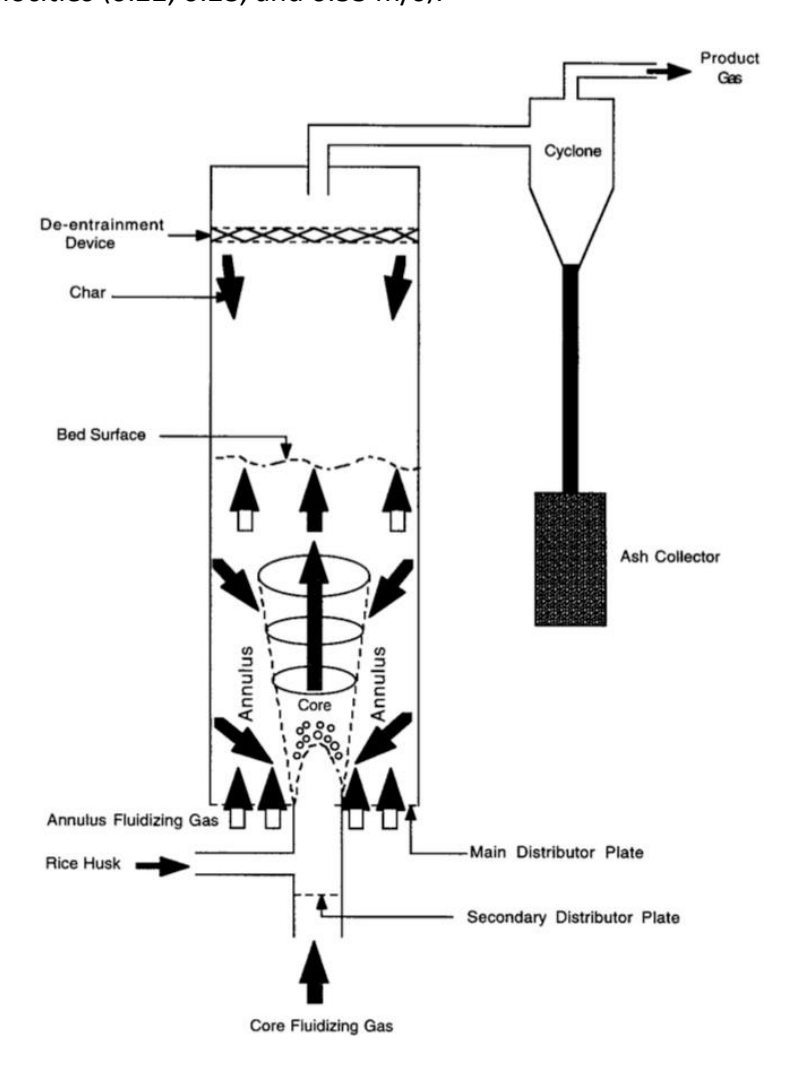


Figure 3.7: Gasifier diagram showing the continuous exchange of gases and solid particles (Mansaray et al., 2000).

The two-compartment model was presented in the first of three paper of the series (Mansaray et al., 2000). The model takes into account the complex hydrodynamic conditions of fluidized bed gasifier, and it has two parameters (carbon conversion in the core and annular regions) as shown in Figure 3.8.

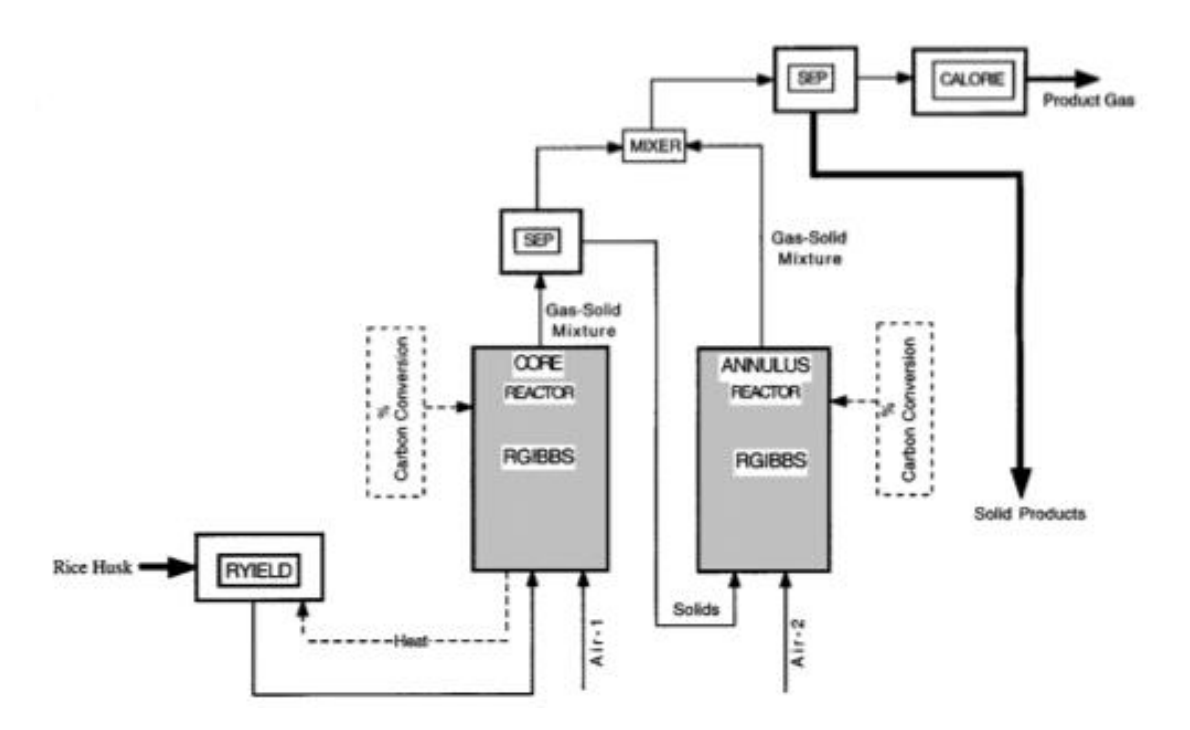


Figure 3.8: ASPEN PLUS simulation flow diagram developed to model the fluidized bed gasifier based on the two-compartment approach (K G Mansaray A E Ghaly A M, 2000).

In the CORE REACTOR (core region), the RGIBBS module calculates the adiabatic temperatures, and equilibrium product composition achieved in this reactor. The unconverted biomass removed from the CORE REACTOR is fed into the ANNULAR REACTOR (annular region), where it undergoes gasification reactions with the annular air. A RGIBBS module also calculates the adiabatic temperatures and the equilibrium products composition.

The model presented reasonable results for temperature, higher heating value (Figure 3.9) and mole fraction (Figure 3.10) for both core and annulus regions.

Nevertheless the overall carbon conversion was overestimated. The reason for the

inconsistencies in experimental and calculated overall carbon conversions must be attributed to uncertainties in the sampling procedure.

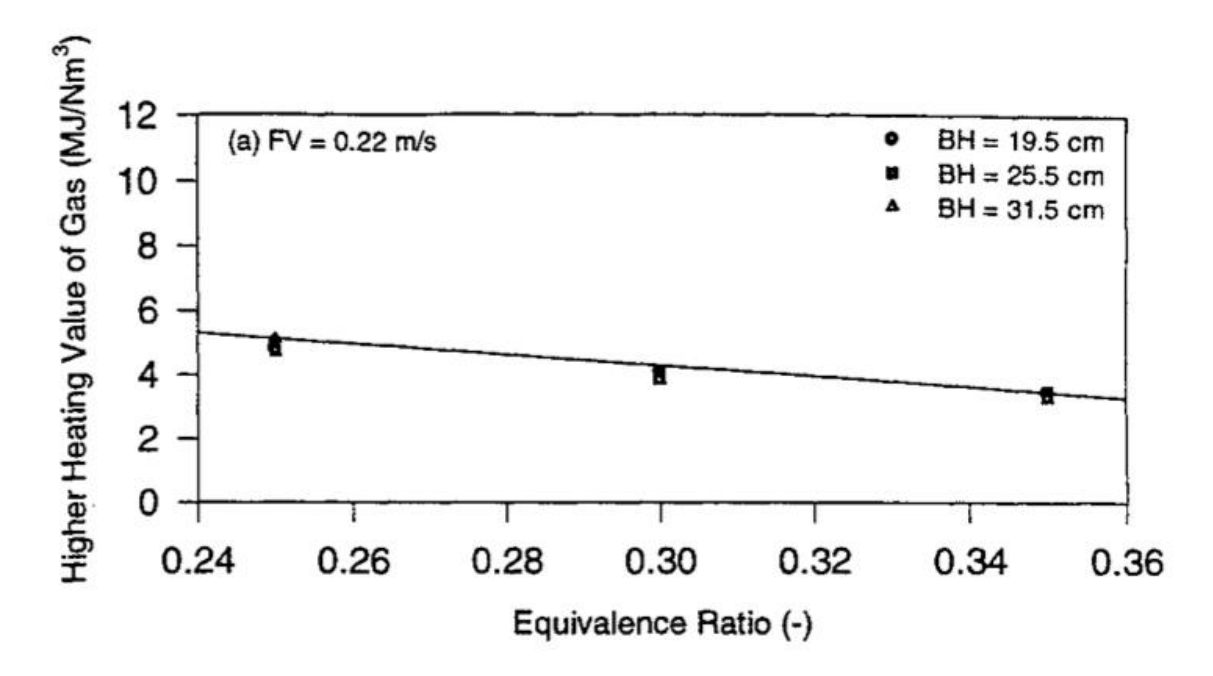


Figure 3.9: Comparison of predicted and measured exit temperatures at various equivalence ratios and bed heights at the fluidization velocity (FV = 0.22).

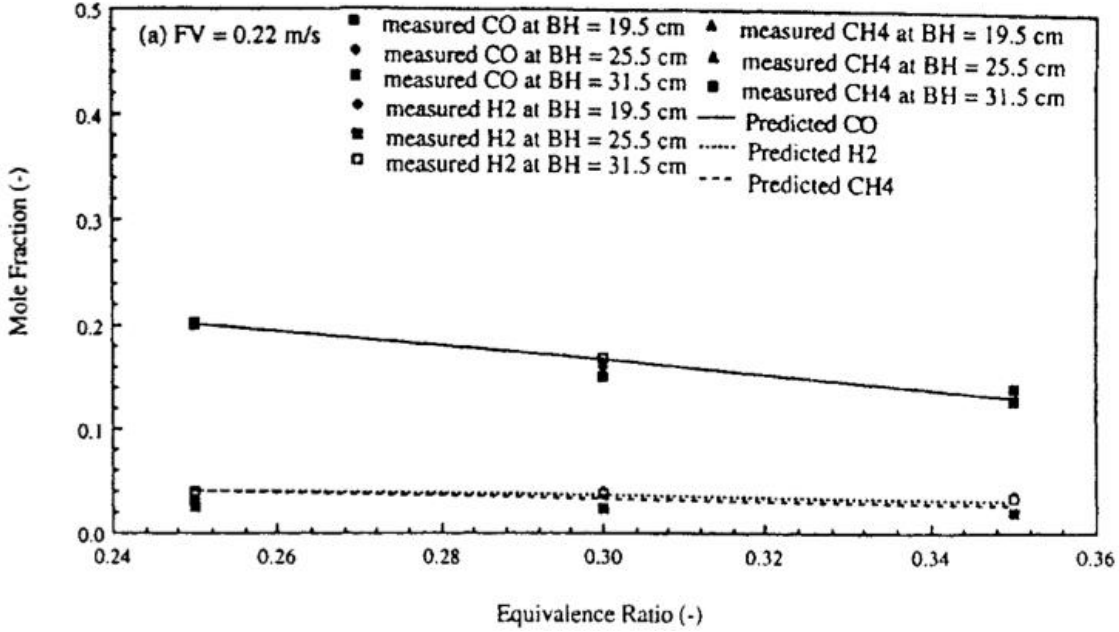


Figure 3.10: Comparison of predicted and measured mole fractions of carbon monoxide, hydrogen and methane at various equivalence ratios, fluidization velocities and bed heights.

3.2.5 Performance analysis of a biomass gasifier (Mathieu & Dubuisson, 2002)

This work modelled wood gasification in a fluidized bed using Aspen Plus. The model is based on the minimization of the Gibbs free energy and it was uncoupled into four basic processes: pyrolysis, combustion, Boudouard reaction and gasification as shown in Figure 3.11.

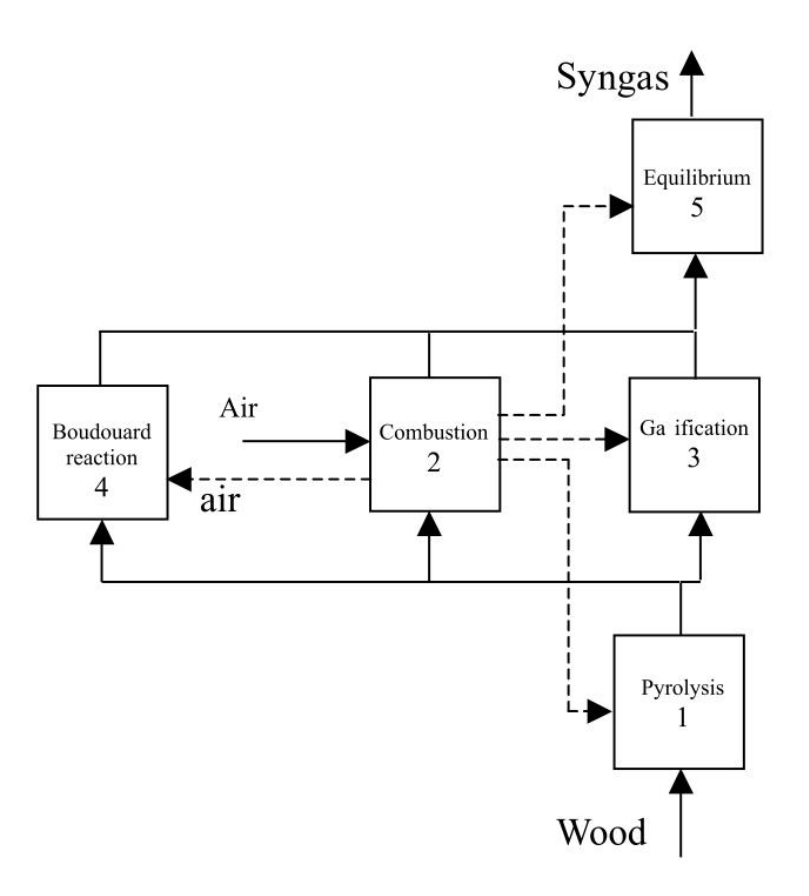


Figure 3.11: Gasifier model

At the beginning of the process, a prompt pyrolysis of the fuel occurs as soon the biomass is injected in the gasifier, fractions of the products of the pyrolysis are either burnt, gasified or take part to the Boudouard reaction as shown in Figure 3.11. From a thermal balance a single reaction temperature, the same in all the processes or boxes, is derived.

At the end of the process, the products of combustion, gasification and Boudouard reaction wait until a new chemical equilibrium is reached and this gives the final calculation of the producer gas.

By performing a sensitive analysis, the authors concluded that there is an optimum oxygen factor 12 (25%), that the enrichment of the air in O_2 up to 30% vol. increases the gasification efficiency provided that this air is not pre-heated, that there is a critical air temperature above which preheating is no longer efficient, and that the operating pressure has only a slight positive effect on process efficiency.

 $^{^{12}}$ It is defined as the ${\rm O_2}$ fraction of the stoichiometric ${\rm O_2}$ amount used in a neutral and theoretical combustion process.

3.3 Kinetic and computational fluid dynamics (CFD) models

In this section, the most relevant previous work in the field of kinetic based models of reactive flows in fixed bed gasifiers is reviewed. The publications presented here cover the majority of the types of gasification models developed. These include steady state kinetic models, dynamic kinetic models and computation fluid dynamics (CFD) models.

3.3.1 Pressurized Downdraft Combustion of Woodchips (Purnomo et al., 1990)

This is one of the first studies that simulated a reacting flow in a fixed bed using a kinetics-based approach. The model of the downdraft combustor considers a bed of wood particles on top of refractory pebbles. Air is fed at the top across the fuel bed, which undertakes drying, pyrolysis and char oxidation. The gas phase in the process consists of oxygen, hydrocarbons, carbon monoxide, carbon dioxide, and water vapour. The composition of these components varies depending on location and time, whereas the composition of nitrogen remains constant during the whole process.

Both wood volume and velocity of flow remain constant in the drying and pyrolysis zones, as density decreases. The product formed in this stage is only a hydrocarbon ($C_1H_{0.335}O_{0.00461}$). In the char zone, the fuel density remains constant, and the thickness shrinks causing the fuel velocity to decrease gradually to zero at the particle interface. Conservation of mass and energy for the solid and gaseous phases are formulated in one-dimensional unsteady form.

3.3.2 Numerical Modelling of a Deep, Fixed Bed Combustor (Bryden & Ragland, 1996)

This paper presents the development of a computational model to estimate the anticipated performance characteristics of a deep, fixed bed combustor/gasifier utilizing whole trees as the source of fuel. The work presents a computational model of a fixed bed deep reactor, which simulates the gasification of large thermally thick woody biomass in segments of approximately 20 cm diameter. This model was used to examine the expected behaviour of the reactor providing subsidies for the design of the combustor. The areas investigated include the heat release per unit plan area and bed depth, and the impact of changing moisture content, fuel size, and under fire velocity.

The model is one-dimensional and steady-state, and it describes an open-top updraft fixed bed combustor. For simplification of the calculations a set of assumptions were made:

- There is no heat loss through the surrounding walls and bed;
- The surface area to volume ratio of the fuel is determined at each location step in the bed as a function of diameter.
- Only seven gas phase species are considered: oxygen, nitrogen, hydrogen, water vapour, carbon dioxide, carbon monoxide, and hydrocarbons (C₁H_{1.522}O_{0.0028}). Hydrocarbons include all gaseous pyrolysis products except water, carbon dioxide, carbon monoxide, and hydrogen. Tars are included with hydrocarbons, which react with oxygen to form water and carbon dioxide.

As soon as the reactions with oxygen begin the load starts to shrink, and carbon dioxide, water vapour, moisture and wood volatiles are released from the wood. This model solves the equations of conservation of mass and energy for the

solid and gas. The entire gas phase physical properties - including specific heat, diffusion coefficients and density - are functions of species and temperature.

This model differs from the other fixed bed models due to the thermally thick biomass fuel. Additionally, the two-point boundary problem is reduced to an iterative process to find the particle diameter as a function of height.

3.3.3 Dynamic behaviour of stratified downdraft gasifiers (Di Blasi, 2000)

This is a major work in the development of fixed bed reacting flow modelling and comprises of a one-dimensional unsteady model for biomass gasification in a downdraft reactor. Heat and mass transfer equations are coupled with drying, pyrolysis, char oxidation and reduction, as well as, gas-phase combustion and thermal cracking of tars. The simulations carried out allowed prediction of the impact of model parameters variations, the structure of the reaction front, as well as the quality of the producer gas. The species taken into account are: oxygen, nitrogen, hydrogen, water vapour, carbon dioxide, carbon monoxide, methane and hydrocarbons (including tars).

The gasifier models perform mass and energy balances for the solid and gas phases, for a one-dimensional and unsteady state system. The pressure drop in the reactor is modelled using the generalized Darcy law. The model equations describe the co-current flows of solid and gas descending across the reactor where several processes take place in the following order: moisture evaporation, biomass pyrolysis, combustion of gases and thermal cracking of the tars, and also char combustion and gasification.

The work was validation by the experimental result presented in the Table 3.2 and they present good agreement with literature.

Table 3.2: Comparison between the predicted and measured composition of the producer gas

% vol	(Groeneveld & van Swaaij, 1980)	(Walawender et al., 1985)	This study (Di Blasi, 2000)
СО	17	18-20	20.3-18.5
H_2	14	12-16	16.8-9.8
CO ₂	13.6	14-16	15.3-9.4
CH ₄	0.9	2.5	4.5-2.4
N_2	46.5	53-45	43-60
air feed rate divided by the biomass feed rate	_	1-2	1.4-2.2

What distinguishes this work from the previous works is the capacity of evaluating a larger number of gases that included tar and methane, in addition to the fact that it has an accurate prediction of the behaviour of time dependent variables.

3.3.4 Performance Analysis of a Fixed-bed Biomass Gasifier Using High-temperature Air (W. Yang et al., 2006)

This paper is the second stage of development of the Fluid Dynamic Incinerator Code (FLIC), developed at Sheffield University. The code was initially designed for MSW incineration on a travelling bed (Y. B. Yang et al., 2002), but was adapted to satisfy the following assumptions for a packed bed:

- One-dimensionality assumption: The major bed properties, namely temperatures (of gas and solid phases inside the bed), gas compositions (O₂, H₂, CO, CO₂, etc.) and solid compositions (moisture, volatiles, fixed carbon and ash) can be described one-dimensionally as functions of the bed height.
- Porous bed assumption: The bed can be treated as a porous medium where mass and heat transfer takes place between the solid and gas phases.
- Spherical particle assumption: The shape of the particle is spherical and the averaged surface-volume diameter is used.

The whole geometrical domain of the bed is divided into many small cells. All partial differential equations (PDEs) used can be represented in a standard form, which are then discretised over each cell and solved using the SIMPLE algorithm. The computer code (FLIC), mentioned above was used to solve the governing equations.

FLIC is available for downloading at http://www.suwic.group.shef.ac.uk/flic and one of the advantages of the code is that, in comparison with the previously mentioned codes, it has a friendly interface that permits the user to change parameters, such as kinetics constants, change state between steady and unsteady, continuous feeding as well as other changes.

3.3.5 The 2D Eulerian Approach of Entrained Flow and Temperature in a Biomass Stratified Downdraft Gasifier (Rogel & Aguillon, 2006)

This is the first work that describes biomass gasification from a 2D approach. Their work uses a "1-D+2-D" (two dimensional time dependent) approach to model the gasification of wood pellets in a downdraft gasifier. The model uses an Eulerian approach to solve the equations of conservation of mass, energy and momentum for the solid and gas phase. The model describes the biomass particle undergoing heating up, drying, primary pyrolysis of biomass, tar thermal cracking, homogeneous reactions and heterogeneous combustion/gasification reactions, as well as particle size shrinkage. This CFD model predicts temperature and gas profiles, producer gas lower heating value and carbon conversion efficiency, as well as the reactor efficiency when operating parameters and feed properties are changed.

The model was programmed into a commercial CFD code, known as PHOENICS, which discretizes the equations using a finite volume method, and solves them through an Inter-Phase Slip algorithm (IPSA).

Despite the sophistication of this software, there are limitations in the gas species treatments that were taken into account in the work (Di Blasi, 2000). For simplification of the process, volatiles are described as methane (CH₄); consequently, it limits the analyses of tar formation and destruction.

CHAPTER 4

WORK PROGRAM

The aim of this work was to investigate the reduction zone of a downdraft gasifier, to provide the necessary data for development and validation of 2D CFD codes to simulate the behaviour of the gasification zone of a downdraft gasifier, and to develop an Aspen Plus model for char gasification.

4.1 Literature review

Based on Chapter 3 – Previous Work, the scope of the project could be defined.

There are a series of reference experimental papers on fixed bed downdraft biomass gasification, but the majority focus on the measurement of temperature and producer gas composition at the exit of the reactor. Fewer references, as presented in section 3.1, explore the interior of the reactor and perform measurements of gas composition and temperature in the longitudinal direction.

On the subject of numerical equilibrium modelling of downdraft biomass gasifiers, there are several reference papers using both the equilibrium constant and the Gibbs free energy minimization methods. Most models present fair agreement with the experimental results for most gases. But the models always underestimate methane concentrations. A few models do not calculate methane and just use the value of the experiments, others correct the methane underestimation by applying empirical correction coefficients.

The majority of those numerical models are implemented in Fortran, C++, EES, etc. Fewer papers, as presented in section 3.2, use Aspen Plus with the RGibbs reactor; however, the authors have mainly used non-stoichiometric methods, and have not applied advanced instruments within the RGibbs reactor, such as restricted equilibrium with temperature approach (global and reaction-specific), and sensitivity analysis.

Therefore, the focus of the experimental part of this work is on the analysis of pressure, temperature, and gas concentration within fixed bed downdraft gasifiers. The numerical side explores chemical equilibrium numerical modelling using Aspen Plus with restricted equilibrium, by either applying whole-system or reaction-specific temperature approaches. The main objectives are detailed in the following section.

4.2 Objectives

- Carry out gasification experiments with charcoal in a continuous fixed bed reactor;
- Perform biomass gasification in a throated downdraft gasifier for three different types of biomass;
- Modify a commercially available throated biomass gasifier to measure axial and longitudinal temperature in the reduction zone;
- Measure temperature and gas profiles in axial and longitudinal directions in a continuous fixed bed reactor fed with charcoal;
- Measure temperature profiles in axial and longitudinal directions of the reduction zone of throated biomass gasifier;
- Develop a gas sampling line according to the orientation of European tar protocol (Neeft, 2005);

- Develop and validate orifice plates to measure the gasifier inlet airflow and outlet producer gas flows;
- Characterize all the biomasses used in terms of ultimate and proximate analysis
- Design multipoint thermocouples to measure longitudinal temperature of the reduction zone of the throated downdraft gasifier;
- Apply restricted equilibrium (temperature approach) corrections to
 Aspen Plus gasifier models to improve results accuracy.

4.3 Work Plan

4.3.1 Experimental work

Gasification experiments were performed in two different reactors as described.

4.3.1.1 Char gasification in a continuous fixed bed reactor - CFiBR

The following activities were performed:

- Reassembling of the CFiBR and checking for leakages;
- Calibration of thermocouple, pressure sensors, flow meters, feeding system and steam generator and other auxiliary systems;
- Biomass characterization;
- Processing of ashy samples;
- Definition of the experimental procedures and parameters;
- Commissioning experiments;
- Validation experiments;
- Compilation and analysis of the results.

4.3.1.2 Gasification in a 25kW Throated fixed bed biomass gasifier

The following activities were performed:

- Assembling of the gasifier and checking for leakages;
- Design of multipoint thermocouples;
- Adaptation of the lid of the gasifier to allow the insertion of thermocouples;
- Design, fabrication and installation of orifice plates to measure inlet and outlet flow of gasses;
- Design, fabrication and installation of a sampling line according to the European tar protocol (Neeft, 2005);
- Substitution of the metallic hopper by and transparent grass hopper;
- Calibration of thermocouple, pressure sensors, flow meters, feeding system and other auxiliary systems;
- Programing of the gasifier control unit GCU
- Biomass characterization;
- Definition of the experimental procedures and parameters;
- Commissioning experiments;
- Valid experiments;
- Compilation and analysis of the results.

4.3.2 Modelling work

The modelling work utilised the Aspen Plus simulator. The following activities were performed:

- Development of a non-stoichiometric equilibrium method (minimization of the Gibbs free energy),
- Development of a non-stoichiometric restricted equilibrium method with whole-system temperature approach;
- Development of a non-stoichiometric restricted equilibrium method with reaction-specific temperature approach.

CHAPTER 5

CHAR GASIFICATION IN A CONTINUOUS FIXED BED REACTOR - CFIBR

The Continuous Fixed Bed Reactor (CFiBR) consists of a reactor designed to simulate either the charcoal gasification stage of a two-stage gasifier (Henriksen et al., 2006) or the gasification zone of a traditional downdraft throated gasifier. The CFiBR used in this work is located at the facilities of CIRAD Persyst in Montpellier, France.

Three experiments were performed. Experiments A and B were performed with the same inlet atmosphere and Experiment C was performed with a different atmosphere.

5.1 Experimental Apparatus (Continuous Fixed Bed Reactor – CFiBR)

The CFiBR, shown in Figure 5.1, was designed and manufactured by CIRAD. It consists essentially of a refractory stainless steel tube of 20 cm diameter and 160 cm length, surrounded by refractory insulation. At the top of the reactor, there is a conveyor belt (a) that enables the feeding of charcoal to the top of the reactor. A system of two pneumatic valves (b) ensures that no air can enter the reactor when the char is introduced.

The atmosphere of the reactor; i.e. the inlet gas composition and its associated temperature, is intended to correspond to the output from the oxidation zone of a fixed bed downdraft gasifier, assumed here to be a mixture of the products of oxidation of a hydrocarbon mixture with additional water vapour. It is generated by

the exhausts of two propane burners with controllable air-fuel ratio (c), together with the addition of water vapour via a high-pressure steam generator (d) - see section 5.1.1.

Inside the reactor, the char settles as a bed, which can reach up to 80 cm in height. At the bottom of the reactor there is a grate with orifices of 1 cm diameter and a scraper (e), which is activated manually and enables ash removal from the reactor. To be able to extract particles greater than 1 cm – especially near the beginning of the experiment when the char has not fully reacted – the grate can be moved vertically downwards to a position below the reactor section where the particles can escape via the periphery.

The major part of the produced gas is extracted from the bottom of the reactor and is taken to a post combustion chamber, after passing through a cyclone (g) which separates fine particles.

The entire system is automatically controlled from a console.

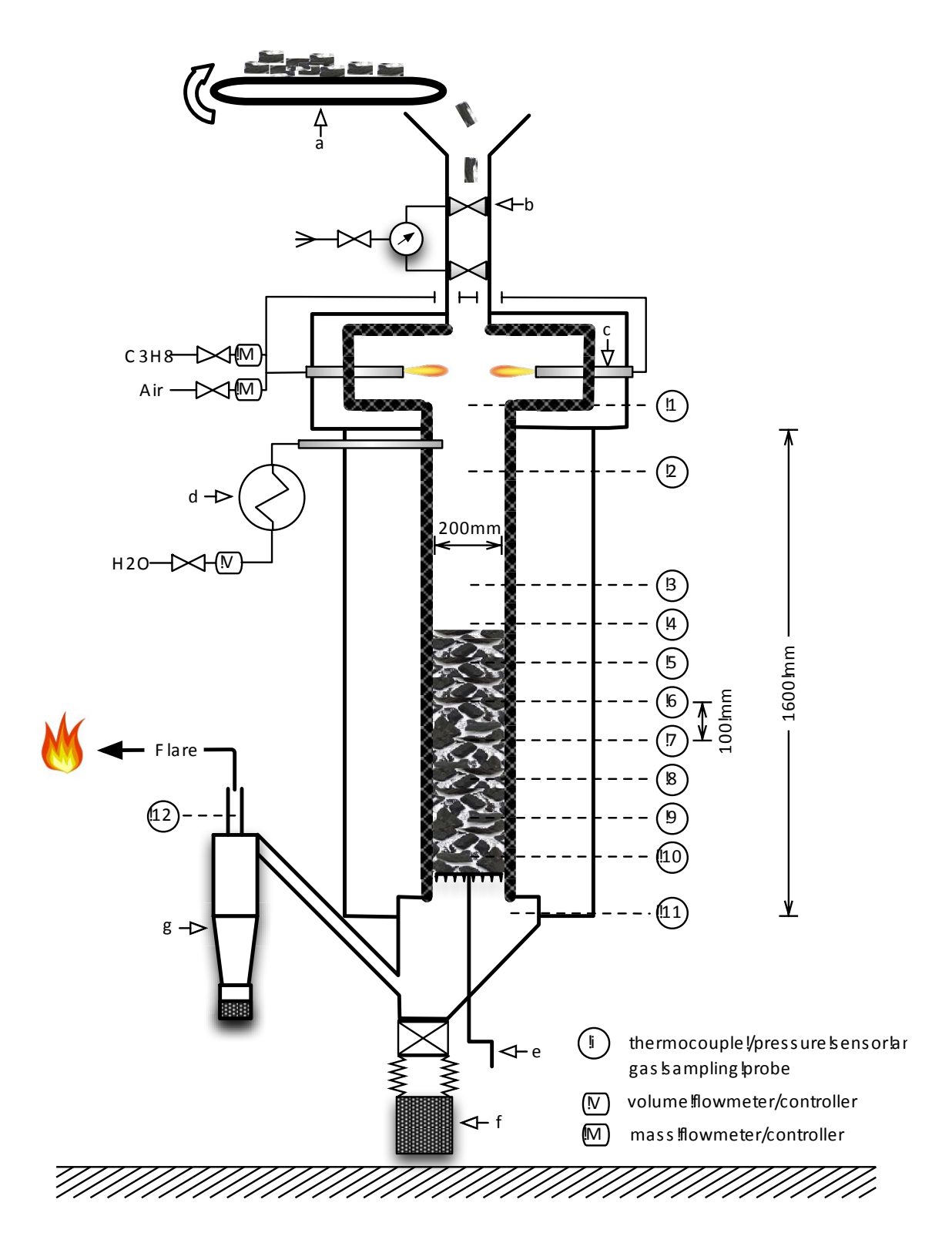


Figure 5.1: Continuous Fixed Bed Reactor - CFiBR

5.1.1 Reactive atmosphere

The reactive atmosphere consists of a gas mixture comprised of products from the combustion of propane in a combustion chamber (O_2 , CO_2 , H_2O , N_2), as well as additional water vapour provided by a steam generator.

The control of combustion parameters (% excess air, gas temperature, air flow and propane flow), in addition to the flow of water vapour, can precisely define the environment of the gasification process. This allows different gasification conditions to be tested and analysed. The reactive atmosphere used for this work is shown in the section 5.4.2 .

5.1.1.1 Combustion chamber

The combustion chamber consists of two 15 kW burners that provide the energy required to heat the reactor, as well as the gasification medium itself.

Each of the two burners is arranged tangentially to the wall of the chamber and is protected by refractory concrete as shown in Figure 5.2. This design creates a vortex regime in order to ensure a good homogeneity of the gas mixture before it enters the reactor.

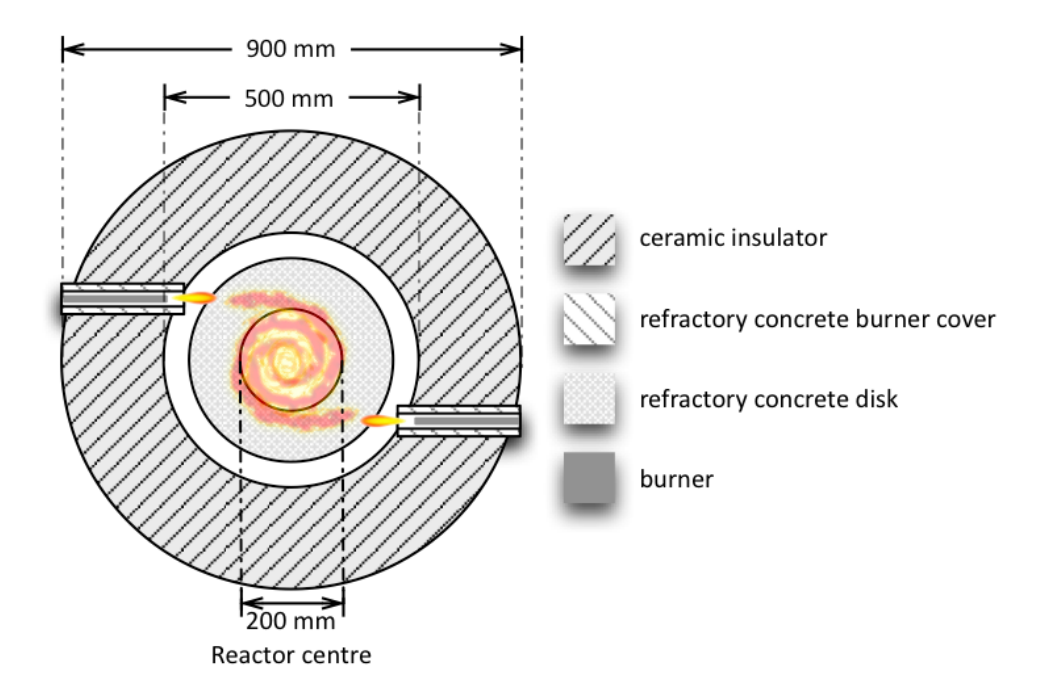


Figure 5.2: Position of the burners in the combustion chamber

The chamber itself is constructed from rigid plates of ceramic wool that provide support and thermal insulation. A concrete refractory covers the burners to protect against the high local temperatures. A refractory concrete disc, 10 cm thick and 20 cm high, is placed directly above the reactor.

The gas supply to the burners (propane and air) is accurately controlled by two mass flow meters calibrated respectively for propane and air (M). The power output of the burners is regulated by the flow of propane. The airflow determines the equivalence ratio of the mixture, which is adjusted to operate with an excess of air. This excess air provides oxygen to the reactive gas, allowing the heterogeneous oxidation of a small fraction of the charcoal in the bed, as would be expected in a full fixed bed gasification process where the oxidation of carbon is one of the main reactions.

5.1.1.2 Steam generator

The steam generator is designed to provide up to 6 kg/h of steam at a temperature of up to 1050 °C. It consists of a furnace and a heat exchanger equipped with a control system.

The furnace is electrically heated and has an installed capacity of 10 kW. Its external dimensions are 700 mm x 880 mm x 1600 mm and its mass is around 350 kg.

The evaporator is a tube exchanger that consists of an "Inconel 600" coiled tube 10 meters in length, 20 mm outside diameter and 16 mm internal diameter, located in the furnace.

The water used comes from the main utility network. It is first purified using a water ion exchange demineralizer. All dissolved salts; silicic acids and carbon content in the domestic water are thereby removed before it enters the preheater. This prevents corrosion risks of the evaporating tube/warm and secures a pure water vapour without the presence of other elements that might disrupt or influence the gasification process.

An automatic valve and a volumetric flow meter with a digital display regulate the steam flow. These are located after the demineralizer and control the flow of liquid water from 0 to 6 kg/h (~100 cm3/min at 20 °C and 1 atm). Volumetric flow rate is automatically calculated to take account of ambient conditions of temperature and pressure. Regulation can either be performed manually or via the system software.

5.1.2 Continuous fixed bed operation

The CFiBR reactor is designed on the principle of continuous fixed bed operation, where the height of the bed is maintained constant during the gasification process. To do this, the ash removal must be continuous or semi-continuous.

5.1.2.1 Charcoal feeding systems

The feeding device consists of a conveyor belt and a hopper equipped with two pneumatic valves installed as shown in Figure 5.1. The conveyor has a total length of 200 cm, a height of 11 cm and a width of 12 cm (Figure 5.3).

The charcoal flow rate can be varied between 0 and 3 kg/h. A known mass of charcoal is distributed on the belt, and knowledge of the belt speed enables a precise control of the charcoal flow rate.

According to the literature, most gasification plants operate at a mass flow-rate per reactor cross sectional area of between 25 and 75 kg m²/h (Knoef, 2005; Mermoud et al., 2006; Van de Steene et al., 2010). The mass flow-rate per reactor cross sectional area was specified to be a value within this range for the present experiments; (see Section 5.4.1).

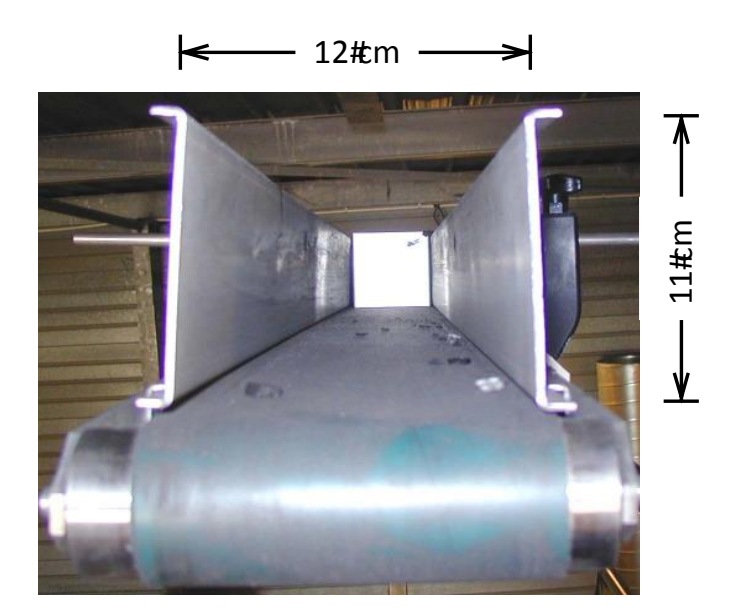


Figure 5.3: Front view of the conveyor belt

The pneumatic valves operate in periodic cycles lasting 1 minute, allowing a semi-continuous feeding of the reactor every minute. The valves open and close in an alternating sequence as follows: i) the superior valve opens, ii) charcoal falls into the hopper trap, iii) the exterior valve closes and the internal valve opens, allowing the charcoal to fall into the reactor. This sequence is used in order to seal the reactor during the feeding process, thereby not permitting any extra oxygen to enter the reactor.

In order to protect the valves against damage by conduction of heat from the combustion chamber, they are cooled by a water heat exchanger. This exchanger is a double jacket containing helical paddles and supplied with cold-water.

5.1.3 Ash and residues removal system

The bed height is kept constant during gasification by controlling the rate of residue extraction. The residence time of particles in the reactor is estimated to be several hours while gases have a residence time of less than one second. The method used for estimating the residence time of solids in the reactor is discussed in s 5.3.4.3.

The ash removal device located in the lower part of the reactor consists of a grate (a perforated plate with holes of 1 cm diameter) attached to a scraper. This grate can move vertically within a range of 10 cm. In its normal operating position, the grate is located at a height of 5 cm above the base of the reactor section and only particles of less than 1 cm in size can cross. However, in the open position (5cm below the base of the reactor) the grate allows the removal of particles larger than 1 cm. Figure 5.4 shows the grate position when open or closed.

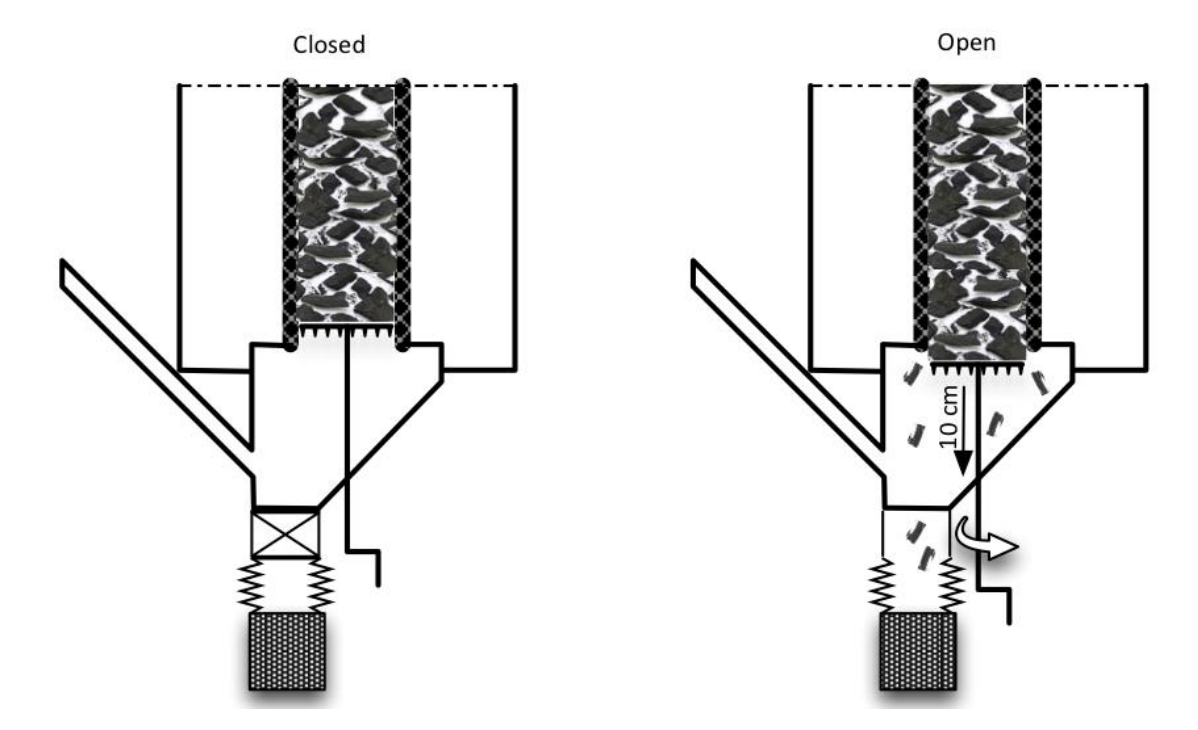


Figure 5.4: Ash removal system

5.2 Production and characterization of the biomass used

The char used was produced from wood chips in a screw pyrolysis reactor located at the CIRAD facilities, and the wood chips used were from maritime pine. The pyrolysis conditions used for charcoal preparation was: temperature 750 ° C, 1 hour residence time and 15 kg/h feed rate. These conditions were selected to represent the environment that the wood chips would experience in a full fixed bed downdraft gasification process as they pass through the drying, devolatilization and oxidation zones. Charcoal that is not prepared under these conditions will have different physical and chemical structures.

About 200 kg of charcoal was produced for use in the experiments.



Figure 5.5: (A) raw wood chips, (B) charcoal after wood chip pyrolysis

5.2.1 Granulometric analysis and particles size distribution

Granulometric distribution play an important role in process engineering (Allaire & Parent, 2003; Hairui et al., 2004). There are many existing methods for characterizing particle size distribution. The method selected in this work was the Rosin-Rammler method (Allaire & Parent, 2003). This method allows a distribution of particles in different size categories to determine the average particle size and the coefficient of dispersion around this average. Sieving separates the particles.

5.2.1.1 Sampling Methodology

In all industrial processes operating with powders or bulk solids, sampling is fundamental to any characterization.

The sampling method used is known as "cone and quartering" and is well documented (Allen, 1996). This method consists of forming a conical pile of all the material, which has previously been well mixed and homogenized. The pile is then divided into four equal parts and two halves are formed from two diametrically opposite quarters of piles. Next, two conical piles separated and mixed to form another conical pile. The subdivision of each of these two lots is continued on the same principle until the amount of the desired sample is reached as shown in Figure 5.6.

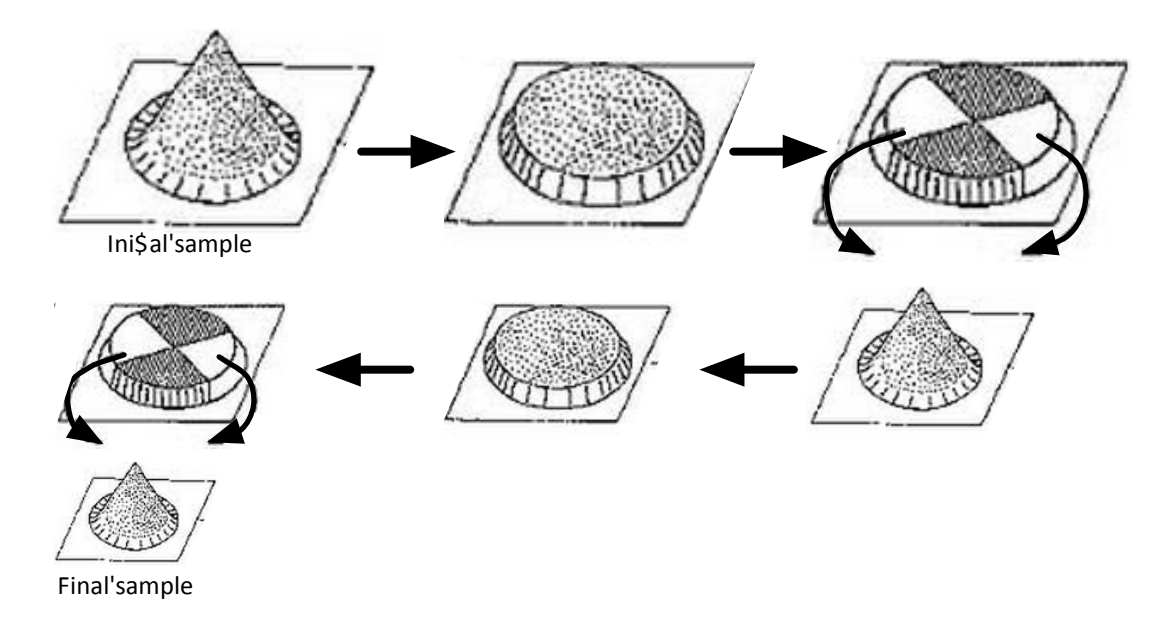


Figure 5.6: Illustration of the cone and quartering sampling method

5.2.1.2 Particle size distribution

Three bags of charcoal (about 15 kg) were randomly selected for characterization. Length distribution was achieved by sieving the charcoal samples, while thicknesses were based on the average of 500 particles that were measured using an electronic calliper. The particle size distributions (length and thickness) are displayed in Figure 5.7 and Figure 5.8. The results showed that about 60% of the particles are <5 mm long; while nearly 75% are < 2 mm wide.

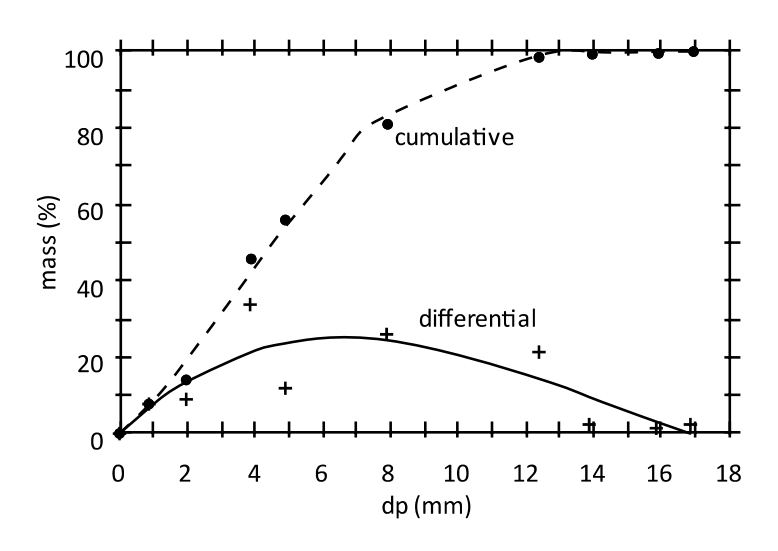


Figure 5.7: Particle size distribution of char - lenght

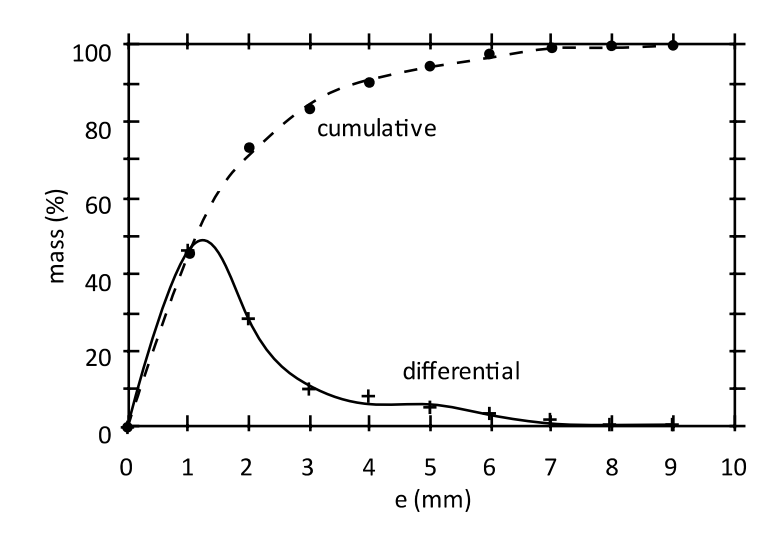


Figure 5.8: Particle size distribution of char - thickness

The Rosin-Rammler model was used to determine the coefficients of dispersion (m) and the average dimensions (d_m and e_m) for length and thickness respectively. The distribution of particle length is more diffuse than the thickness, as the coefficients of dispersion are $m_l = 1.7366$ and $m_t = 1.1723$. Moreover, the average particle length and thickness are $d_m = 5.6$ mm and $e_m = 1.66$ mm.

5.2.2 Physicochemical characterization

5.2.2.1 Proximate and ultimate analysis

Proximate and ultimate analyses were performed using the standards NF EN 1860-2 and XP CEN/TS 15104. Results for both biomass and char are presented in Table 5.1. Calorific values were measured using a calorimetric bomb.

Table 5.1: Proximate and ultimate analysis of maritime pine char and woodchips

	Woodchips	Charcoal		
Proximate (wt. % db)				
Volatile matter	82.6	4.9		
Fixed carbon	17.2	93.7		
Ash	0.20	1.4		
Ultimate				
С	45.0	89.8		
Н	5.70	2.2		
0	42.8	6.1		
N	<0.3	<0.2		
S	<0.1	<0.002		
Ratios				
H/C	0.13	0.025		
O/C	0.95	0.068		
Calorific value (MJ/kg)				
HHV		32.42		
LHV		31.71		

5.2.2.2 Analysis of minerals

The composition of inorganic matter in the charcoal is shown in Table 5.2. The results were obtained using ICP-MS (Inductively Coupled Plasma Mass Spectrometry) (Tagutchou, 2008). There is a strong dominance of calcium, potassium and principally manganese.

Table 5.2: Composition of mineral materials in the charcoal samples

Mineral elements	(wt % in char sample)	(wt % in the ash)
Manganese (Mn)	0.434	30.46
Calcium (Ca)	0.351	24.61
Potassium (K)	0.218	15.30
Iron (Fe)	0.213	14.96
Magnesium (Mg)	0.080	5.64
Aluminium (Al)	0.072	5.06
Phosphor (P)	0.030	2.13
Silicic (Si)	0.015	1.08
Sodium (Na)	0.007	0.47
Nickel (Ni)	0.002	0.16
Zinc (Zn)	0.001	0.09
Cupper (Cu)	0.001	0.04
TOTAL	1.425 ± 0.003	100 ± 0.03

5.2.3 Morphological and structural characterization of the char particles

The charcoal samples were analysed at EMI (European Institute of Membranes) in Montpellier and at the RAPSODEE Centre of the Ecole des Mines d'Albi-Carmaux. The morphological and structural characterization obtained is presented in the table below.

Table 5.3: morphological properties of charcoal samples

Properties	Values
Porosity	0.75
Density of the solid phase (kg/m³)	1600
Particle density (kg/m³)	402.5
Bulk density (kg/m³)	180
BET surface (m ² /g)	182
Surface of micropores (m ² /g)	45.8
Average pore diameter (µm)	4.13
Specific surface (m ² /m ³)	25.5 x 10 ⁶
Micropore volume (cm³/g)	0.021
Average hydraulic diameter of the micropores (Å =10 ⁻¹⁰ m)	4.58

The porosity (ε) is calculated from the bulk density ($\rho_{particle}$) of the reference particle and its solid phase density (ρ_{solid}) according to the Eq. 5.1.

$$\varepsilon = \frac{\rho_{particle}}{\rho_{solid}}$$
 5.1

The dimensions of the reference particle (not to be confused with the average particle size) are defined by assuming that the particle shape is parallelepiped (5.5 mm X 5.5 mm X 10.5 mm). Its volume (3.18 x 10-7 m 3) and mass (128 mg) are used to calculate the particle density (402.5 kg/m 3). The solid density (1600 kg/m 3) of the char was measured using a pycnometer.

5.3 Instrumentation, measurements and calculations

The control of the gasification process is based on a precise metrology. Experimental measurements allow the control of the process input parameters such as: feed flow rates, concentration of reactants, power output of the burners, bed height, etc. Temperature and pressure are recorded and backed up every 10 seconds using a data acquisition module for processing and displaying the collected data continuously.

In order to comprehend the phenomena occurring during gasification of the charcoal bed, the reactor is equipped with numerous sensors and sampling points. All the measured sensor values can be observed and recorded instantaneously and enable the supervision of the experiment. Once all data is properly recorded and samples are analysed, calculations of mass and energy balances, in addition to conversion and residence time, can be performed.

5.3.1 Temperature

The temperature measurement system consists of 12 units of 1 mm k-type thermocouples installed as shown in Figure 5.1. These can be divided into two categories, fixed and movable, as follows.

5.3.1.1 Fixed

These thermocouples do not enter in contact to the charcoal bed and measure only gas temperature.

- Combustion chamber (T1);
- Outlet of the steam generator (T2);
- 10 cm above the charcoal bed (T3);

- Below the ash removal (T11);
- Outlet of the cyclone (T12).

5.3.1.2 Movable

These thermocouples (T4 to T10) are inserted within 4 mm o.d. refractory steel tubes which are positioned every 10cm along the reactor from the base of the reactor to a height of 80 cm. They can slide in the radial direction in order to obtain longitudinal and radial profiles of temperatures in the bed. They are placed in a helical pattern in order to limit the perturbation on the charcoal bed while particles are circulating.

5.3.2 Pressure

Two pressure sensors (0-500 mbar) are placed before and after the char bed, in order to measure pressure drop across the bed. The pressure can also be measured everywhere in the bed via the thermocouple probes. The obtained pressure profile can show the point of ash collapse.

5.3.3 Gas composition

The gases are sampled through the thermocouple probes, providing direct correspondence between temperature and gas concentration. The gases are then cooled in order to remove the condensables, and analysed using a micro-GC (Varian Chrompack CP-2003), which is connected directly to the sampling line. The sampled gas can be analysed every thirty minutes during the experiment, to give the

concentrations of CO, CO₂, N₂, H₂, CH₄, C₂H₄ and C₂H₆. Water content is analysed off line using the Karl Fisher method¹³ (ASTM Standard E203, 2008).

Initially, the thermocouples are placed in the centre of the reactor, but they can be shifted horizontally to provide radial profiles of concentrations and temperature.

5.3.3.1 Sampling line

The sampling line shown in Figure 5.9 is divided into four modules:

- Module 1: gas sampling probe heated by an electric tape;
- Module 2: ceramic filter to retain particulates;
- Module 3: condenser;
- Module 4: flow control/measurement unit.

The gas sampling process follows the European Tar Protocol as described by Good (2005).

-

¹³ It is a classic titration method that uses coulometric or volumetric titration to determine trace amounts of water in a sample.

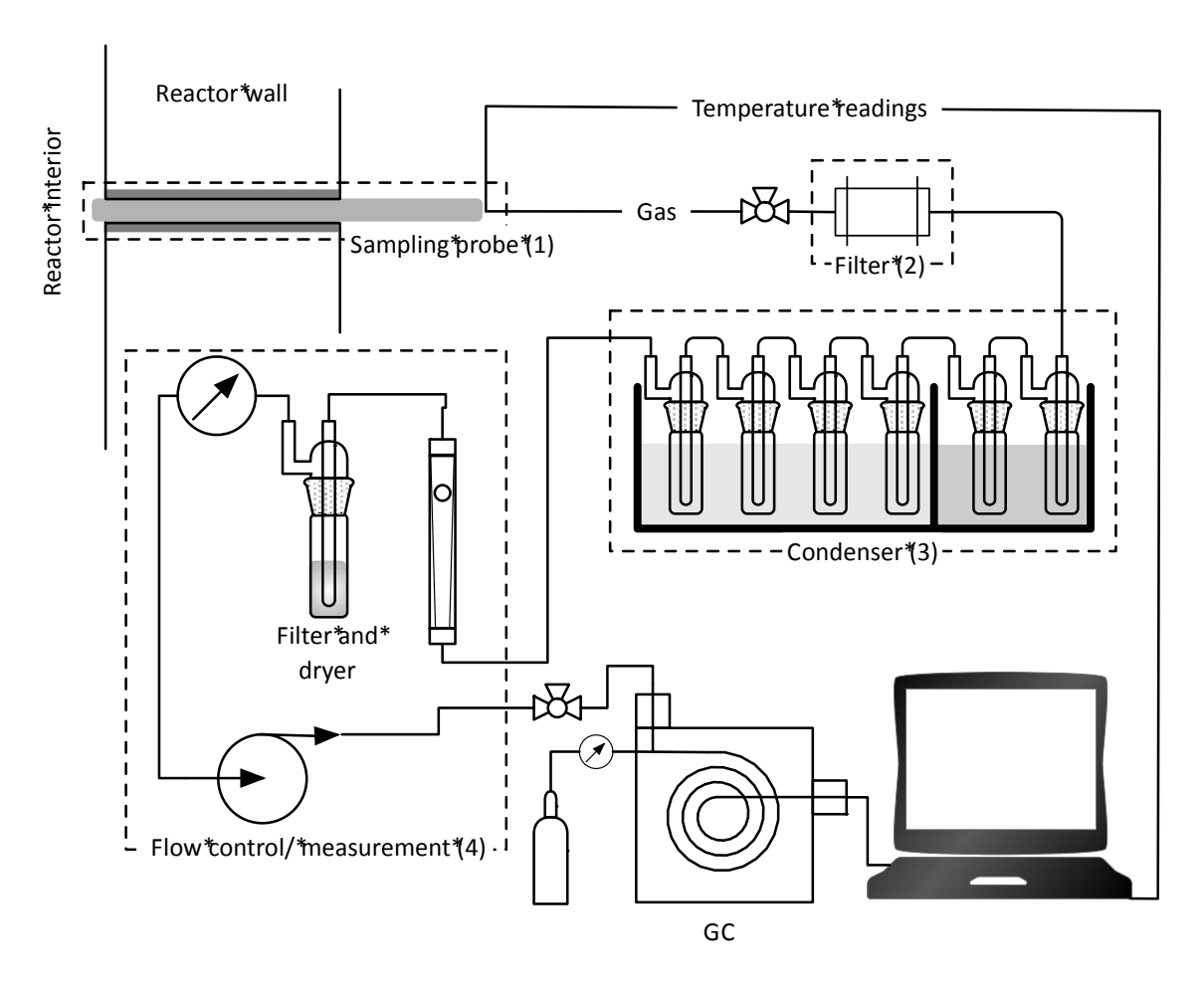


Figure 5.9: Diagram of the producer gas sampling line

Module 1 ensures that the sample is kept at temperatures similar to the sampling point. This reduces temperature drops avoiding condensation and disturbance of the flow regime.

Module 2 traps solids particles, allowing only gases to enter the condenser.

Module 3 separates condensable gases (tar + H_2O) and non-condensable gases (CO, H_2 , CO₂, CH₄ and light C_xH_y). Condensable gases are trapped in the impinger bottles as the non-condensable gases move to the next module. Tar amount is calculated from a mass balance..

Module 4 measures and controls the volumetric flow withdrawn. An accurate control of the sampling flow is required, as excessive volumetric flow will disturb the isokinetic sampling regime. A sampling pump allows relatively low flow rates

(≈10l/min); the gases are then directed to a gas chromatograph for concentration analysis.

5.3.3.2 Analysis of non-condensable gases

The non-condensable gases are analysed using a micro-gas chromatograph (micro-GC). This device samples the gas every 180 seconds and injects them into two columns (column A and column B). Both columns are molecular sieves, which operate by separating the molecular gas species according to their retention time. Each column is connected to a TCD (Thermal conduction Detector). The TCD detects a difference of thermal conductivity during the passage of gas, which from cross referencing with the data of the calibration gases used returns the gas concentration. Each column has specific characteristics for analysing well-defined species; a detailed characteristic of these columns is presented in Table 5.4.

Table 5.4: Micro-GC columns operational parameters

Column	Carrier Gas	Temperature (°C)	Pressure (kPa)	Species
Α	Argon	120	100	N ₂ , O ₂ , H ₂ , CO, CH ₄
В	Helium	45	75	CO_2 , CH_4 , C_2H_4 , C_2H_6

The micro-GC is calibrated using standard gases that are specified according to the species and their concentrations expected in the producer gases. A calibration is performed regularly every two experiments, and always before the first analysis of the day.

The samples analysed in the micro-GC give the final molar fraction of each gaseous species relative to the total amount of non-condensable gases. For the final composition of the producer gas, it is necessary to take into account the fraction of

condensates (water vapour and traces of tar) trapped in Module 3 (condenser) of the sampling line.

5.3.3.3 Analysis of condensates

A rotary evaporator is used to recover the condensates dissolved in isopropanol, and the difference between the mass of the mixture and the mass of isopropanol gives the mass of the hydrocarbon condensate. The separated part of the mixture contains isopropanol and water; this mixture is then analysed in a Karl Fischer titrator. This method is based on the reaction between Bunsen iodine and sulphur dioxide in an aqueous medium as described by Eq. 5.2.

$$I_2 + SO_2 + H_2O \rightarrow H_2SO_4 + 2HI$$
 5.2

Karl Fisher titration determines the mass content of the water in the mixture (water and isopropanol) recovered from the rotary evaporator. Adding this amount of water to the total amount of condensable gases and dividing by the sampling time gives the average flow of condensates.

5.3.3.4 Producer gas flow rate

Each gas flow-rate is calculated separately and nitrogen is used as a tracer as shown in Eq. 5.3.

$$\dot{m}_{pg} = \frac{[N_2]^{ag}}{[N_2]^{pg}} \dot{m}_{ag}$$
 5.3

 $[N_2]^{ag}$, $[N_2]^{pg}$ and \dot{m}_{ag} are respectively nitrogen concentration in the attack gases (inlet) and producer gases (outlet), and mass flow-rate of attack gases.

The mass flow-rate of gas components is calculated using the component mass fraction [j] from Eq. 5.4.

$$\dot{m}_l = [j]^{pg} \dot{m}_{pg} \tag{5.4}$$

5.3.4 Solid residues measurements and characterization

During the gasification process, samples of solid residues are collected every 10 minutes from the bottom of the reactor using a device consisting of a waterproof flexible aluminium connection and a steel vessel as shown in Figure 5.10. This device prevents the further conversion of residues during the cooling process. The conversion rate is determined directly by weighing the masses of the samples or indirectly by analysis of their ash. The conversion rate will be discussed in more detail in Section 5.3.4.1.

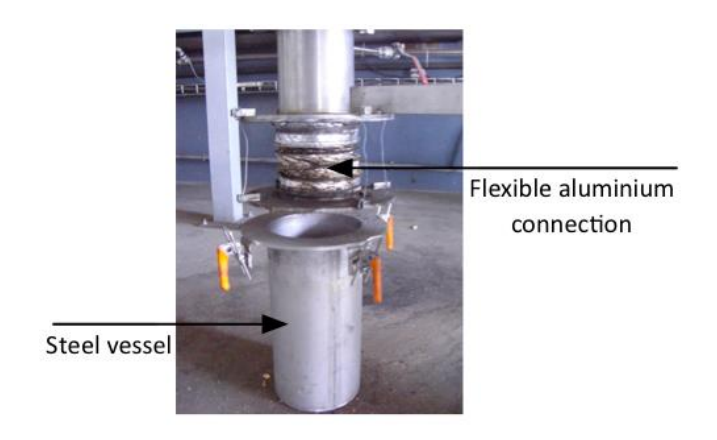


Figure 5.10: Solid residues collection device

5.3.4.1 Measurement of conversion rate

The calculation of the char conversion rate (χ) is done by two parallel methods, direct and indirect, as described below.

A) Direct method

The conversion is given by the ratio between the inlet flow of char and the solid products removed (ash and char residues collected every 10 minutes). Fine

particulates trapped in the cyclone are not taken into consideration due to their minimal influence on the mass balance. The direct method is so called because it can be performed while the experiments are running and the conversion rate can be calculated every time residues are removed, by means of Eq. 5.5.

$$\chi_d = \frac{\dot{m}_C - \dot{m}_{RC}}{\dot{m}_C} \tag{5.5}$$

where $\dot{m}_{\it C}$ and $\dot{m}_{\it RC}$ represent respectively the feed rate of char and solid residues removal rate.

B) Indirect method

The indirect method is based on the mass conservation of mineral materials (ash) throughout the reactor. It is assumed that ash does not react; therefore its mass is kept constant and can be used as a tracer. The Eq. 5.6 describes ash mass conservation.

$$\dot{m}_{ash} = a_C \dot{m}_C = a_{RC} \, \dot{m}_{RC} \tag{5.6}$$

where $a_{\it C}$ and $a_{\it RC}$ represent respectively the ash content (%) in the char and in the solid residues removed.

Then, knowing the rate of ash in the char and in the solid residues, Eq.5.7 can be used to calculate the conversion rate.

$$\chi_i = 1 - \frac{a_C}{a_{RC}}$$
 5.7

The indirect method is so called because it cannot be performed while the experiment is running, as it requires proximate analysis to measure the ash content of the solid residues.

5.3.4.2 Bulk density across the bed

Once the experiment is finished, the supply of reactive gas and charcoal is stopped and nitrogen is injected at the reactor to cool down the bed. The nitrogen flow is maintained until it reaches room temperature, thereby avoiding gasification reactions and keeping the bed structure.

When the reactor reaches room temperature, the load (charcoal bed) is removed from the reactor. The charcoal removed allows the calculation of the bulk density across the bed, as well as conversion ratio using the indirect method.

5.3.4.3 Residence time of char in the reactor

The calculation of residence time is based on charcoal particles moving downwards until they exit the reactor. Knowing the charcoal feed and the ash removal rates, one can calculate the velocity that the bed travels downwards as gasification occurs and the charcoal is consumed (Barrio et al., 2001) with the use of Eq. 5.8. The bulk density of the charcoal chips, as well as the height of the bed, are assumed to remain constant.

$$v_{\text{bed}} = \frac{\dot{m}_C - \dot{m}_{RC}}{\rho_{bulk} S_{reactor}}$$
 5.8

where $\,\,\rho_{bulk}$ is the bulk density of the charcoal bed and $S_{reactor}$ represents the cross sectional area of the reactor.

Assuming the height of the bed to be constant it is possible to calculate the residence time according to Eq. 5.9.

$$t = \frac{v_{bed}}{H_{hed}}$$
 5.9

where H_{bed} is the height of the charcoal bed.

The calculation of velocity is an approximation, as the bulk density change due to chemical reaction is not taken into account. The solid residues removal also interferes with the accuracy of the results since it promotes variation in the bed height.

5.3.5 Mass and energy balances

The energy balance is calculated according to the principle of conservation of energy (1st Law of thermodynamics) as expressed in Eq. 5.10.

$$0 = \dot{Q}_{lost} + \dot{W}_{cv} + \sum_{in} \dot{m}_{in} \left(h_{in} + \frac{u_{in}^2}{2} + gz_{in} \right) - \sum_{out} \dot{m}_{out} \left(h_{out} + \frac{u_{out}^2}{2} + gz_{out} \right)$$
5.10

where Q_{lost} represents the heat lost by the system, W_{cv} is the variation of the mechanical work and m, h, $u^2/2$ and gz are respectively the mass flow, enthalpy, kinetic and potential energy in and out of the control volume (cv).

As there is no mechanical work being produced by the system and kinetic and potential energy are negligible, Eq. 5.10 can be reduced to

$$0 = \dot{Q}_{lost} + \sum_{in} \dot{m}_{in} \, h_{in} \, - \sum_{out} \dot{m}_{out} \, h_{out}$$
 5.11

The mass balance is given by the difference between inlet reagents and outlet products (producer gas and residues). It can be mathematically expressed by Eq. 5.12.

$$0 = \sum_{in} \dot{m}_{in} - \sum_{out} \dot{m}_{out}$$
 5.12

The inlet reagents are charcoal and the reactive atmosphere gases are composed of O_2 , N_2 , CO_2 , H_2O . The outlet products are the producer gas (H_2 , CO, CH_4 , H_2O , CO_2 and N_2) in addition to solid residues removed from the bottom.

Therefore,

$$\sum_{in} h_{in} \dot{m}_{in} = \dot{m}_C h_C + \sum_{j} \dot{m}_i h_i$$
 5.13

and,

$$\sum_{out} h_{out} \dot{m}_{out} = \dot{m}_{RC} h_{RC} + \sum_{j} \dot{m}_{j} h_{j}$$
5.14

where h and m are respectively the specific enthalpy and mass flow of each gaseous compound going in (i) or out (j) of the reactor. The specific enthalpy can be calculated as:

$$h_{i,j}(T) = h_{i,j}^{0}(T) + \int_{T_0}^{T} C_{p(i,j)}(T) dT$$
5.15

where $h^0_{i,j}$ is the standard enthalpy of formation of the component i,j, $\mathsf{Cp}_{(\mathsf{j})}$ is the specific heat and T is the medium temperature.

Combining Eq. 5.11 and Eq. 5.14, the final equation for calculating the energy balance is:

$$\dot{m}_C h_C + \sum_i \dot{m}_i h_i - \dot{m}_{RC} h_{RC} - \sum_j \dot{m}_j h_j - \dot{Q}_{lost} = 0$$
 5.16

The heat loss is calculated according to Eq. 5.17

$$\dot{Q}_{lost} = h_c A dT 5.17$$

where h_c is the convective heat transfer coefficient of the process, A is heat transfer area of the surface and dT is the temperature difference between the surface and the ambient.

5.4 Operational parameters

Three experiments were performed. Experiments A and B were performed with the same conditions. They were intended to provide two set of gas measurements, one in the wall and another in the centre of the reactor, thus they would allow the study of the gas variation in the radial direction. Experiment C was performed with a different atmosphere.

Airflow was constant for all experiments while propane and water vapour flow were changed.

The bed height was fixed at 65 cm for all experiments in accordance with industrial practice for traditional downdraft and two-stage gasifiers where the height of the char bed stays within 50 - 100 cm (Van de Steene et al., 2010).

The two different operational conditions were chosen to be within the operational parameter range of industrial gasifiers. The two sets of data generated in these experiments are intended to be an input source for development and validation of numerical simulation.

5.4.1 Char flow

The raw char feeding rate was set to be 1.680 kg/h (28g/min), which is equivalent to a mass flow-rate per reactor cross sectional area of 53.47 kg m 2 /h. This value is within the operational range of two-stage gasifiers, which operate between 25 – 75 kg m 2 /h (Knoef, 2005).

In the literature, stoichiometric ratios are most often presented in relation to raw biomass (Franco et al., 2003; Mahishi & Goswami, 2007). However they can also be presented in relation to fixed carbon content in the char (Kumabe et al., 2007) and

this practice has been adopted here. After subtracting moisture, ash and residual volatiles, the char feeding rate used for stoichiometric purposes is 25g/min.

5.4.2 Reactive atmosphere

The inlet temperature, velocity, and composition of the attack gases are imposed by a precise control of the mixture of air, propane and water vapour injected into the combustion chamber.

Air mass flow was kept constant in all experiments, while propane and water vapour were balanced in order to provide an approximately constant superficial velocity.

Analysis of the attack gases was routinely performed before each experiment to validate the results of calculations. This allowed the determination of the combustion conditions and validation of the bed input parameters.

Table 5.5: Operating conditions of the CFiBR gasification experiments

	Experiment A and B					Experiment C			
Reactants (inlet conditions)	•				•				
Char feeding rate (m _c)	2.1	(mol/min)	25	(g/min)	2.1	(mol/min)	25	(g/min)	
Q _{air} ¹⁴	8.031	(mol/min)	235.50	(g/min)	8.103	(mol/min)	237.61	(g/min)	
Q _{N2}	6.494	(mol/min)	181.93	(g/min)	6.553	(mol/min)	183.57	(g/min)	
Q_{02}^{15}	1.674	(mol/min)	53.57	(g/min)	1.689	(mol/min)	54.05	(g/min)	
Q _{C3H8}	0.286	(mol/min)	12.59	(g/min)	0.303	(mol/min)	13.35	(g/min)	
Q _{H2O} (added water vapour)	0.67	(mol/min)	12.20	(g/min)	1.02	(mol/min)	18.41	(g/min)	
2,120 (0.000 1.000 1.000 1.000 1.000		(,		(8)		(,		(6)	
Products (attack gases)									
Q ₀₂	235.50	(mol/min)	7.883	(g/min)	0.18	(mol/min)	5.61	(g/min)	
Q _{CO2}	181.93	(mol/min)	37.699	(g/min)	0.91	(mol/min)	39.98	(g/min)	
Q _{H2O}	53.57	(mol/min)	33.238	(g/min)	2.30	(mol/min)	40.73	(g/min)	
Q _{N2}	12.59	(mol/min)	181.928	(g/min)	6.55	(mol/min)	183.57		
Total Flux of attack gases	235.50	(mol/min)	260.748	(g/min)	9.94	(mol/min)	269.89	(g/min)	
Properties (attack gases)									
Superficial Velocity	0.55	(m/s)			0.57	(m/s)			
Products Temperature	1060	°C			1080	°C			
Total Pressure	1.01	atm			1.01	atm			

¹⁴ Q stands for gas flow.
¹⁵ Oxygen is provided in excess of 2.70% in Experiment A/B and 1.78% in Experiment C

5.5 Experimental Procedures and Parameters

5.5.1 Preliminary verification tests

Before any of the experiments, a series of verification tests need to be done to ensure that the apparatus does not suffer from any flaws that may compromise the experiment. These verifications tests take place on the day of the experiment and consist of the following steps:

- Check the availability of nitrogen and propane, as well as ensure the availability of reserve bottles;
- Check the functioning of the line of compressed air; the pressure must be between 2.5 and 3 bar for the first line; and between 5 and 6 bar for the second line;
- Check the operation of the various meters (water vapor, propane, compressed air, nitrogen), different management interfaces (Flow vision, Smart DDE, Smart Control, LB2) and data acquisition interface (Agilent BenchLink Data Logger);
- Check the operation of valves and the conveyor belt;
- Conduct a leak test of the system;
- Test the operation of the burners.
- Install and verify proper operation of the sampling line and the "micro-GC";
- Check the availability of solvent (isopropanol) in sufficient quantity;
- Analyze the fumes from the burnt propane in the empty reactor (without coal bed), to ensure that the results of the "micro-GC" are comparable with those of a theoretical simulation the combustion of propane. The obtained results after several rounds of testing show that data from combustion calculations are comparable within 2% of those measured by the "micro-GC."

5.5.2 Gasification experiments

For the gasification experiments performed, the following steps were followed:

- Load the reactor with charcoal to a height of 75 to 80 cm, as well as the conveyor belt with charcoal enough for 1h of operation;
- Ignite the propane burners: the burner ignition power is 5.5 kW, equivalent to a rate of 3.6 NL/min of propane and 90 NL/min of air;
- Increase the power of the burners gradually until it reaches ≈14 kW, the ratio of propane/air flow must be 9/220 (no excess air);
- Switch on the extractor and light up the flare;
- Start pneumatic valves cooling system;
- Set the steam generator temperature;
- Launch of the data acquisition and temperature monitoring software;
- Reduce propane burners power to ≈11 kW once the temperature in T₂ reaches 1080 °C; the ratio of propane/air flow should be 7/200 (3% O₂)in the combustion gasses);
- Feed the reactor as soon as it is noticed a sudden increase in bed level temperature (T₄), the surface of the bed is at T4 (65 cm);
- Set water vapour flow to the desirable amount;
- Start ash removal from the moment temperature in T₄ begins to decrease, repeat the process every 10 minutes;
- Once the steady state is established (see the Section 5.5.4), start sampling of producer gas;
- Stop the experiment by stopping the supply of reactive gas and charcoal. A nitrogen flow is then injected to stop reactive flow and cool the reactor and the charcoal bed;
- Keep the inert atmosphere until reactor is completely cooled.

5.5.3 Data collection and processing

Temperature and pressure are collected and recorded every 10 seconds as described in Sections 5.3.1 and 5.3.2 Gases are sampled and the condensates are stored to be further analysed after the experiment as described in Section 5.3.3

Once the charcoal bed is sufficiently cooled in an inert atmosphere¹⁶ to avoid further chemical reaction and preserve the physical state of the char bed at the end of the experiment, the following procedure is carried out:

- ullet Empty the reactor by removing the remaining charcoal through the bottom. The charcoal must be removed in increment (h_z) . Mass and bulk density of the charcoal removed can determine the volume occupied by the charcoal; therefore, the corresponding height of this increment;
- Determine the height (h_z) corresponding to each "slice" removed;
- Weigh all samples taken from the reactor;
- Calculate bulk density of the charcoal bed removed, as well as those of ash residues from the day of the experiment;
- Grind and homogenize all samples according to the requirements for proximate and ultimate analysis;
- Determine the different conversion rates of each sample by indirect method;
- Calculate various balance sheets.

5.5.4 Establishment of steady state

5.5.4.1 From start to steady state

Before reaching steady state the CFiBR passes through three distinct phases: heating, bed level stabilisation and thermal stabilisation. The entire process lasts on average 8 h. In the heating phase (the first 2 h) the CFiBR is heated by the hot gases from

¹⁶ This inert atmosphere is composed of ambient temperature nitrogen that is forced downwards the bed.

propane combustion, the bed is loaded with char, but the continuous feeding is off. During the next 3 h (the thermal stabilisation phase), char starts to be fed at a constant flow-rate, while the excess is removed from the bottom. Temperatures during this stage are stabilising, but the bed height still fluctuates excessively. In the bed level stabilisation phase (the next 3 h) a constant char conversion rate is reached and all the temperatures are in quasi-equilibrium. Once the necessary data s collected, charcoal stop being fed and room temperature nitrogen is injected to cool down the bed. A graphical visualisation of the distinct phases is shown in Figure 5.11.

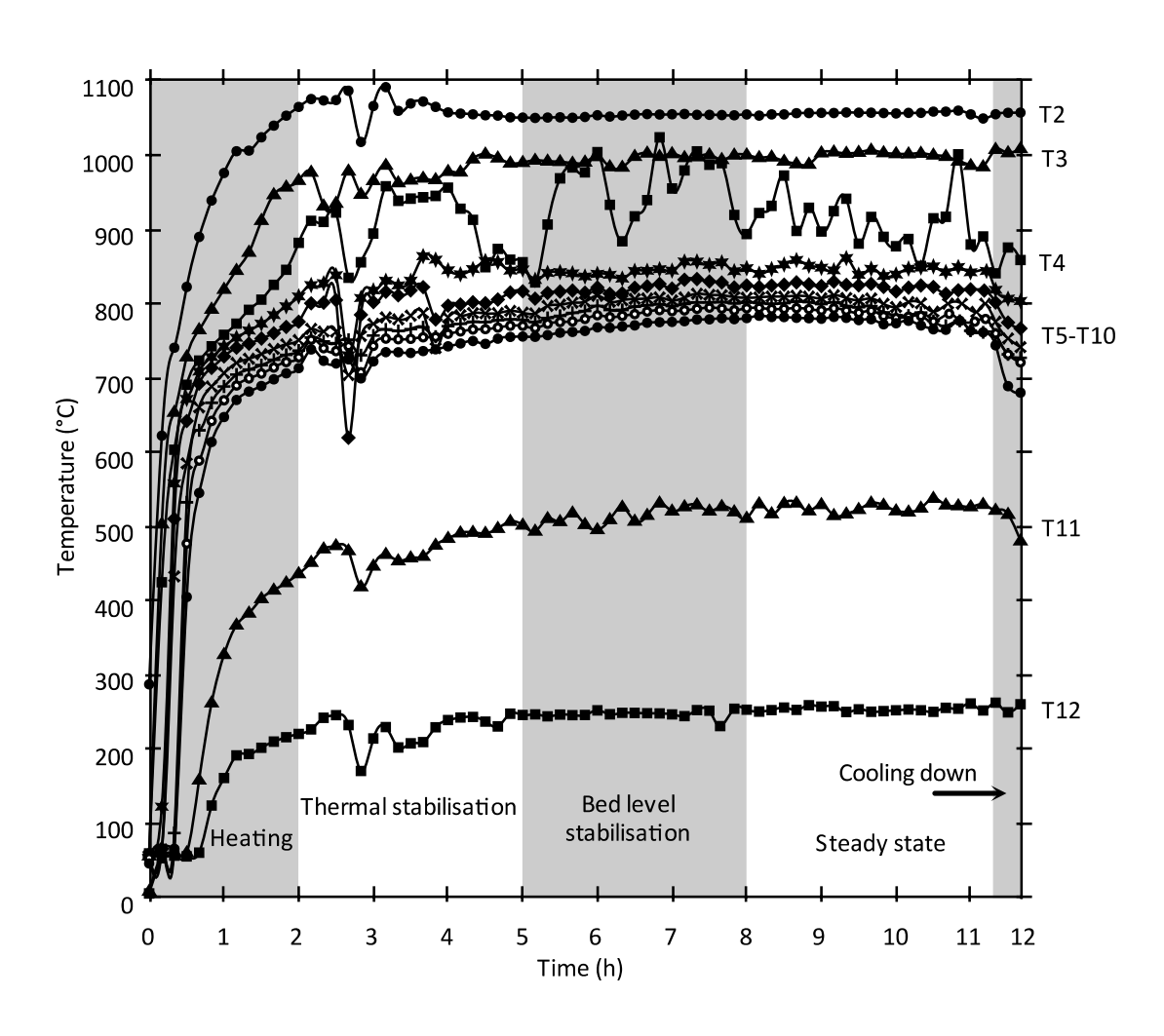


Figure 5.11: The phases to reach steady state.

5.5.4.2 Bed level

During the experiment, the bed level varies for 3 reasons: chemical reactions of the charcoal, continuous feeding of new charcoal, and periodic solid residues removal. It is very difficult to control the bed level directly using sensors, so the temperature indicated by a thermocouple (T4) at the desired height of the bed was used. A lower temperature means that the thermocouple is immersed in the bed; a higher temperature means it is clear. Figure 5.12 shows the obtained variations of temperature. Solid residues rich in ash are extracted from the bottom every 10 min until the temperature rises; indicating the bed surface has fallen below the required height, and then the bed is allowed to rise again (the continuous char feed rate exceeds the rate of consumption of char). For these sets of experiments the bed level was kept at 650 mm.

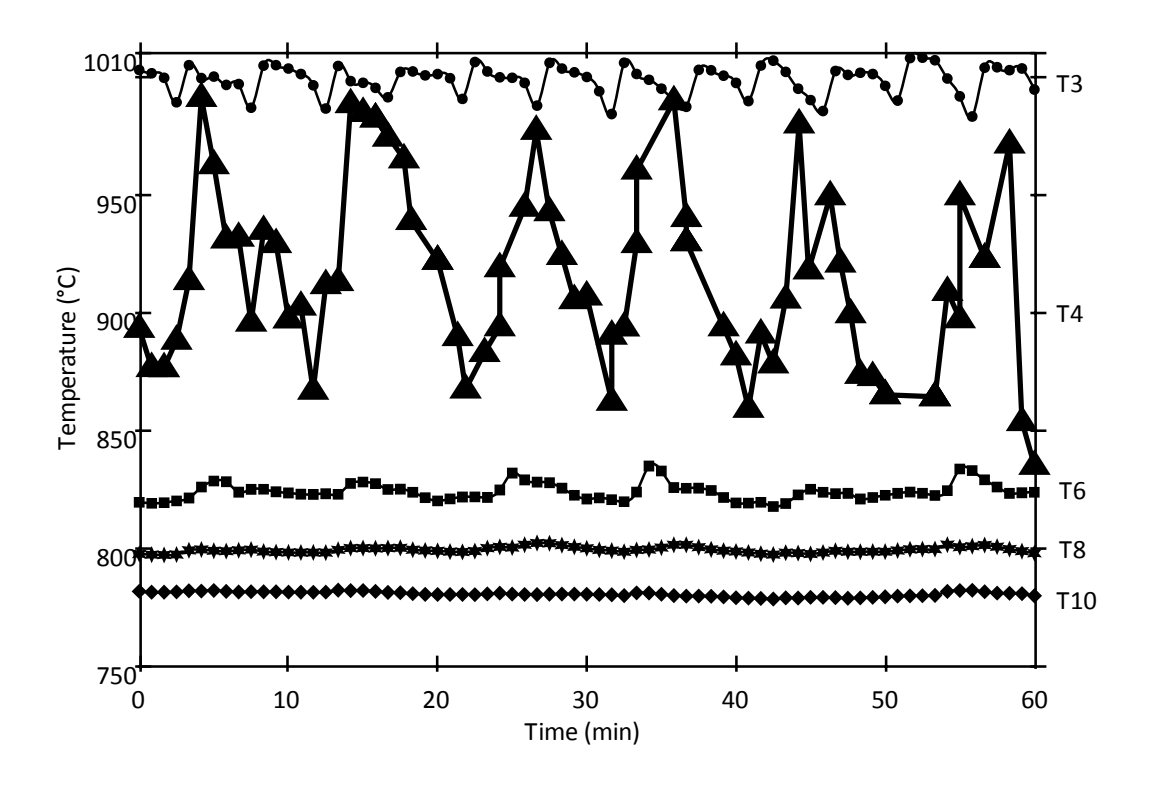


Figure 5.12: Bed level monitored by T4

5.6 Experimental results

Over 100 hours of gasification experiments were conducted to produce the results presented in this section. Every experiment can only last a maximum of 13 hours, as the time is limited to the opening times of the facilities (06h - 19h).

The results presented here were acquired under the operating conditions presented in Section 5.4 The results are analysed to provide mass and energy balances, as well as profiles of temperature, pressure, mole concentration and conversion, both in transient and steady states.

The results complement the work on the CFiBR previously performed at CIRAD (Tagutchou, 2008; Van de Steene et al., 2010; Mermoud, 2006), and are a valuable database for development and validation of numerical methods.

5.6.1 Reaching steady state

5.6.1.1 Temperature

As previously described in Section 5.5.4 a complete experiment passes through three stages until it reaches steady state. Once the system stabilises the temperature only varies ± 10 °C, except at thermocouple T4 which is the reference for bed height (Figure 5.12). This profile of the dynamic behaviour until the system reaches steady state is identical to previous studies (Mermoud, 2006; Tagutchou, 2008; Van de Steene et al., 2010) as expected.

5.6.1.2 Solid residues removal and charcoal conversion

Charcoal conversion is inversely proportional to solid residues removal. As described in Section 5.5.4.2, solid residues rich in ash are removed from the bottom to keep the bed height constant. During the thermal stabilization stage, nearly no residue

is removed due to the low conversion ratio. As the system moves to bed stabilization stage, solid residues are removed every 10 minutes. Therefore the removal rate is not constant as the temperature and reaction rate have not reached stability and the insulation is still raising its temperature. Once the system reaches steady state, solid residues removal is constant.

Figure 5.13 and Figure 5.14 show the conversion profiles for the two operational conditions described in Section 5.4 It can be observed in both graphs that in the beginning of the experiments; the charcoal conversion is under 50%. As the overall temperature increases and stabilises (Figure 5.11) less residues are removed and charcoal conversion increases until it reaches 75% conversion for Experiment A/B and 71% for Experiment C. The conversion is calculated using the directed method described in Section 5.3.4.1

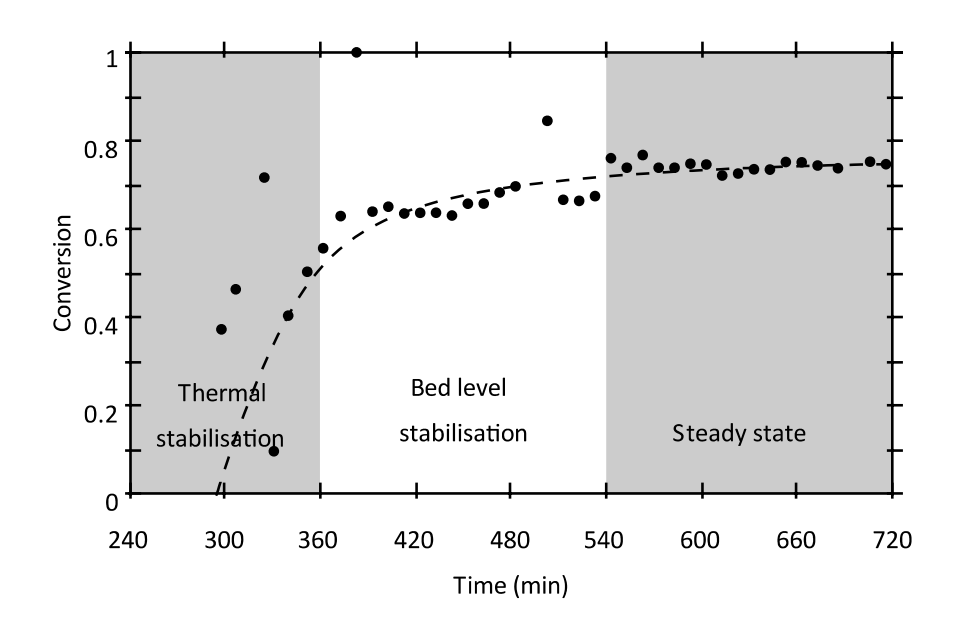


Figure 5.13: Conversion profile of Experiment A/B using direct method.

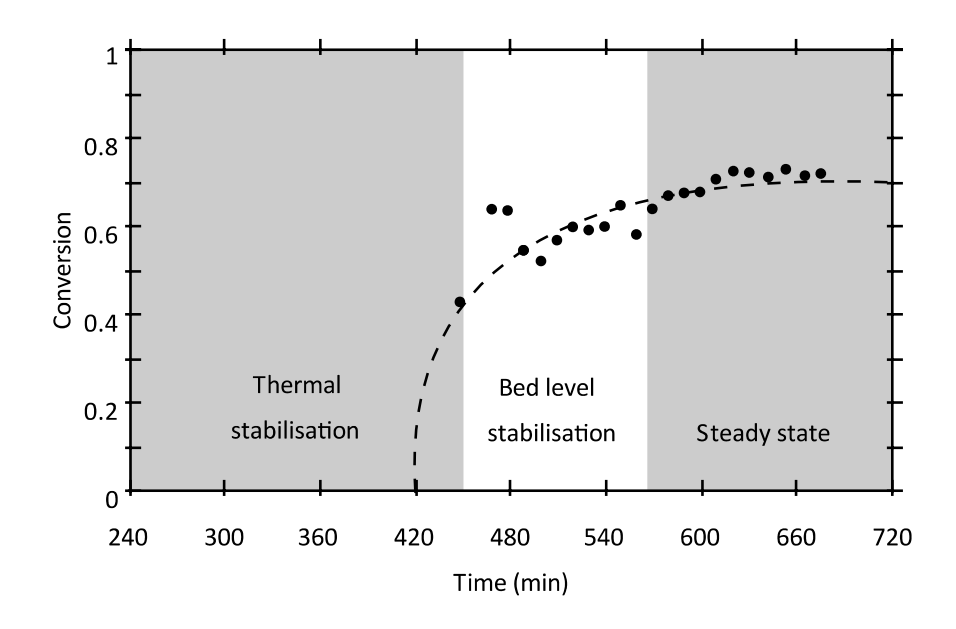


Figure 5.14: Conversion profile of Experiment C using direct method.

5.6.2 Steady state: variation of properties across the reactor

To understand reactor internal behaviour and the influence of design parameters on performance, it is necessary to acquire data beyond the traditional "black box" approach where only inlet properties of the biomass and outlet properties of the gas are taken into account. In trying to achieve this, previous work has characterized only the longitudinal direction of the gasifier bed (Zainal, 1996; Sharma, 2011; Susanto & Beenackers, 1996; Sharma, 2009; Plis & Wilk, 2010; Tagutchou, 2008; Van de Steene et al., 2010).

This section presents the steady state results for temperature in longitudinal and radial directions; as well as the longitudinal profiles for the producer gas, pressure drop, charcoal conversion and bulk density.

5.6.2.1 Temperature

Figure 5.15 shows the temperature profile for the two operational conditions.

Three regions can be observed.

Region 1: Above bed level (T4 = 60 cm from the bottom) a decrease of temperature is observed due to convective heat loss to the wall only, as the reactive atmosphere has not yet encountered the char bed. This is supported by the change of temperature in the radial direction which is typical of laminar flows within ducts (Lienhard IV & Lienhard V, 2011).

Region 2: Between T4 and T6, once the reactive atmosphere reaches the charcoal bed, the temperature drops rapidly. This temperature decrease is due to the endothermic nature of the gasification reactions as well as the heating up and drying of the charcoal entering the reactor and settling on top of the bed. In this region, the radial gradient increases and the temperature in the wall is up to 60°C lower than in the centre.

Region 3: Under T6, the temperature decrease is less pronounced and the longitudinal gradient reduces. The radial gradient becomes stable, where the maximum radial temperature variation between the centre and the wall is 65 °C for Experiment A/B and 38 °C for Experiment C.

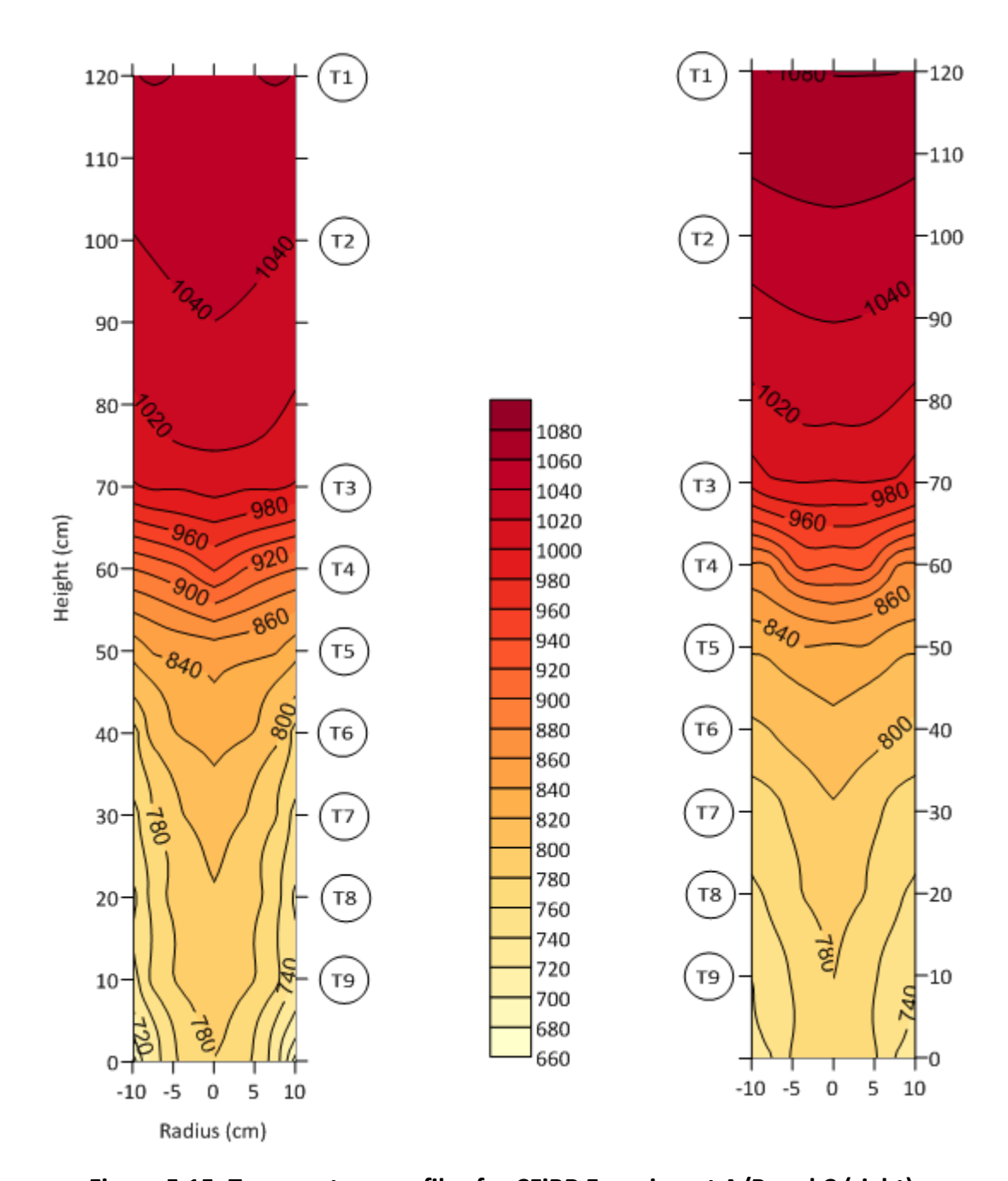


Figure 5.15: Temperature profiles for CFiBR Experiment A/B and C (right).

This supports other obsevations that in a fixed bed gasifier, the longitudinal gradient of temperature drops rapidly in the first 1/5th of the bed before decreasing gradually along the rest of the bed (Hobbs et al., 1993).

5.6.2.2 Gas composition profiles

To measure the gasses it was applied the method presented in the section 5.3.3. The knowledge of the gas concentrations across the gasifier bed assists the determination of the location of the chemical reactions occurring. These data together with temperature profiles can guide reactor improvements in addition to the development of new designs. This section presents the molar concentration and mass flow longitudinal profiles for the tested conditions. Methane molar concentration is multiplied by 10 to be seen in the graph.

Resembling the temperature profiles earlier presented, the concentration and mass flow profiles, shown in Figure 5.16 and Figure 5.17, also have three distinct regions:

A) Region 1: Above bed level (T4 = 60 cm from the bottom).

A reduction in the concentration of O₂, H₂O and CO₂ can be observed, while CO and H₂ start being formed. The temperature in the centre of the bed decreases promptly to under 850 °C in Region 2. This drop in temperature indicates the dominance of endothermic reactions, in addition to devolatilization and drying of the charcoal. The turbulence in this zone, caused by the sudden increase in the gas velocity from encountering a porous media, influences the chemical reactions at the surface of the bed. Therefore, the conditions for gas sampling at this location are not optimum, therefore the data collected are likely to not be precise and may be use as reference for order of magnitude.

B) Region 2: Between T4 and T6.

The concentrations of CO and H_2 increase considerably as the concentrations of H_2O and O_2 fall. The concentration CO_2 remains almost constant. At this region there is competition between exothermic and endothermic reactions in both homogeneous and heterogeneous phases. This is the main region of reaction where over 80% of the producer gases are formed.

C) Region 3: Under T6 (the remaining 50 cm of bed, about 80% of the total height).

The variations in the gas concentrations are very small, since the reduction in temperature reduces the reaction kinetics. Previous studies have shown that it takes 32 min to completely convert an isolated 10 mm particle in 20% steam at 930 °C, but by reducing the temperature to 830 °C the conversion time increases to 108 min (Mermoud et al., 2006); equivalent tendencies are observed during particle gasification by CO₂ (Tagutchou, 2008). Homogeneous reactions also play an important role in the gasification process, and in particular the water gas shift is very sensitive to temperature (Higman & Van Der Burgt, 2008).

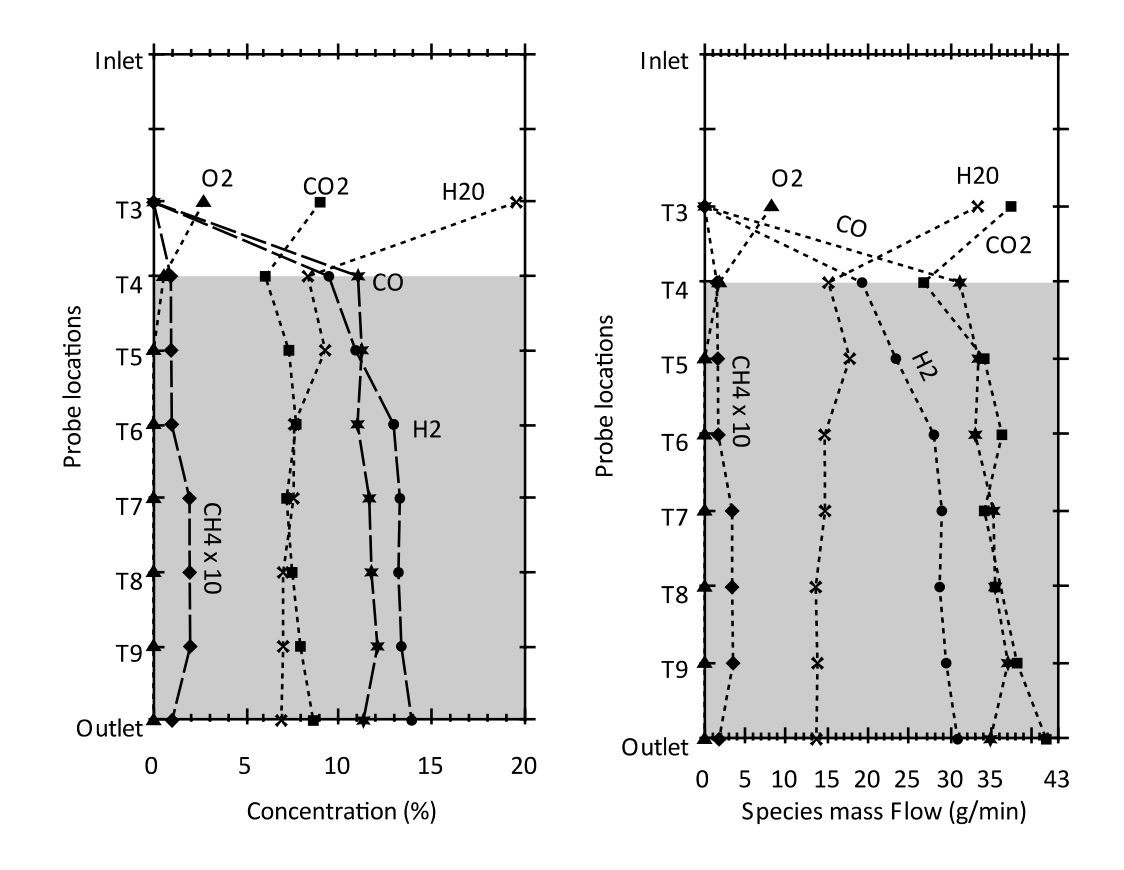


Figure 5.16: Longitudinal profiles of molar concentration and species mass flow in Experiment A.

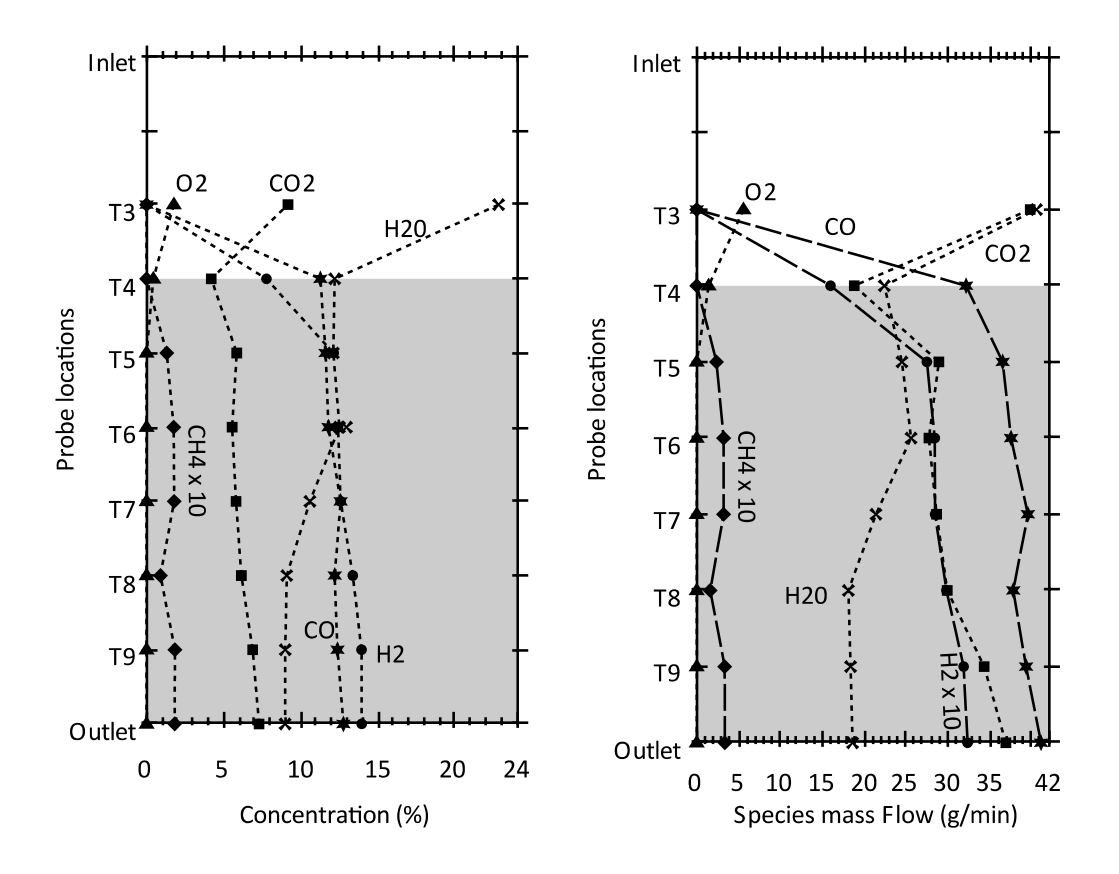


Figure 5.17: Longitudinal profiles of molar concentration and species mass flow in Experiment C.

At first sight, the nearly constant concentration of CO_2 suggests that it is not participating in any of the reactions. However this is not the case. All the O_2 that enters the systems goes to CO_2 production by the char combustion reaction, while the Boudouard reaction consumes CO_2 and the water gas shift reaction also involves CO_2 .

Unlike the temperature radial profile shown in Figure 5.15, no significant radial variation in the gas concentration can be observed in the data shown in Table 5.6 and Figure 5.18. Although there is a clear radial temperature gradient and it is known that changes in temperatures influence reaction kinetics, in this case the temperature differences were not enough to change the composition to a significant degree.

Table 5.6: Comparison of concentration on the radial and longitudinal profile of Experiment A/B.

	H2 (%)			CO (%)			CH4 (%)		
	Centre	Wall	Diff	Centre	Wall	Diff	Centre	Wall	Diff
T4	9.47	Χ		11.05	Χ		0.93	Χ	
T5	10.91	11.04	-0.13	11.25	11.63	-0.38	0.95	0.97	-0.02
T6	12.97	13.40	-0.43	11.02	12.10	-1.08	0.98	1.00	-0.02
T7	13.30	12.37	0.92	11.65	11.22	0.42	1.94	1.92	0.02
T8	13.23	12.95	0.27	11.77	11.03	0.73	1.95	1.92	0.03
T9	13.38	13.20	0.18	12.10	11.37	0.72	1.98	1.93	0.05
Outlet	13.94	Χ		11.34	Χ		1.00	Χ	

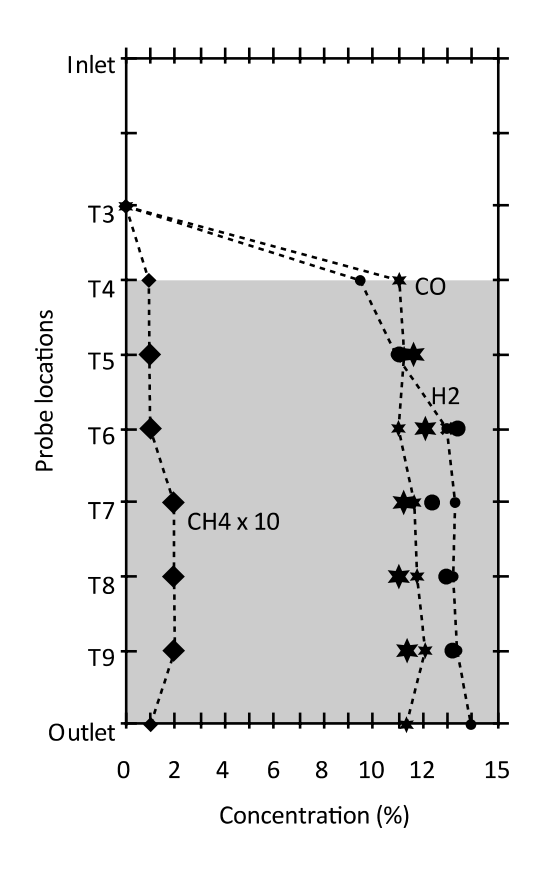


Figure 5.18: Comparison of concentration on the radial and longitudinal profile of Experiment A/B. Lines represent samples in the centre of the reactor and larger symbols represent samples extracted by the wall.

5.6.2.3 Charcoal conversion and bed bulk density

For experiment A/B, Figure 5.19 shows that in the first 10 cm of the bed, coal has a conversion rate of about 85%. This conversion rate then slowly evolves until it reaches 90% of final conversion rate. Similarly the bulk density reduces from 180 kg/m 3 to 120 kg/m 3 in the top 10 cm, then slowly reduces until it reaches 113 kg/m 3 as the final bulk density.

For experiment C the conversion rate in steady state is 89% according to the indirect method.

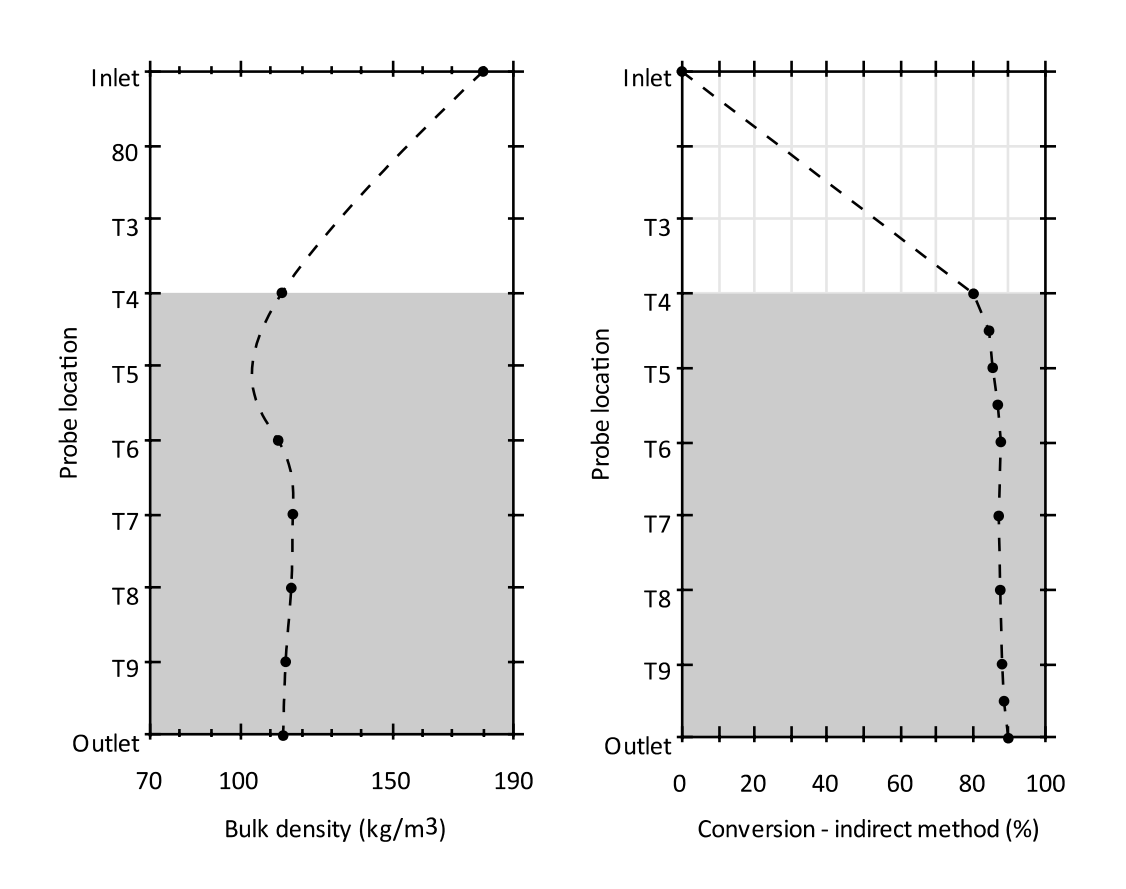


Figure 5.19: Bulk density and conversion rate across the bed for Experiment A/B

5.6.3 Mass and energy balances

To perform a mass and energy balance a control volume was defined as shown in Figure 5.20. The control volume was restricted to the area that covers the char bed to minimize the error. A larger volume that covered all the gasifier would require a calculation of heat losses in areas where temperature was not measured.

Both mass and energy balances only apply to steady state, where fluctuations of the gas species are limited to <2%.

The methodology to perform these calculations is described in Section 5.3.5

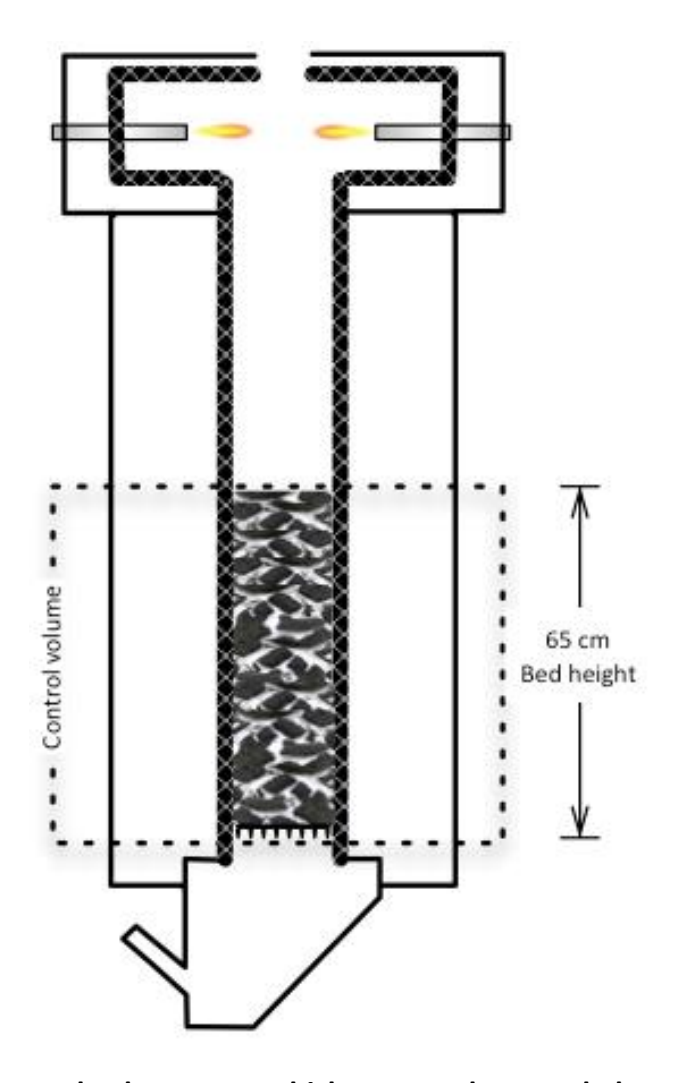


Figure 5.20: Control volume over which mass and energy balances are applied

The mass balance is given by the difference between inlet reagents and outlet products (producer gas and residues). The inlet reagents are charcoal and the reactive atmosphere gases presented in Table 5.5, and the outlet products are the producer gas and the solid residues removed from the bottom. The solid particles trapped in the cyclone are not taken into account. The calculation of the mass balanced is performed according to Eq. 5.12.

The energy balance takes into account the enthalpy of the mass flow in addition to the heat loss going out of the control volume. The energy balance is calculated according to Eq. 5.16.

The heat loss is calculated according to Eq. 5.17, using the dimensions of the control volume (0.65 m height and 0.6 m diameter). The heat transfer coefficient of natural convection is 10 W/m^2 -K.

Mass and energy balances for the two experimental conditions are presented in Figure 5.21 and Figure 5.22.

For Experiment A/B the temperature for the inlet gases is 1060 °C and charcoal is assumed to be 560 °C (the mean temperature between the inlet gases and the charcoal on the conveyer). The results presented in Figure 5.21 show good closure, with a mass balance error of 1.6% and an energy balance error of 6%.

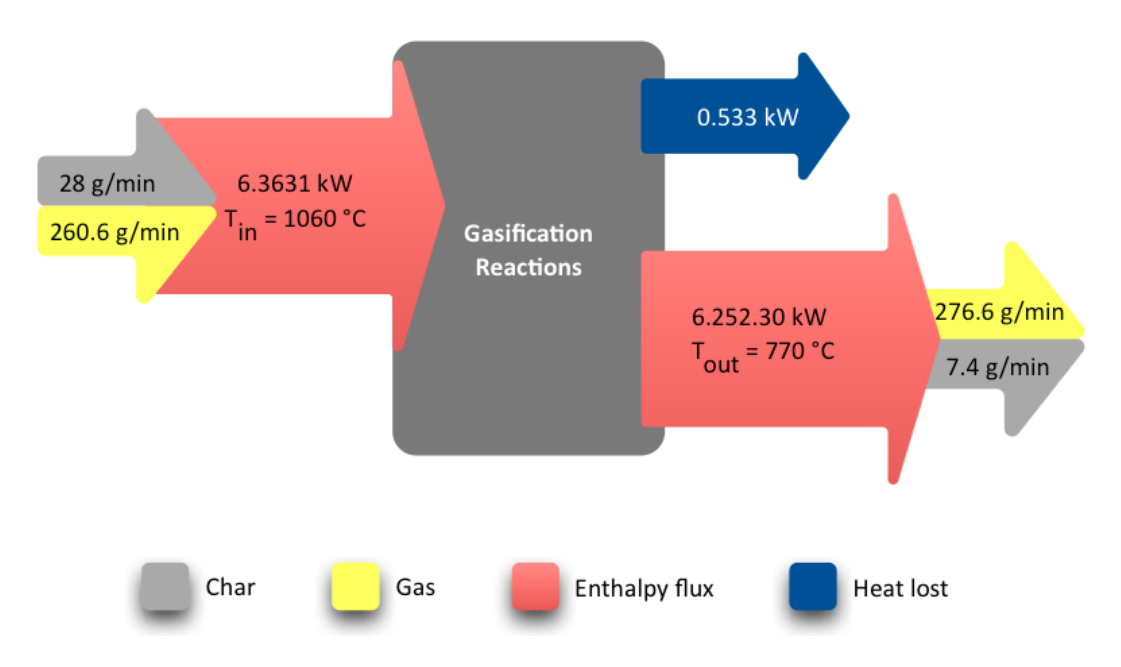


Figure 5.21: Mass and energy balance for Experiment A/B

For Experiment C the temperature for the inlet gases is 1080 °C and charcoal is assumed to be 570 °C (again the mean temperature between the inlet gases and the charcoal on the conveyer). Again the results presented in Figure 5.21 show good closure, with a mass balance error of 1.3% and an energy balance error of 1.9%.

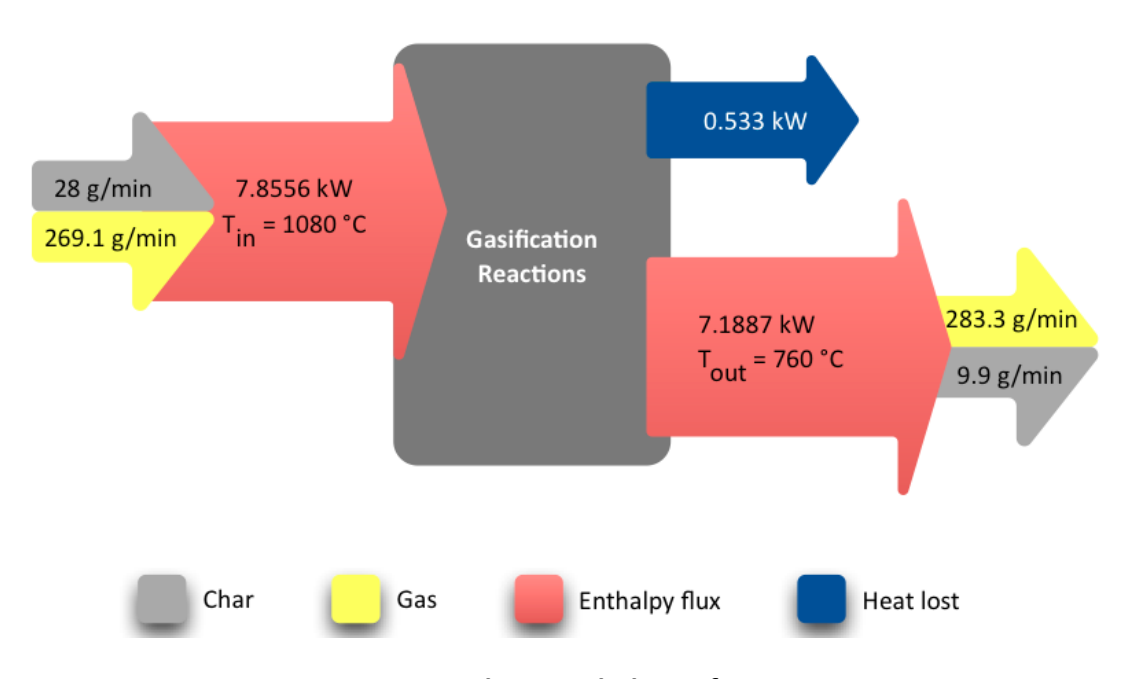


Figure 5.22: Mass and energy balance for Experiment C

The small errors in the mass balances can be attributed to the fine particulates trapped in the cyclone and/or uncertainties in the gas sampling. The energy balance errors may also be related to assumptions in the charcoal inlet temperature and the natural convection heat transfer coefficient.

5.7 Conclusions

The main objective in this chapter is to perform an experimental study of charcoal gasification in a continuous fixed bed reactor, providing a radial and longitudinal characterization of the bed. Several hundred hours of experiment were necessary to commission the gasifier and over a hundred hours of experiments were perform to deliver the two different conditions presented in this chapter.

It was described how to control the operational regime and the bed level by measuring the temperature of the top of the bet and monitoring the ash removal. Furthermore, it was presented results for time evolution for gas concentration, temperature and charcoal conversion. At steady state data for temperature, pressure and gas composition profiles for longitudinal and radial directions were also presented.

The data collected under these conditions allowed the analysis and interpretation of the phenomena occurring within the charcoal bed during gasification; with focus on how the concentration of reactive atmosphere and water vapour, effects the temperature and gas concentration on the bed, as well as density and charcoal conversion profiles.

These profiles have shown the existence of temperature gradients across the bed, which decreases from the top to the bottom and from the centre to the wall. Gas concentrations changes in the longitudinal direction, nevertheless it did not present

any relevant change in the radial direction. The radial profile of temperature is of great value for reactor design, as it can identify "colder" zones within the bed that may become channels were tar could pass through the bed without being cracked.

The temperature gradient data in cross reference to the gas longitudinal profile allow a clear picture of the gasification of the charcoal and generation of producer gas, as well as showing that most of chemical reactions took place in the first 15 centimetres of bed, therefore confirming the observations made by several authors which used similar facilities. Three main areas have been identified along the reactor, from top to bottom they are:

- Region 1: Above bed level (T4 = 60 cm from the bottom) a decrease of temperature is observed due to convective heat loss to the wall only, as the reactive atmosphere has not yet encountered the char bed.
- Region 2: Between T4 and T6, once the reactive atmosphere reaches the charcoal bed, the temperature drops rapidly; the radial gradient increases and the temperature in the wall is up to 60 C lower than in the centre.
- Region 3: Under T6, the temperature decrease is less pronounced and the longitudinal gradient reduces. The radial gradient becomes stable, where the maximum radial temperature variation between the centre and the wall is 65 °C for Experiment A/B and 38 °C for Experiment C.

As a conclusion, it can be stated that the results presented allow the understanding of several continuous fixed bed gasification phenomena. The diagnostics made regarding temperature, gas composition profile, conversion rate, ash removal flow as well as the, represents a valuable input for reactor design, as well as operations parameters improvement. The overall data can be also used for numerical model development and validation, which ultimately constitute an effective contribution to the conception, design and development of gasification reactors.

CHAPTER 6

GASIFICATION IN A 25KW THROATED FIXED BED BIOMASS GASIFIER

In order to understand the behaviour of a downdraft gasifier, a commercially available 25kg/h throated reactor was modified to be able to measure pressure drop, gas composition (longitudinal direction) and temperature (radial and longitudinal directions).

The device consists of a metal reactor (280mm id, 76.2mm throat) surrounded by refractory insulation. An auger enables the feeding of biomass to the top of the reactor. The biomass flow rate is controlled by the consumption of the reactor. Air inlet and gas outlet are both measured using orifice plates installed in the device.

The gas is extracted through the bottom of the reactor and taken to a flare for final oxidation, after passing through a cyclone which separates the fine particles and a biomass filter that traps condensables in the aerosol phase.

6.1 Experimental Apparatus (GEK – Gasifier Experimenters Kit)

The whole system is called the Gasifier Experimenters Kit (GEK) and comprises a reactor, cyclone, PyroCoil, auger feed drying bucket, hopper, filter and flare. The system is designed and manufactured by All Power Laboratories in the USA. A diagram of the GEK is shown in Figure 6.1.

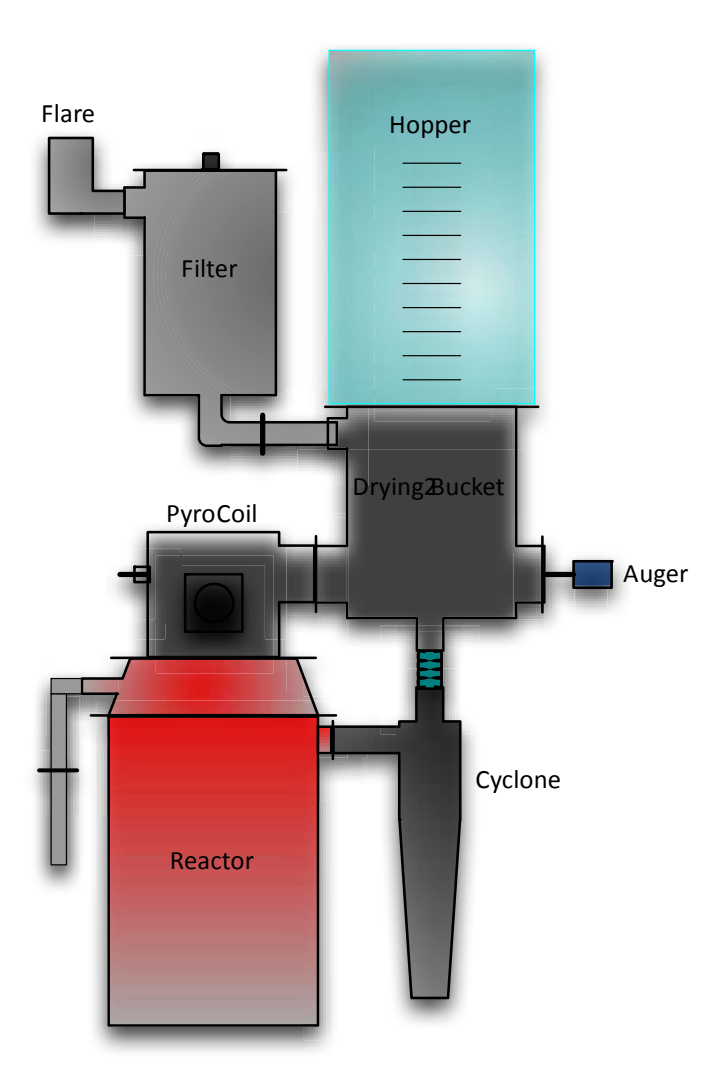


Figure 6.1: GEK with full thermal integration

The system as supplied (shown in Figure 6.1) is not intended to provide data for the detailed understanding of the process. Therefore, the only process indicator provided is the pressure drop across the system, indicated by a manometer.

In order to make the system suitable for researching fixed bed gasifier dynamics, it was necessary to create strategic points of temperature, gas and pressure data collection. Intrusive instruments were carefully installed in the reactor in such a way as not to disturb the flow of biomass.

6.1.1 Reactor

The default reactor for the GEK system is an Imbert type (throated downdraft gasifier named after its inventor Jacques Imbert) (Reed & Das, 1988). An Imbert is the usual starting point for generating low tar wood gas to power internal combustion engines. The GEK Imbert (Figure 6.3 and Figure 6.2) is able to deliver 60-75 kWth (20-25 kWe in a generator set) consuming 20-25 kg/h of dry lignocellulosic biomass. This model is a double jacket reactor, which uses the excess of heat generated by the process to pre-heat the inlet air that exit the nozzles. This makes tar cracking more efficient by increasing the operating temperature.

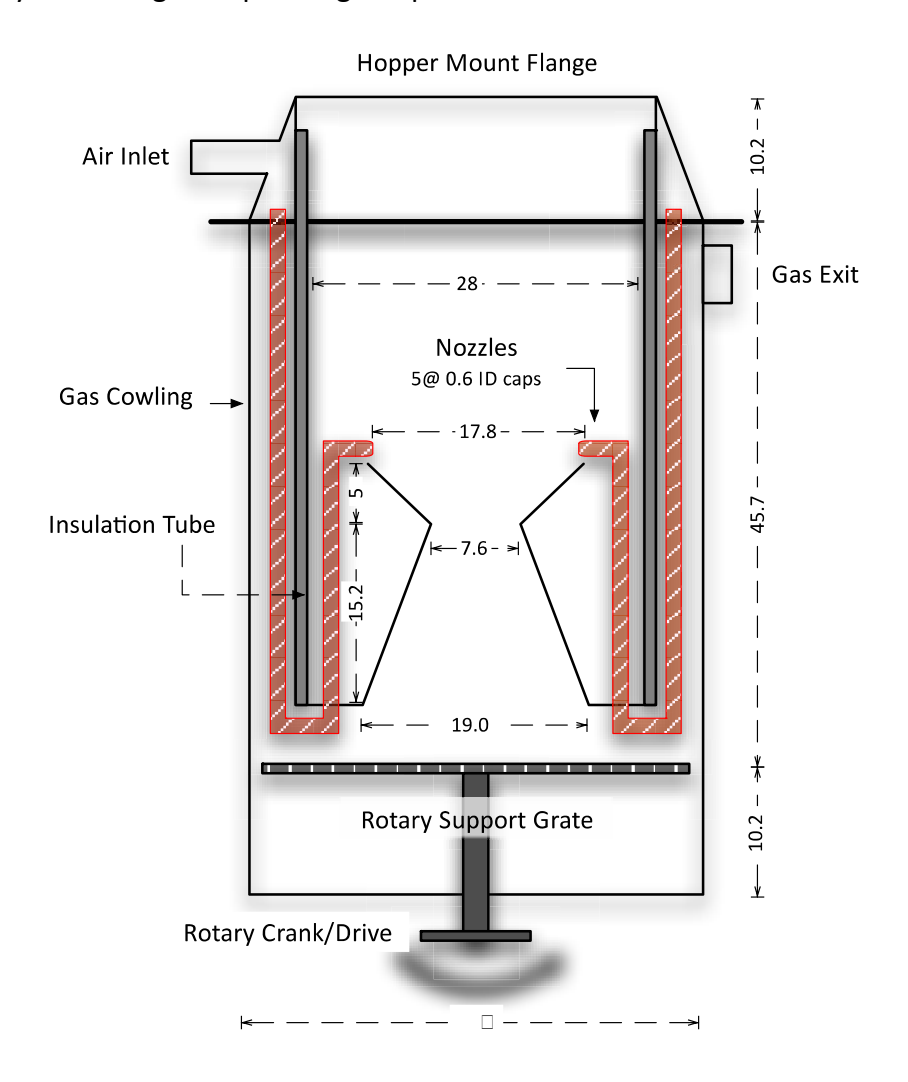


Figure 6.2: Imbert reactor adapted from All Power Labs (All Power Labs, 2008). All units are in centimetres.



Figure 6.3: Disassembled reactor showing air tubes on the left and top view of the reactor on the right

6.1.2 Cyclone

The cyclone Installed at the exit of the reactor (see Figure 6.4) receives the hot producer gas from the gasifier and delivers it to the filter. During the transfer process, the cyclone removes particulates and cools down the producer gas. The detailed dimensions are available at All Power Labs (2008).

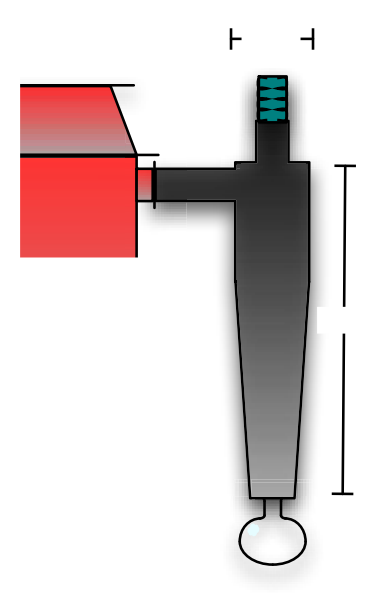


Figure 6.4: Diagram of cyclone attached to the reactor.

6.1.3 Auger feed and drying bucket

The auger feed and drying bucket assembly (shown in Figure 6.5) bolts on to the side of the PyroCoil of the GEK reactor and has the cyclone connected to the base as shown in Figure 6.1. The auger and drying bucket are double jacketed so that outgoing product gas from the cyclone is circulated through the assembly to transfer heat to the fuel. There is a series of internal baffles in the double jacket to create an accelerated gas flow across the inner surface for better heat transfer. Fuel level sensing is via a simple mechanical plunger, which directly controls the auger motor. The drive motor is a pdm (positive displacement motor) controlled 12vdc brushless gear motor for speeds of between 10 and 50rpm. The preheating of the biomass provided by this system increases the efficiency of the whole process through predrying. The detailed dimensions are available at All Power Labs (2008).

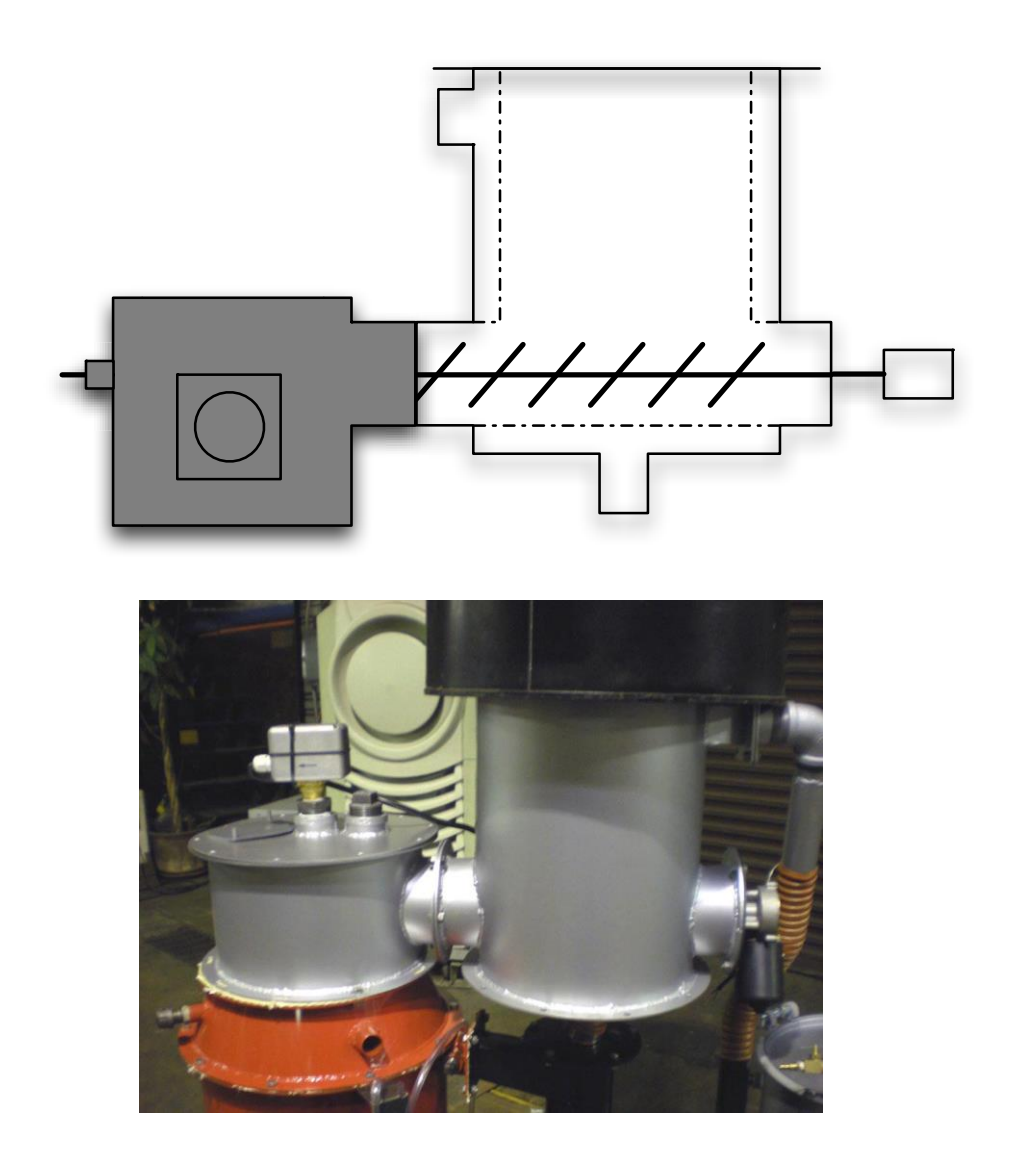


Figure 6.5: Auger and drying bucket

6.1.4 Filter

The filter is a simple vessel filled with charcoal and iron wool. Once the product gas leaves the drying bucket with temperatures lower than 100 °C, they enter the filter where remaining condensables and particulates are removed. When the charcoal inside the filter needs to be changed, it can be used as a gasification fuel.

6.1.5 PyroCoil:

The GEK PyroCoil (shown in Figure 6.6) is attached to the top of the reactor. It was designed by All Power Labs as a gas heat exchanger that recovers heat from engine exhaust gases and introduces the heat to the pyrolysis zone of a downdraft gasifier. For the experiments performed in this work, the PyroCoil was used to connect the auger to the reactor. The detailed dimensions are available at All Power Labs (2008).

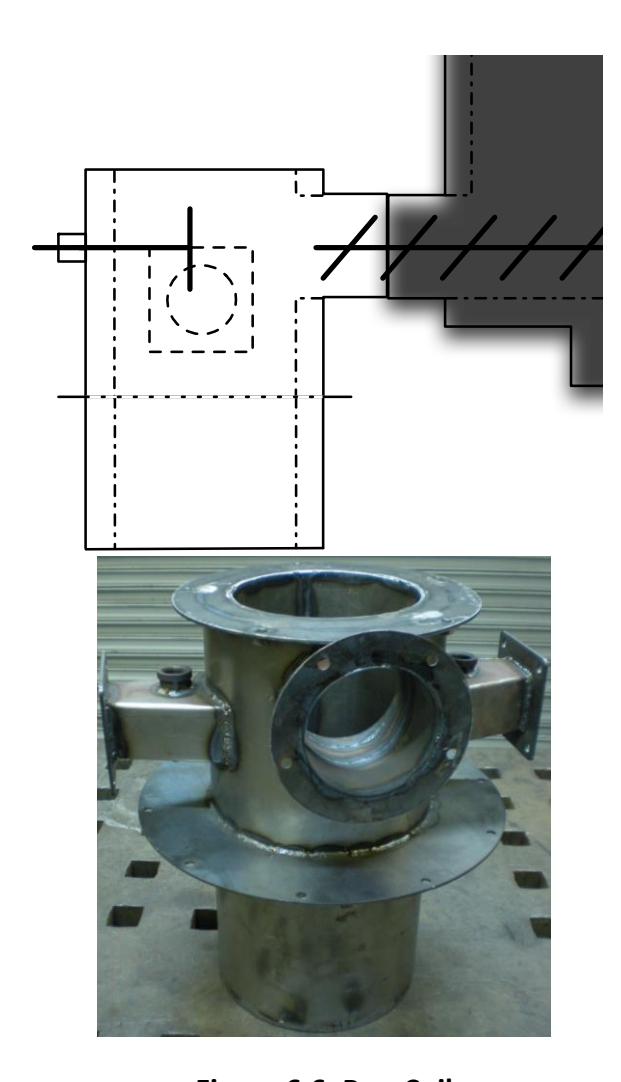


Figure 6.6: PyroCoil

6.2 Instrumentation and Measurements

In order to comprehend the phenomena occurring during gasification of the bed, the reactor is provided with various sensors. All the values measured can be observed and recorded instantaneously and enable real-time monitoring of the experiment.

6.2.1 Temperature:

Three 3.17mm k-type multipoint thermocouple probes specially designed for this system (shown in Figure 6.7) are inserted from the top of the PyroCoil crossing the full longitudinal span of the gasifier. The three thermocouple probes measure 16 temperature points, covering a broad area of the gasification zone in both longitudinal and radial directions.



Figure 6.7: Base of the k-type multipoint thermocouple probe showing its wiring, and 3.17mm probe.

The TCs are installed in the reactor as shown in Figure 6.8. The two central TCs record 6 temperatures each; at 2.5cm intervals starting from the bottom tip. The external TC measures 4 points located at the following locations starting from the bottom tip: 0, 7.5, 10, and 12.5 cm.

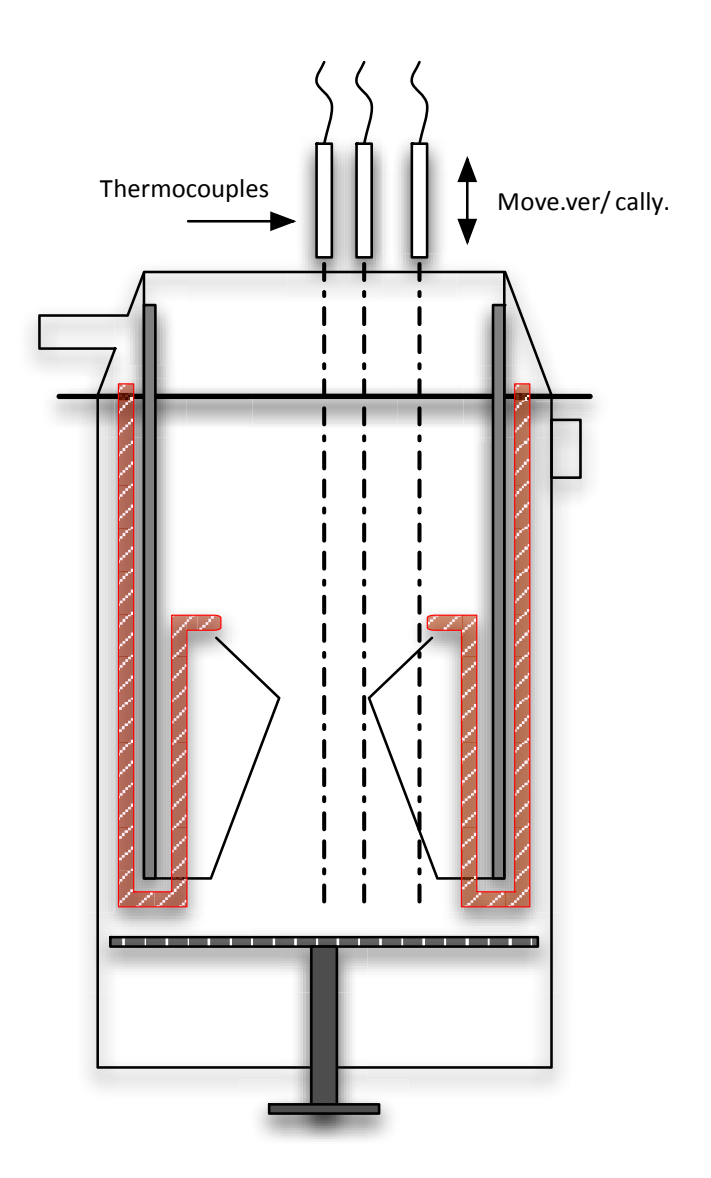


Figure 6.8: Thermocouple positioning inside the reactor. (The dash lines represent TCs).

Calibration results provided by the manufacturer of the thermocouples are shown in Table 6.1. The error is less than 1% for temperatures up to 650 $^{\circ}$ C.

Table 6.1: Calibration report provided by ILC – Idaho Laboratories Corporation

Actual Temperature °C	Measured Temperature °C	Deviation	Error %
229.51	229.31	-0.20	-0.08
405.70	404.64	-1.06	-0.26
652.12	650.90	-1.22	-0.18

6.2.2 Pressure

Fixed pressure measuring points are located at the bottom of the reactor and after the filter. The pressure can also be measured everywhere in the bed via the insertion of probes into the TC probe channels.

6.2.3 Mass flow rate

6.2.3.1 Air and producer gas

The air is sucked into the reactor by an ejector attached between the filter and the flare, the flow can be controlled by the speed of the air that passes through the ejector, that is controlled by an butterfly valve. Air inlet and gas outlet streams are measured using orifice plates (OPs). The inflow OP is installed at the air inlet of the reactor (see Figure 6.9); the outflow OP is at the inlet of the filter (see Figure 6.10). Both OPs were manufactured and calibrated at Aston University. The temperatures required to calculate the density of the fluid are acquired by two thermometers installed adjacent to each OP. Air flow rate is monitored during all experiments. Air is taken to be 21% O_2 and O_2 and O_2 by volume with no moisture.

Producer gas flow rate can only be calculated once the gas composition is known.

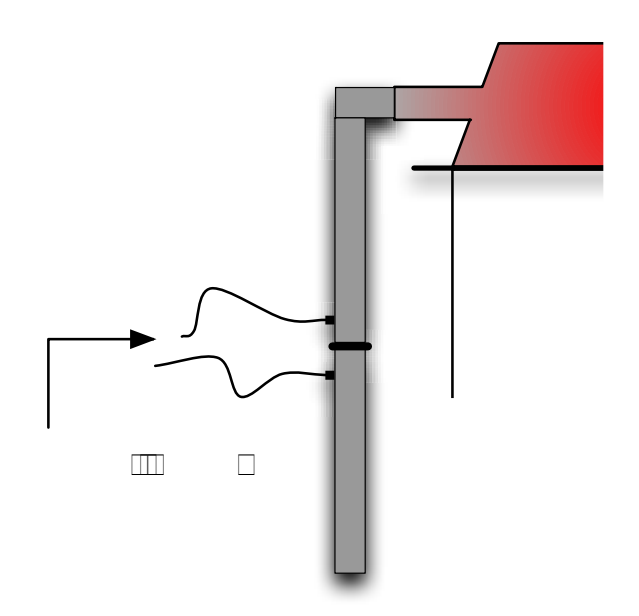


Figure 6.9: Diagram of the inflow OP.

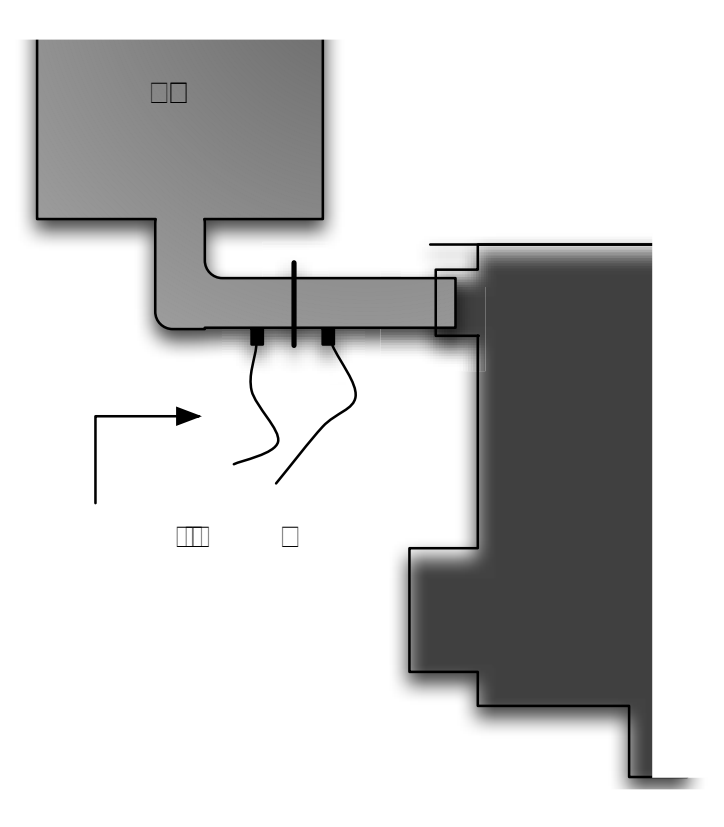


Figure 6.10: Diagram of the outflow OP.

6.2.3.2 Biomass pellets

During the experiment biomass consumption is calculated, every 20 min, based on the volumetric reduction of the biomass inside the hopper, which carries a scale as

shown in Figure 6.11. The biomass flow rate can also be calculated through mass balance once air, producer gas and particulate flows are known.

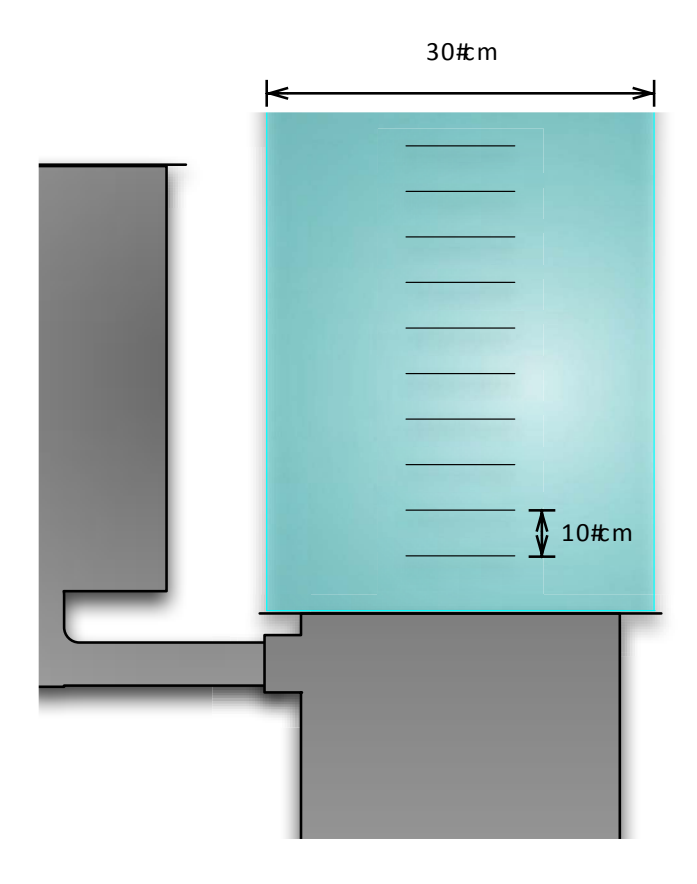


Figure 6.11: Diagram of the hopper.

6.2.4 Gas composition

The gases can be sampled through the central thermocouple probe along the whole longitudinal span of the reactor, as well as at the gas outlet, providing direct correspondence between temperature and gas concentration. The gases are then cooled in order to remove the condensables, and analysed using a GC (TCD detector and carboxen-1000 column), which is connected directly to the sampling line. The sampled gas can be analysed every thirty minutes during the experiment, to give CO, CO₂, N₂, H₂ and CH₄ concentrations. Water is analysed off line using the Karl Fisher method, and tars have their concentration calculated by weight difference.

The Gas Chromatograph used was a Hewlet Packard HP-5890 series II with Carboxen 1000 column. At every injection a sample of approximately 150 micro litres of clean product gas was used. This samples was extracted via the sampling line described below.

6.2.4.1 Sampling line

The sampling line shown in Figure 5.9 is divided into four modules:

- Module 1: gas sampling probe heated by an electric tape and iron wool filter
- Module 2: 6 impinger bottles, glass beads and connectors
- Module 3: sampling tube
- Module 4: membrane vacuum pump and a mass flow meter

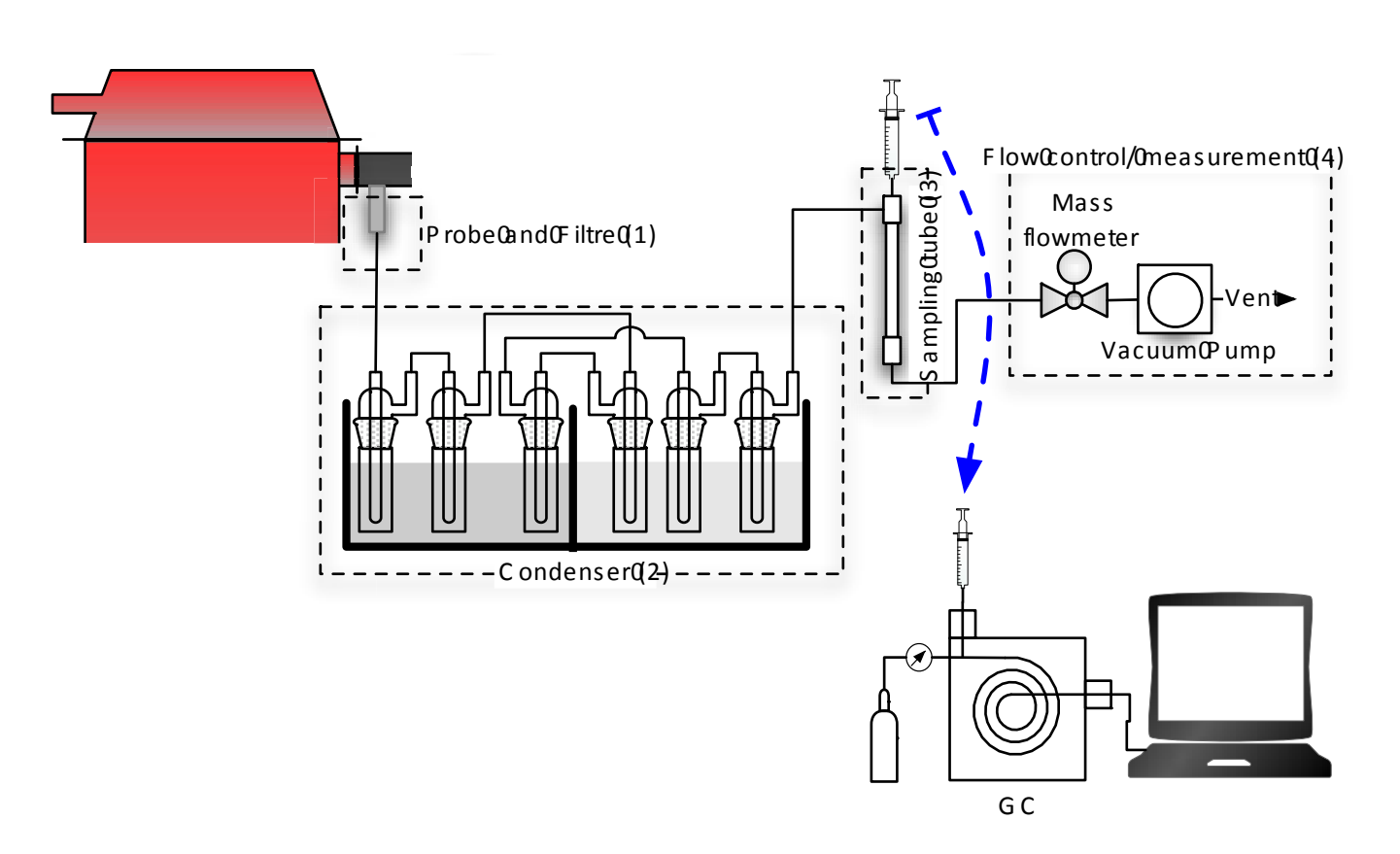


Figure 6.12: Diagram of the producer gas sampling line

The gas sampling process follows the European Tar Protocol (Neeft, 2005).

This system works in similar fashion to the system presented in Chapter 5.

6.2.4.2 Tar collection and analysis

The tar sampling and analysis follow the following steps as defined by (Neeft, 2005).

A) Sampling line preparation steps:

- Step 1: Verify that the impinger bottles, connectors, and glass fritz are clean.
- Step 2: Connect the modules as shown in the diagram.
- Step 3: Fill impinger bottles 2, 3, 5 and 6 with glass beads (note: the glass beads need to be just above the gas outlet).
- Step 4: Fill impinger bottle 1 to 5 with ≈50ml of isopropanol.
- Step 5: Ensure that the line is gas tight and free from blockage.
- Step 6: Ensure that the cold and hot baths are respectively at -20 and 40 °C.

B) Gas Sampling Steps:

- Step 1: Verify that the gasifier is at steady state condition.
- Step 2: Set the flow to 0.3Nm3/h (5NL/min).
- Step 3: Record the start time of gas meter reading.
- Step 4: Monitor the flow.
- Step 5: Occasionally agitate the condenser cooling liquid of the impinger bottles.
 - Step 5: Stop the vacuum pump, close the stop valve in the sampling line and record the time of the end of the sampling.

C) Sample Storage:

• Step 1: Decant the content of the impinger bottles into a dark vessel.

- Step 2: Soak the impinge bottles and glass beads with isopropanol and pour the solvent into the dark vessel.
- Step 3: Identify and store the dark bottle and keep it at a temperature <5 °C until analysis.

D) Tar quantification steps:

Tar is measured by weight difference, where the isopropanol is evaporated by a rotary evaporator (Stuart model RE-300).

- Step 1: Weigh the tar/water/isopropanol mixture collected from the tar sampling line.
- Step 2: Pour the mixture in the rotary evaporator flask and set it up for 40 rpm in a 50 °C water bath.
- Step 3: Visually monitor the separation of water and isopropanol. Once no water or isopropanol is leaving the condenser switch off the system. This means that only tar remains in the evaporator flask.
- Step 4: Measure the mass of the tar in the evaporator flask.
- Step 5: Collect the water/isopropanol from the condenser flask to analyse the water content via Karl Fischer titration.

6.2.5 Data collection:

Temperature and differential pressure are measured and logged every second with the help of a GCU (gasifier control unit).

The full features of the GCU are presented in Table 6.2.

Table 6.2: Input and output signals of the GCU

Quantity	Items
1	Atmel ATmega 1280 processor
16	K-type thermocouple inputs
6	Differential or gauge pressure/vacuum inputs
8	PWM FET outputs
4	Auxiliary analogue inputs
1	Frequency counter input
3	R/C hobby servo outputs
1	Display and four button keypad
1	USB serial host interface
1	SD-card slot
1	CANbus interface
1	Auxiliary RS-232 interface

6.3 Production and characterization of the biomass used

Four types of biomass were used to perform the experiments. Mixed wood chips, mixed wood pellets, wheat straw pellets and Miscanthus pellets. Over 500kg of biomass were used. Mixed wood chips were only used to perform the commissioning of the gasifier.

All the biomasses were sieved to eliminate fine particulates. After pretreatment, they were sent to Marchwood Scientific Services Ltd for proximate and ultimate analysis. Bulk density and mean dimensions were measured at EBRI facilities; the results are shown in Table 6.3.

Table 6.3: Feedstock characteristics.

	Wood chips	Mixed wood	Wheat straw	Miscanthus
Proximate				
analysis wt.% db.				
Moisture	3.7	10.0	12.2	7.28
Volatiles	89.9	80.05	71.96	79.05
Fixed carbon	9.8	18.45	17.96	16.74
Ash	0.3	1.5	10.08	4.2
HHV (MJ/kg)	15.4	19.8	17.7	19
Ultimate analysis				
wt.% (dry basis)				
Carbon	45.6	45.6	47.1	42.1
Hydrogen	5.8	5.8	7.4	6.5
Oxygen	48.0	48.0	43.2	40.5
Nitrogen	0.3	0.3	0.5	0.59
Sulphur	0.1	0.1	0.1	0.1
Dimensions				
Bulk Density	-	FFC 1	F20 /	401.0
(kg/m^3)		556.1	528.4	481.9
Length (mm)	-	21	26.6	20.4
Diameter (mm)	-	6.9	9.2	6.9

6.4 Experimental procedures and parameters

6.4.1 Commissioning

To prepare the GEK for the runs, a series of cold and hot trials were performed. The cold runs were intended to check for leakages and calibrate the auger and the orifice plates. The hot runs used mixed wood chips as feedstock, and were intended to provide understanding of the operational conditions of the GEK, as well as determine the optimal experimental conditions.

At the start of the first two hot runs, it was noticed that a substantial quantity of tar was being formed during the start up and warming up process. This situation was solved at the third run by pre-loading the gasifier with charcoal up to the throat of the reduction zone. Having a charcoal bed at the start up is indispensable, because it is in the charcoal bed where the heterogeneous reactions take place (Reed & Das, 1988).

For the third run, activated carbon was also added to the filter that precedes the flare; this allowed the capture of condensable vapours formed during the gasification process. These modifications improved the operation of the system and the third run was successful, as the tar trapped in the sampling line was about 2g/Nm³. A steady flare was also achieved once the gasifier reached 1000 C as the air inlet kept an average of 10 m³/h. The parameters tested over the three commissioning runs established the verifications tests and operating parameters for the subsequent experiments.

6.4.2 Preliminary verification tests and setup of the grid

Prior the experiments, a series of verification tests need to be done to ensure that the GEK does not present any flaws that may compromise the run. These verifications tests take place on the day of the experiment and consist of the following steps:

- Check the availability of charcoal and diesel to light the reactor;
- Check the functioning of the line of compressed air; the pressure must be between 2.5 and 3 bar for the first line; and between 5 and 6 bar for the second line;
- Check the operation data acquisition interface (CGU and flow meter data acquisition software);
- Check the operation of the auger motor;
- Conduct a leak test of the system;
- Verify proper operation of the sampling line and the GC;
- Check the availability of solvent (isopropanol) in sufficient quantity;
- Check the availability of calibrations gases.

Once all the preliminary requirements have been checked, the GEK can be prepared for the run. The following stets must be done to run a gasification experiment at the GEK.

- Load the reactor with charcoal;
- Load the hopper with the feedstock;
- Inject diesel in the charcoal bed;
- Install the sampling line and the GC;
- Connect the TCs and orifice plates to the CGU;
- Attach and turn on the compressed air line;
- Light the gasifier.

6.4.3 Operational parameters

Three types of pellets comprising mixed wood, Miscanthus and wheat straw were used to make six feedstock mixtures to run 11 experiments as shown in Table 6.4.

The commissioning test allowed defining the operational parameters. The air inlet was chosen to be the variable, as it can be controlled via the ejector and accurately measured by an orifice plate.

Initially it was intended to fix the following airflows, \approx 8 kg/h and \approx 16 kg/h. Although, at the first run two thermocouples were damaged do to high temperature when used an airflow of 16kg/h. It was also noticed that at low airflows (<8kg/h) the GEK had difficulties to keep a steady state. Therefore, for the remaining runs, the airflows used were \approx 10.7 and \approx 12.8kg/h.

Table 6.4 presents the runs, which were performed using the GEK.

Table 6.4: Gasification runs series

Run	Feedstock	Airflow (kg/h)
1	100% mixed wood pellets	8.10
2 a	75% mixed wood pellets and 25% Miscanthus pellets	10.7
2b	75% mixed wood peliets and 25% Miscantilus peliets	12.8
3 a	50% mixed wood pellets and 50% Miscanthus pellets	10.7
3b	3b	12.8
4a	25% mixed wood pellets and 75% Miscanthus pellets	10.7
4b	25% Illixed wood peliets and 75% Miscantilus peliets	12.8
5a	100% wheat straw pollets	10.7
5b	100% wheat straw pellets 5b	12.8
6a	50% mixed wood pellets and 50% wheat straw pellets	10.7
6b	30% mixed wood peliets and 30% wheat straw peliets	12.8

6.5 Gasification runs

6.5.1 Run 1: 100% mixed wood pellets

Mixed wood pellets was the feedstock used in the first run. The Table 6.5 presents the mass flow, including tar. The mass balance presents good closure of 97.4%.

In overall, the disparities in the mass balance can be explained mainly by pressure fluctuations in the outlet gas orifice plate.

Table 6.5: Mass balance for the Run 1

Mass balance	Run 1
Air flow (kg/h)	8.1
Pellets flow (kg/h)	4.6
Flow of unreacted material (kg/h)	0.14
Gas outlet flow (kg/h)	12.2
Tar (g/Nm3)	1.5
ER – equivalence ratio	0.33
Closure	97.4%

The thermocouples setup explained in the section 6.2.1 gave the longitudinal and radial temperature profile shown in the Figure 6.13. This profile covers the section of the reactor that is just below the throat to the grate. It can be noticed a clear decrease in the temperature towards the grate due to the endothermic nature of the gasification reactions. The gas leaves the combustion zone at a higher temperature (>1000 C), and as soon reaches the char bed they provide heat to the reactions (de Souza-Santos, 2004; Reed, 1985). A radial gradient can also be observed; therefore, the gradient is higher at 12 cm height and is decreases as it becomes closer to the grate.

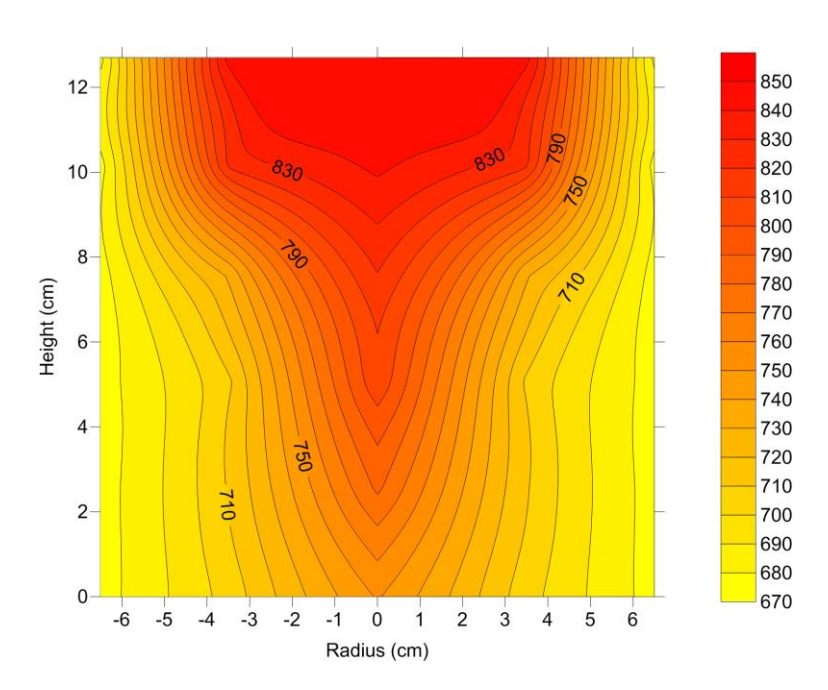


Figure 6.13: Temperature profile - Run 1

Higher airflows were experimented, up to 16kg/h, but these promoted temperatures around 1400 C, which were higher than the supported by the TCs. The exposure to these temperatures damage the two TCs near the wall, as they were near the air inlet nozzles described in the section 6.1.1 The remaining experiments will only present the centre longitudinal profile of temperature.

The Table 6.6 presents the gas concentrations, including the water content. The measurements were performed according to the procedures presented in the section 6.2.4.

Table 6.6: Gas concentrations - Run 1

Species	Run 1 (vol %)
CO	18.4
CO ₂	9.1
CH ₄	1.8
H ₂	20
H_2 H_2O N_2	11.3
N ₂	39.4

6.5.2 Run 2: 75% mixed wood pellets and 25% Miscanthus pellets

A blend of 75% mixed wood pellets and 25% Miscanthus pellets was the feedstock used in the Run 2. The Table 6.7 presents the mass flows, including tar, as well as the equivalence ratio for two distinct experiments (a and b) using the same feedstock.

Table 6.7: Mass balance for the Run 2

Mass balance	Run 2a	Run 2b
Air flow (kg/h)	10.7	12.8
Pellets flow (kg/h)	7.4	7.66
Flow of unreacted material (kg/h)	0.22	0.38
Gas outlet flow (kg/h)	17.2	19.2
Tar (g/Nm3)	1.30	1.10
ER – equivalence ratio	0.27	0.31
Closure	96.5%	95.7%

The longitudinal temperature profile shown in the Figure 6.14 presents a decrease in temperature from the top to the grate as expected. The reasons for this behaviour are the same introduced in the Run 1.

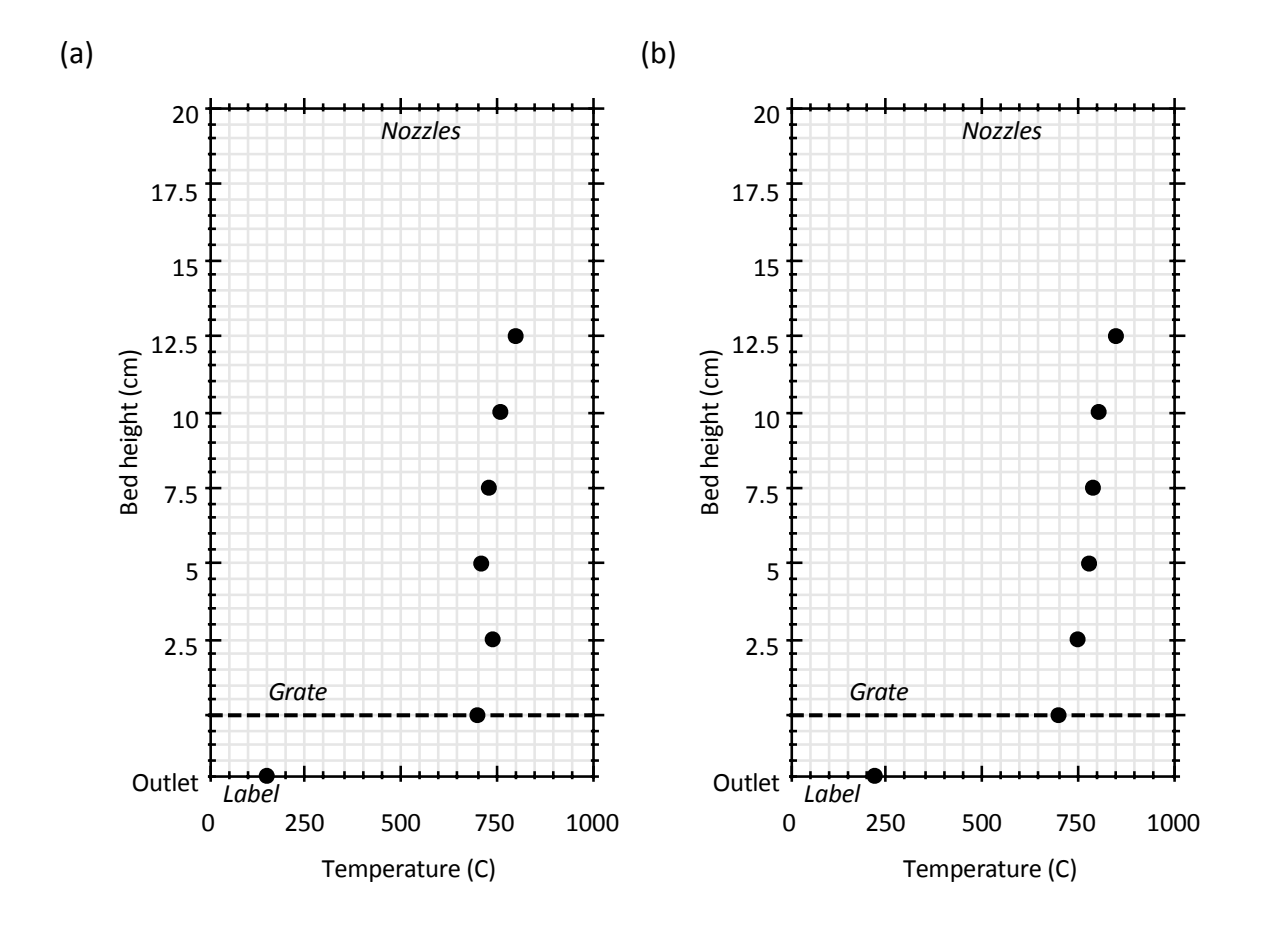


Figure 6.14: Temperature profile - Run 2

The table below presents the gas concentrations, including the water content. The measurements were performed according to the procedures presented in the section 6.2.4.

Table 6.8: Gas concentrations - Run 2

Species	Run 2a (vol %)	Run 2b (vol %)
СО	22.3	21
CO ₂ CH ₄	8.4	7.7
CH ₄	1.7	1.8
H_2	24.4	19
H ₂ O N ₂	8.3	11.4
N_2	34.9	39.1

6.5.3 Run 3: 50% mixed wood pellets and 50% Miscanthus pellets

A blend of 50% mixed wood pellets and 50% Miscanthus pellets was the feedstock used in the Run 3. The Table 6.9 presents the mass flows, including tar, as

well as the equivalence ratio for two distinct experiments (a and b) using the same feedstock.

Table 6.9: Mass balance for the Run 3

Mass balance	Run 3a	Run 3b
Air flow (kg/h)	10.7	12.8
Pellets flow (kg/h)	7.5	8.02
Flow of unreacted material (kg/h)	0.23	0.40
Gas outlet flow (kg/h)	17.0	20.0
Tar (g/Nm3)	1.40	1.20
ER – equivalence ratio	0.27	0.30
Closure	96.4%	98.0%

The longitudinal temperature profile shown in the Figure 6.15 presents a decrease in temperature from the top to the grate as expected. The reasons for this behaviour are the same introduced in the Run 1.

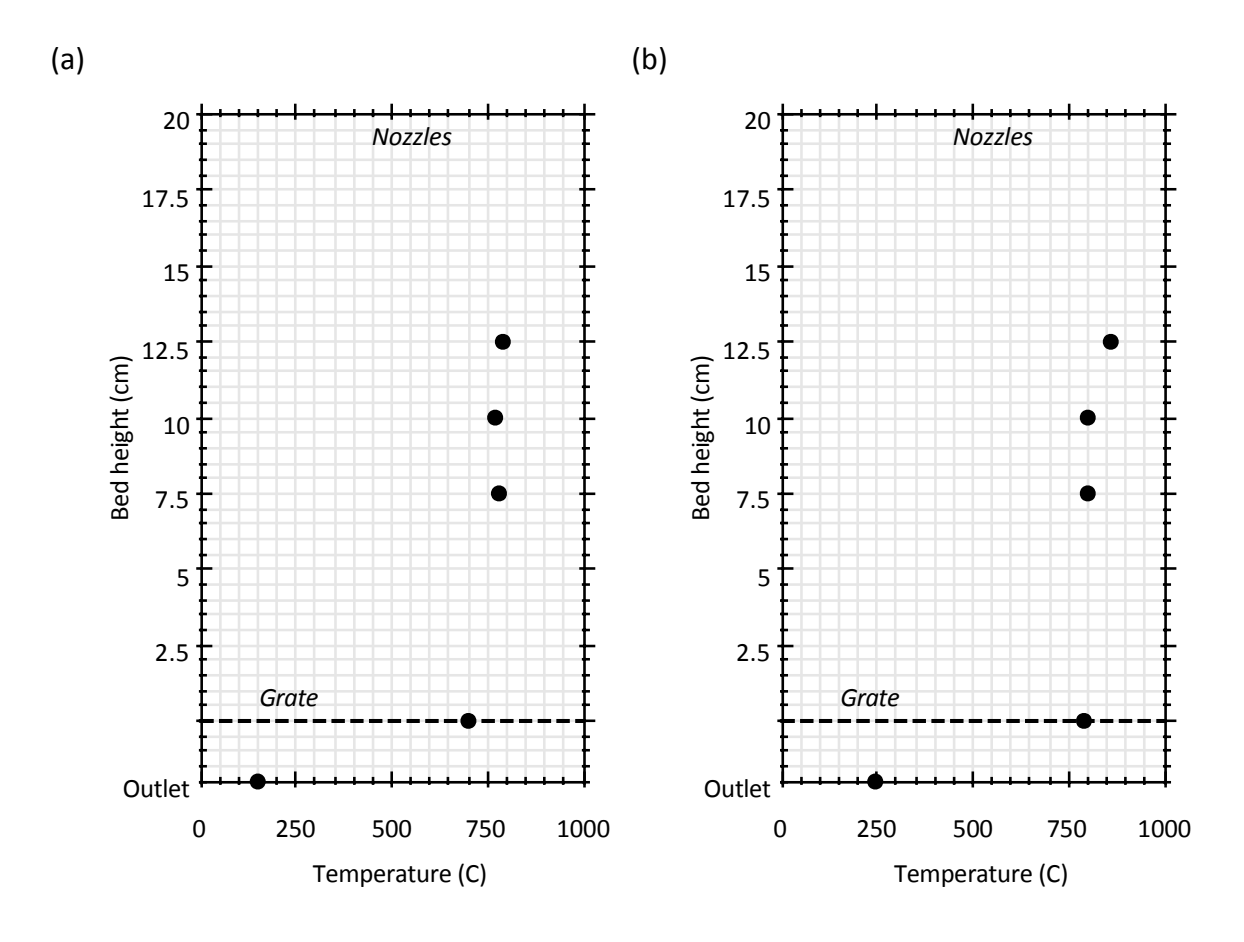


Figure 6.15: Temperature profile – Run 3

The table below presents the gas concentrations, including the water content. The measurements were performed according to the procedures presented in the section 6.2.4.

Table 6.10: Gas concentrations - Run 3

Species	Run 3a (vol %)	Run 3b (vol %)
СО	23.8	22.6
CO ₂	8.2	7.6
CH ₄	1.2	0.9
H ₂	25	21.5
H ₂ H ₂ O N ₂	6.9	9.6
N_2	34.9	37.8

6.5.4 Run 4: 25% mixed wood pellets and 75% Miscanthus pellets

A blend of 25% mixed wood pellets and 75% Miscanthus pellets was the feedstock used in the Run 4. The Table 6.11 presents the mass flows, including tar, as well as the equivalence ratio for two distinct experiments (a and b) using the same feedstock.

Table 6.11: Mass balance for the Run 4

Mass balance	Run 4a	Run 4b
Air flow (kg/h)	10.7	12.8
Pellets flow (kg/h)	7.2	7.97
Flow of unreacted material (kg/h)	0.22	0.40
Gas outlet flow (kg/h)	18.5	19.7
Tar (g/Nm3)	1.20	1.00
ER – equivalence ratio	0.28	0.30
Closure	104.3%	96.8%

The longitudinal temperature profile shown in the Figure 6.16 presents a decrease in temperature from the top to the grate as expected. The reasons for this behaviour are the same introduced in the Run 1.

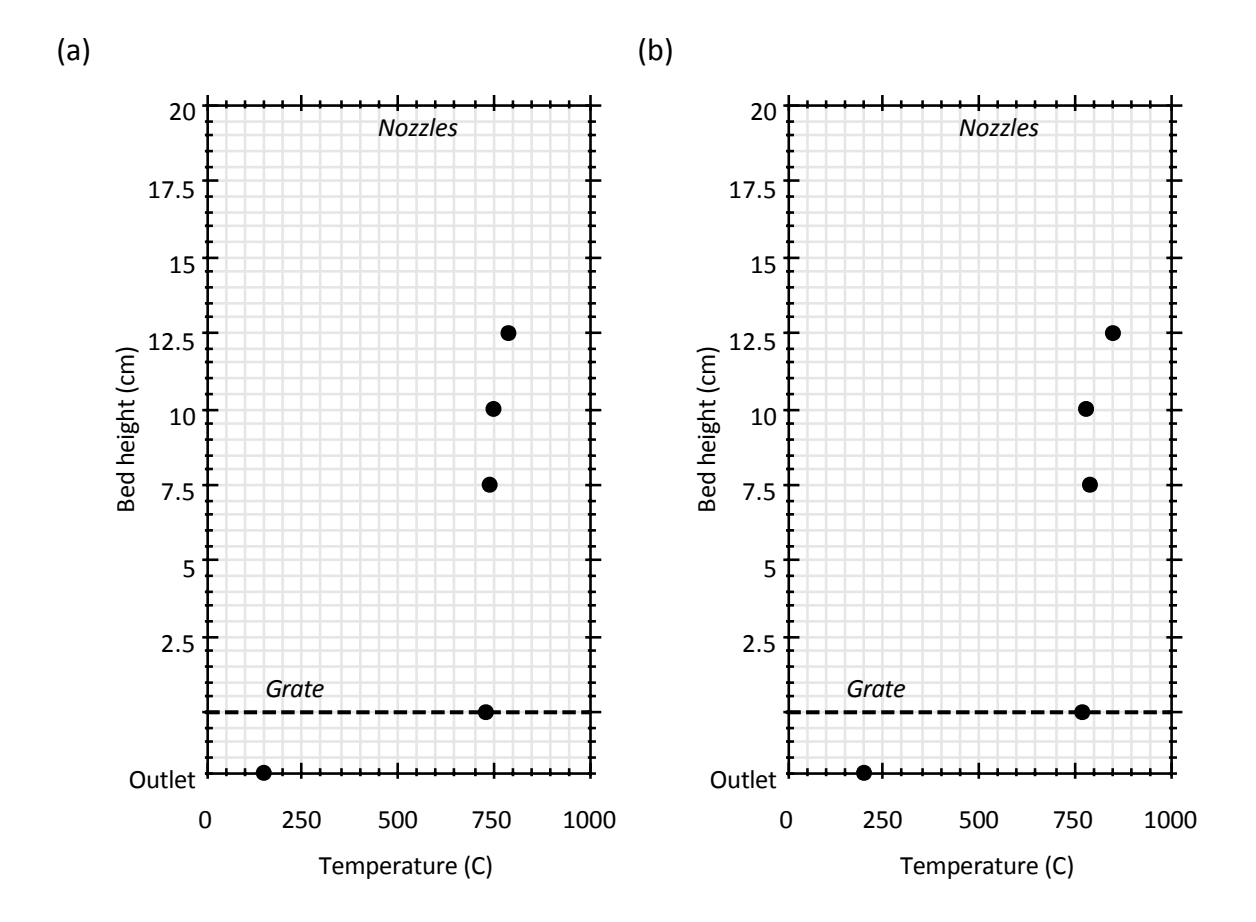


Figure 6.16: Temperature profile - Run 4

The table below presents the gas concentrations, including the water content. The measurements were performed according to the procedures presented in the section 6.2.4.

Table 6.12: Gas concentrations - Run 4

Species	Run 4a (vol %)	Run 4b (vol %)
СО	25.4	22.9
CO ₂ CH ₄	7.6	7.8
CH ₄	1.2	2
H ₂	22.8	17.6
H ₂ O N ₂	6.6	10.3
N_2	36.4	39.4

6.5.5 Run 5: 100% wheat straw pellets

Wheat straw pellets feedstock was used in the Run 5. The Table 6.13 presents the mass flows, including tar, as well as the equivalence ratio for two distinct experiments (a and b) using the same feedstock.

Table 6.13: Mass balance for the Run 5

Mass balance	Run 5a	Run 5b
Air flow (kg/h)	10.7	12.8
Pellets flow (kg/h)	7.2	8.26
Flow of unreacted material (kg/h)	0.21	0.41
Gas outlet flow (kg/h)	16.8	20.1
Tar (g/Nm3)	1.70	1.40
ER – equivalence ratio	0.33	0.34
Closure	95.3%	97.4%

The longitudinal temperature profile shown in the Figure 6.17 presents a decrease in temperature from the top to the grate as expected. The reasons for this behaviour are the same introduced in the Run 1.

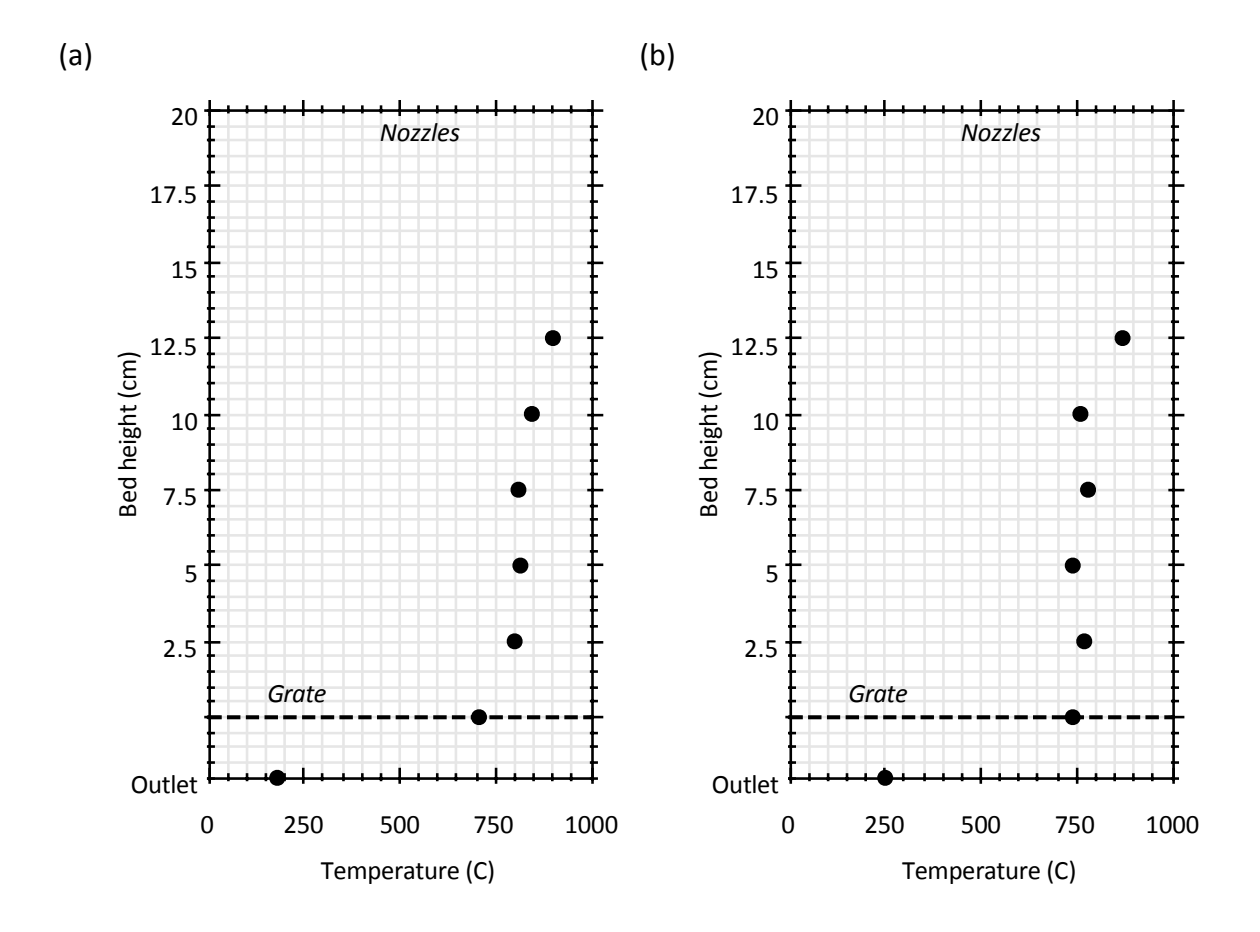


Figure 6.17: Temperature profile - Run 5

The table below presents the gas concentrations, including the water content. The measurements were performed according to the procedures presented in the section 6.2.4.

Table 6.14: Gas concentrations - Run 5

Species	Run 5a (vol %)	Run 5b (vol %)
СО	20.1	18.5
CO ₂ CH ₄	8.5	8.6
CH ₄	1.1	1.7
H_2	21.7	18.2
H ₂ O N ₂	11.6	14.4
N_2	37	38.6

6.5.6 Run 6: 50% mixed wood pellets and 50% wheat straw pellets

A blend of 50% mixed wood pellets and 50% wheat straw pellets was the feedstock used in the Run 6. The Table 6.15 presents the mass flows, including tar, as

well as the equivalence ratio for two distinct experiments (a and b) using the same feedstock.

Table 6.15: Mass balance for the Run 6

Mass balance	Run 6a	Run 6b
Air flow (kg/h)	10.7	12.8
Pellets flow (kg/h)	6.7	7.83
Flow of unreacted material (kg/h)	0.20	0.39
Gas outlet flow (kg/h)	16.5	21.0
Tar (g/Nm3)	1.60	1.30
ER – equivalence ratio	0.32	0.33
Closure	96.2%	103.7%

The longitudinal temperature profile shown in the Figure 6.18 presents a decrease in temperature from the top to the grate as expected. The reasons for this behaviour are the same introduced in the Run 1.

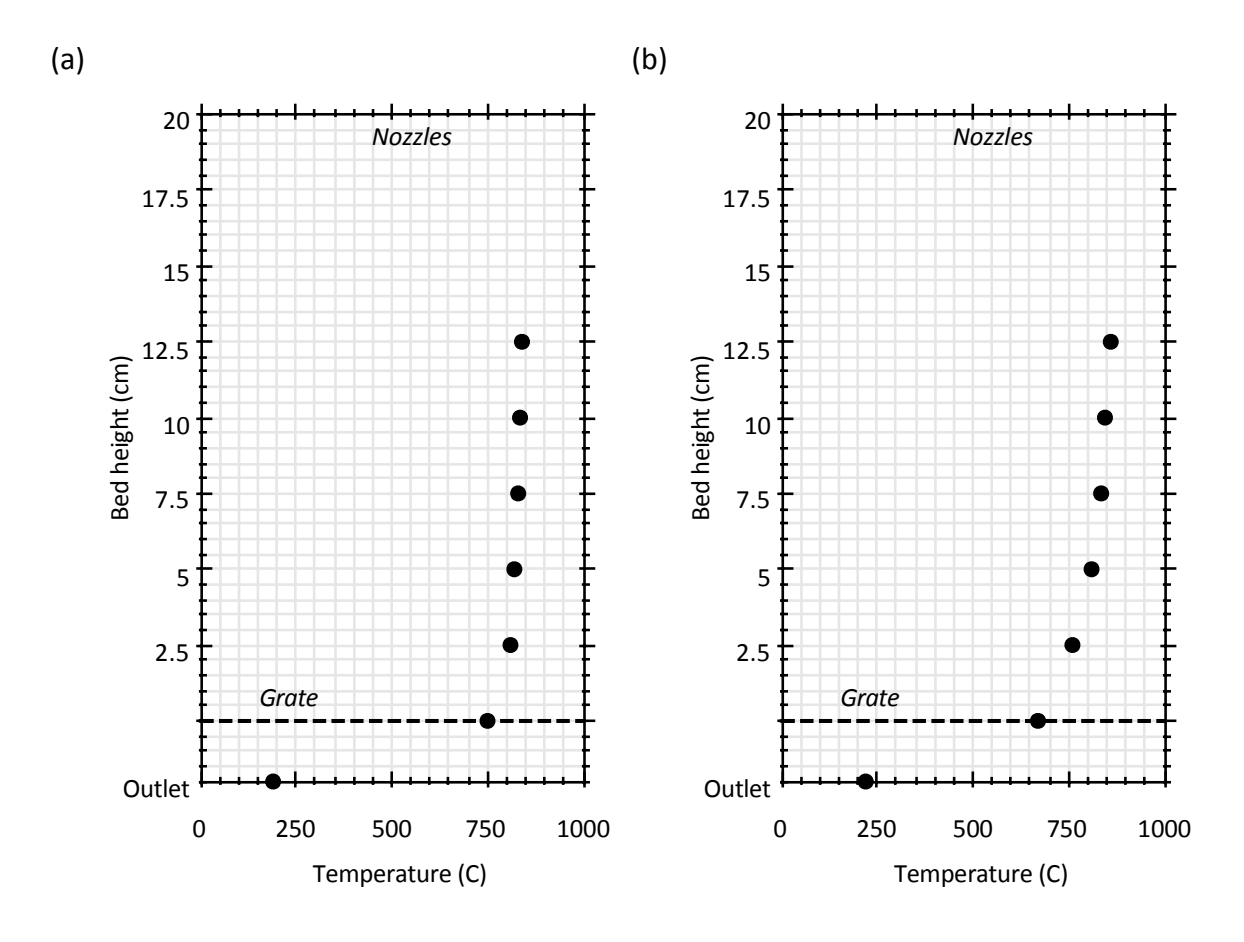


Figure 6.18: Temperature profile – Run 6

The table below presents the gas concentrations, including the water content.

The measurements were performed according to the procedures presented in the section 6.2.4 .

Table 6.16: Gas concentrations - Run 6

Species	Run 6a (vol %)	Run 6b (vol %)
СО	20.5	19.1
CO ₂ CH ₄	8.1	8.1
CH ₄	1.2	1.5
H ₂	21.4	18.8
H ₂ O	11.2	13.6
N_2	37.6	38.9

6.5.7 Summary of the gasification runs

The Table 6.17 presents a summary of the experimental results.

Table 6.17: Summary of the experimental results

Run	Feedstock	Airflow (kg/h)	Feedstock (kg/h)	Producer gas (kg/h)	Tar (g/Nm³)	ER
1	100% mixed wood	8.1	4.6	12.2	1.5	0.3
2a	75% mixed wood and	10.7	7.4	17.2	1.3	0.27
2b	25% Miscanthus	12.8	7.66	19.2	1.1	0.31
3a	50% mixed wood and	10.7	7.5	17.0	1.4	0.27
3b	50% Miscanthus	12.8	8.02	20.0	1.2	0.30
4a	25% mixed wood and	10.7	7.2	18.5	1.2	0.28
4b	75% Miscanthus	12.8	7.97	19.7	1.0	0.30
5a	1000/	10.7	7.2	16.8	1.7	0.33
5b	100% wheat straw	12.8	8.26	20.1	1.4	0.34
6a	50% mixed wood and	10.7	6.7	17.0	1.4	0.32
6b	50% wheat straw	12.8	7.83	21.0	1.3	0.33

For all the cases can be observed that higher the airflow, higher is the feedstock consumption, which increases the producer gas consumption. Therefore, this moves equivalence ratio away from the optimum (0.25) (Reed, 1985). Further from 0.25 and closer to 1, the producer gas reduces its HHV by forming more CO_2 and less hydrogen and carbon monoxide.

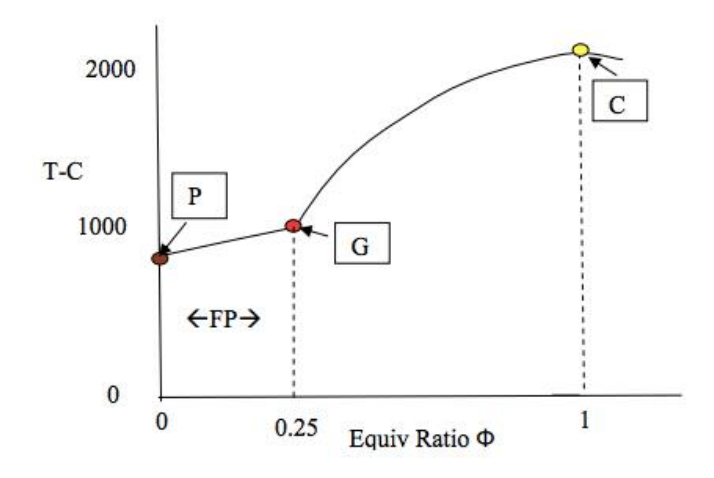


Figure 6.19: Equivalence ratio diagram (Reed, 1985)

Nonetheless, the increase of producer gas increases the superficial velocity, and therefore reduces the tar production. This has already been reported by (Yamazaki et al., 2005).

6.6 Conclusion

The main objective in this chapter is to present an experimental study of biomass gasification in a downdraft gasifier, providing a radial and longitudinal characterization of the bed. A few dozen of hours of experiment were necessary to setup and commission the gasifier and over a hundred hours of experiments were perform to deliver the two different conditions presented in this chapter.

It was described how to assemble and control the operational regime by controlling the airflow into the reactor, and the biomass consumption by marking the auger transparent. It was also describe the setup of the thermocouples and orifice plates to measure the gas flow. Furthermore, it was presented results for mass balance and gas concentration, temperature, tar production and equivalent ratio. A longitudinal and radial directions temperature profile was also presented.

The data collected under these conditions allowed the analysis and interpretation of the phenomena occurring within the throat of the gasifier bed during gasification.

These profiles have shown the existence of temperature gradients across the bed, which decreases from the top to the bottom and from the centre to the wall. The radial profile could only be presented for one of the runs due to the damage of two thermocouples.

CHAPTER 7

SIMULATION OF CHAR GASIFICATION PROCESS IN A CONTINUOUS FIXED BED REACTOR USING ASPEN PLUS

There are a few commercial softwares able to perform biomass gasification simulation by chemical equilibrium. ASPEN Plus was chosen because of the robustness of its physical properties database and sensitivity analysis tools. ASPEN uses unit operation blocks to model specific process operations (reactors, separators, heaters, pumps etc.).

The model developed to simulate the CFiBR is based on Gibbs free energy minimization (RGIBBS block in ASPEN). Restricted equilibrium parameters were used to calibrate the results against experimental data presented in Chapter 5.

7.1 Principles of RGibbs and gasification modelling

The RGibbs block can be used to establish the chemical equilibrium composition between reactants and products. Chemical equilibrium can be performed either by stoichiometric or non-stoichiometric methods, via three different calculation options that can be chosen in the ASPEN Plus RGibbs basic specifications panel:

- Calculate phase equilibrium and chemical equilibrium;
- Restricted chemical equilibrium specify temperature approach (or duty and temperature) of entire system;
- Restricted chemical equilibrium specify temperature approach or molar extent for specified reaction stoichiometry

Non-stoichiometric methods do not require reactions to be specified, while stoichiometric methods require the specification of the reactions.

7.1.1 Non-stoichiometric equilibrium method (minimization of the Gibbs free energy)

This applies minimization of the Gibbs free energy to model the equilibrium of a reacting system (such as combustion and gasification). In ASPEN Plus, this is the standard way to use the RGibbs block. The use of this technique does not require the knowledge of a reaction mechanism, which is an interesting advantage for processes with complex reactions. Restricted chemical equilibrium can be applied either via temperature approach for the whole system, or by specifying temperature and heat duty.

The Gibbs free energy (G_{total}) for the gas products of a gasification process containing N species (i=1...N) is given by:

$$G_{total} = \sum_{i=1}^{N} n_i \Delta G_{f,i}^o + \sum_{i=1}^{N} n_i RT \ln \left(\frac{n_i}{\sum n_i}\right)$$
 7.1

where $\Delta G_{f,i}^o$ represents the Gibbs free energy of formation of species i (pressure of 100 kPa). Eq. 7.1 must be solved for the unknowns ($n_i = n_1 \dots n_7$) to minimize G_{total} , by a complete mass balance of individual elements. For instance, the quantity of hydrogen determined by ultimate analysis must be the same as the total quantity of hydrogen in the producer gas. This is independent of the reaction path or chemical formula. Therefore, for every element j Eq. 7.2 can be written.

$$\sum_{i=1}^{N} a_{i,j} n_i = A_j 7.2$$

The term $a_{i,j}$ represents the quantity of atoms of the element j in the species i, thus A_j accounts for the number of atoms of the element j injected in the reactor. The value of n_i is to be calculated in a fashion that brings G_{total} to a minimum. The Lagrange multiplier method can be used to solve these equations. The Lagrange function is presented in the form of Eq. 7.3, where λ_j is the Lagrangian multiplier for the element j.

$$L = G_{total} - \sum_{j=1}^{K} \lambda_j \left(\sum_{i=1}^{N} a_{i,j} n_i - A_j \right) \frac{kJ}{mol}$$
 7.3

The extremum point can be found by dividing Eq. 7.3 by RT and taking the derivative

$$\left(\frac{\partial L}{\partial n_i}\right) = 0 \tag{7.4}$$

Eq. 7.4 creates the set of non-linear equations into a matrix of that has *i* rows. Those are solved simultaneously by the integration technique with the constraints defined in Eq. 7.2.

7.1.2 Stoichiometric method (reactions enabled)

By enabling chemical reactions a more precise control of quasi-equilibrium conditions becomes possible, where temperature approach can be applied for every specified reaction. The possibility of changing the equilibrium temperature for different reactions is an alternative way to mimic kinetic-controlled behaviour in a chemical equilibrium model.

The stoichiometric method is based on the equilibrium constant; consequently, the model includes the chemical reactions and the species present. For

illustrative purpose, the following equations will be used as the desired gasification set of chemical reactions.

R1
$$CO_2 + C \leftrightarrow 2CO$$
 7.5

R2
$$C + H_2O \leftrightarrow CO + H_2$$
 7.6

R3
$$C + 2H_2 \leftrightarrow CH_4$$
 7.7

$$CO + H_2O \leftrightarrow CO_2 + H_2$$
 7.8

In the first step of the model development, it is necessary to select all species containing C, H and O, and/or other main elements. Minor elements expected in the producer gases are usually neglected. The number of species present in the producer gas dictates the number of unknowns, and, therefore, the number of equations necessary for solving the problem.

To demonstrate a set of equations necessary to solve a problem, the example of one mole of biomass gasified by d moles of steam and e moles of air will be used. The reaction of the biomass with steam and air (3.76 moles of nitrogen and 1 mole of oxygen) can be represented by:

$$CH_{a}O_{b}N_{c}+dH_{2}O+e(O_{2}+3.76N_{2})$$

$$\rightarrow n_{1}C+n_{2}H_{2}+n_{3}CO+n_{4}H_{2}O$$

$$+n_{5}CO_{2}+n_{6}CH_{4}+n_{7}N_{2}$$

$$7.9$$

Where $n_1 \dots n_7$ are stoichiometric coefficients. The chemical formula $CH_aO_bN_c$, found through the ultimate analysis of the biomass, represents a molecule of biomass and a,b and c are the mole ratios $\frac{H}{c}$, $\frac{O}{c}$ and $\frac{N}{c}$. Using a,b and c as input parameters the total number of unknowns is seven $(n_1 \dots n_7)$.

As this is a representation of a simple model, the whole gasification process will be represented by the two sets of equations presented below. The first set of equations to solve the system is generated by the atomic balance of the species (carbon, hydrogen, oxygen, and nitrogen) - the so-called stoichiometric equations.

C
$$n_1 + n_3 + n_5 + n_6 = 1$$
 7.10

$$2n_2 + 2n_4 + 4n_6 = a + 2d 7.11$$

$$0 n_3 + n_4 + 2n_5 = b + d + 2e 7.12$$

N
$$n_7 = c + 7.52e$$
 7.13

The remaining set of equations comes from the equilibrium constants of the gasification reactions. Subtracting steam gasification (R2) by the Boudouard reaction (R1) the result is the water–gas shift reaction (R4), making this equation redundant for this purpose. Subsequently, only the equilibrium of reactions R1, R2, and R3 are necessary, as the equations generated for solving the problem satisfy the number of unknowns.

For a reactor at pressure, P, the equilibrium constants for reactions R1, R2, a R3 are given by (Basu, 2010b):

$$K_{e1} = \frac{y_{CO}^2}{y_{CO_2}} P 7.14$$

$$K_{e2} = \frac{y_{CO}y_{H2}}{y_{H_2O}}$$
 7.15

$$K_{e3} = \frac{y_{CH_4}}{y_{H_2}^2} P 7.16$$

Where y_i represents the mole fraction for species i of CO, H_2 , H_2O , and CO_2 .

The equilibrium constant equations and the stoichiometric equations may be solved at the same time. Hence, by solving the seven equations (Eq. 7.10 to 7.16) the seven unknowns $(n_1 \dots n_7)$ can be found. This will give the composition and yield of producer gas.

This is a simplified example of the stoichiometric modelling of a gasification reactive process. The sophistication and complexity increases with the species and reactions considered.

7.2 ASPEN Plus gasification model

The gasification process is broken down into steps that are represented by operation blocks in a sequence that best fits the gasification process. Basic assumptions

The basic assumptions in the model are:

- **zero-dimensional:** chemical equilibrium model cannot deal with dimentions;
- **steady state regime:** it is not purpose of the model to simulate variation of properties over time;
- **isothermal reactor:** the reactor is considered as a perfectly insulated apparatus, i.e. heat losses are neglected. Gasifiers have heat losses to the environment, but this is incorporated in the enthalpy balance of the equilibrium model;
- N₂ does not react: product containing nitrogen such as NOx are hardly formed in fixed bed biomass gasification process and can be neglected from the model;

• **no tars and other heavy products:** This products are negligible in the producer gas and are not taken into account.

7.2.1 Physical property method

There is a range of thermodynamic models available in ASPEN Plus to calculate the physical properties of components and mixtures. These thermodynamic models calculate properties such as density, heat duty (heat loss), enthalpy and temperature. IDEAL was the method used to calculate all physical properties of the conventional components in the gasification process, as its simplicity provides quick and accurate results.

The IDEAL property method accommodates both Raoult's law and Henry's law, and can be used for solid processing where vapor-liquid equilibrium is unimportant (AspenTech, 2010). This method uses the:

- Ideal activity coefficient model for the liquid phase (2 = 1)
- Ideal gas equation of state Pv = RT for the vapor phase
- Rackett model for liquid molar volume

Biomass is a nonconventional component in ASPEN Plus, as it is not listed in the component list of Aspen, so it requires a different treatment to calculate its properties. As nonconventional components are heterogeneous solids that do not participate in chemical or phase equilibrium, the only physical properties that are calculated for nonconventional components are enthalpy and density (AspenTech, 2010). Therefore its enthalpy and density must be calculated separately. To calculate the enthalpy, the method HCOALGEN was used. It is the general coal model for computing enthalpy in the Aspen Physical Property. As there is no model for computing biomass properties, this was used due to the chemical composition

similarities between biomass and coal. It uses proximate and ultimate analysis of the biomass as input parameters.

DCOALIGT model was selected to calculate the biomass density; this model is also design to calculate the property of coal, where it gives true (skeletal or solid-phase) density of coal on a dry basis, but it was chosen for the same reason presented above. It uses ultimate and sulfur analyses. The model is based on equations from the Institute of Gas Technology (Institute of Gas Technology, 1978).

7.2.2 Model description (breaking down the gasification process)

To model a gasifier using ASPEN Plus, it is necessary to break down the process into several sub-processes that can be represented by the operations blocks available in ASPEN (Paviet et al., 2009; Ramzan et al., 2011).

The CFiBR has two major reacting stages: the formation of the reactive atmosphere (production of attack gases) by the combustion of propane in the combustion chamber; and the gasification of the charcoal by the attack gases. To model the CFiBR, It is necessary to break down these two stages into four operation blocks and eight material streams as shown in the process flow sheet (Figure 7.1).

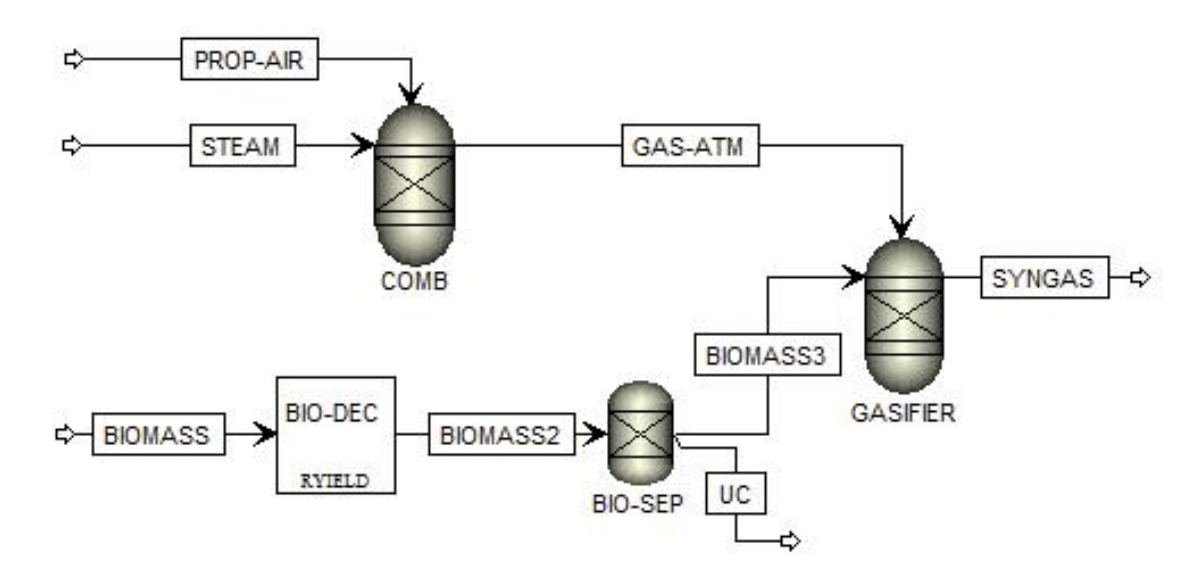


Figure 7.1: ASPEN Plus flow sheet of charcoal gasification in the CFiBR

The Table 7.1 and Table 7.2 describes every component presented in the Figure 7.1.

Table 7.1: Description of ASPEN Plus flowsheet unit operation blocks presented in Figure 7.1

ASPEN Plus ID	Block ID	Description
RYIELD	BIO-DEC	Yield reactor – converts the non-conventional stream BIOMASS into conventional components (C, H, O, N and ash)
SEP2	BIO-SEP	Separator – extracts a portion of the carbon on the feedstock to represent un-reacted charcoal removed from the bottom of the reactor
RGIBBS GASIFIER		Gibbs free energy reactor – calculates the equilibrium composition of the combustion products formed in the combustion chamber
		Gibbs free energy reactor – simulates drying and pyrolysis, partial oxidation

Table 7.2: Description of ASPEN Plus flowsheet streams presented in Figure 7.1

Stream name	Description
PROP-AIR	Specifies the mixture of propane and air composition to be burnt in the block COMB
STEAM	Inject the water vapor in the block COMB
GAS-ATM	Represents the combustion products generated at the block COMB. It transport the products to the bloc GASIFIER
BIOMASS	Specifies the charcoal as a nonconventional stream to be entered at the BIO-DEC. Thermodynamic conditions, as well as ultimate and proximate analysis, and mass flow rate were specified.
BIOMASS2	Resulted from the block BIO-DEC, presents the charcoal in the form of ASPEN Plus conventional components.
UC	Separates the unreacted carbon and ash from the charcoal to be input in the block GASIFIER. The amount is defined by the user
BIOMASS3	Input the remaining charcoal into the block GASIFIER
SYNGAS	This represents the outlet of the block GASIFIER, i.e. the producer gas from the gasifier

From Figure 7.1, the streams PROP-AIR and STEAM enter the block COMB.

The function of this block is to simulate the combustion of the inlet mixture and provide the characteristics of the attack gases.

The stream BIOMASS was specified as a non-conventional stream. Any material, such as charcoal, which is not in ASPEN Plus material library, needs to be introduced as a nonconventional material. Thermodynamic conditions, as well as ultimate and proximate analysis and mass flow rate were specified. The model HCOALGEN was used to calculate the enthalpy based on the value of HHV manually input (see Table 7.3). The model DCOALIGT calculated the density.

The next block is BIO-DEC, its purpose is to decompose the biomass into conventional components (C, H, O, N, and ash) based on the charcoal ultimate and proximate analysis. The results are carried to the next block by the stream BIOMASS2. The block BIO-SEP receives the stream BIOMASS2 and separates the products into two streams, UC and BIOMASS3.

The stream UC contains the unreacted charcoal and ash. To avoid total conversion of the carbon, and therefore the miscalculation of the producer gas composition, the unreacted charcoal and ash are not allowed to enter into the block GASIFIER. The amount of charcoal diverted is defined based on the validation experiments.

The attack gases (GAS-ATM) and the charcoal decomposed into elements (BIOMASS3) go into the block GASIFIER.

Three solutions methods are used to simulate the gasifier, each involving only a change to the block GASIFIER in Figure 7.1. The three methods are:

- Non-stoichiometric equilibrium method (minimization of the Gibbs free energy);
- Non-stoichiometric restricted equilibrium method with system temperature approach;
- Stoichiometric restricted chemical equilibrium method with reactionspecific temperature approach.

Table 7.3 and Table 7.4 show the information of the feedstock and the input parameters used in the model.

Table 7.3: Feedstock Proximate and Ultimate analysis

	Charcoal
Proximate (wt. % db)	
Volatile matter	4.9
Fixed carbon	93.7
Ash	1.4
Ultimate	
С	89.8
Н	2.2
0	6.1
N	<0.2
S	<0.002
Calorific value (MJ/kg)	
HHV	32.42

Table 7.4: Simulation initial properties

	Experiment A and B	Experiment C
Reactants flow (g/min)		
Char feeding rate	25	25
Air	235.50	237.61
Propane	12.59	13.35
Added water vapour	12.20	18.41
Unreacted carbon removed via UC	7.4	8.8
Block temperature (°C)		
PROP-AIR	25	25
STEAM	1000	1000
BIOMASS	25	25
GAS-ATM	1060	1080
GASIFIER	870	870
Total Pressure (atm)	1.01	1.01

7.2.2.1 Non-stoichiometric equilibrium method (minimization of -Gibbs free energy)

Two sets of simulations are presented in this section. The first uses the GASIFIER temperature as the chemical equilibrium temperature. The second simulation restricts the equilibrium by the application of temperature approach for the entire system.

A) Without temperature approach

The overall results in Table 7.5 and Table 7.6 show good agreement with the experiments. However, the producer gas results presents an over calculation of carbon monoxide by 3.3 points; and an under calculation of hydrogen of 1.76 points in Experiment A and B. This margin is even greater in Experiment C.

Table 7.5: Experimental results versus model predictions by Nonstoichiometric equilibrium for Experiment A and B.

	ASPEN	Experiment	Difference
02	6.75E-18	0.00%	0.00
N2	58.67%	60.67%	2.00
H2O	7.53%	6.35%	-1.18
H2	11.76%	13.52%	1.76
СО	14.28%	10.99%	-3.29
CH4	3.66E-06	0.10%	0.10
CO2	7.76%	8.37%	0.60
Total Mole	100.00%	100.00%	

Table 7.6: Experimental results versus model predictions by Nonstoichiometric equilibrium for Experiment C

	ASPEN	Experiment	Difference
02	0.00%	0.00%	0.00
N2	57.44%	56.80%	-0.65
H2O	10.50%	8.99%	-1.51
H2	11.82%	13.96%	2.14
СО	11.46%	7.30%	-4.16
CH4	0.00%	0.18%	0.18
CO2	8.77%	12.77%	4.00
Total Mole	100.00%	100.00%	

B) Temperature approach

A sensitivity analysis was applied to find the overall temperature approach which gives the best results. A variation of ±500 degrees over the GASIFIER temperature was studied. The variation of the mole fraction versus temperature approach (Tapp) can be observed in Figure 7.2 and Figure 7.3.

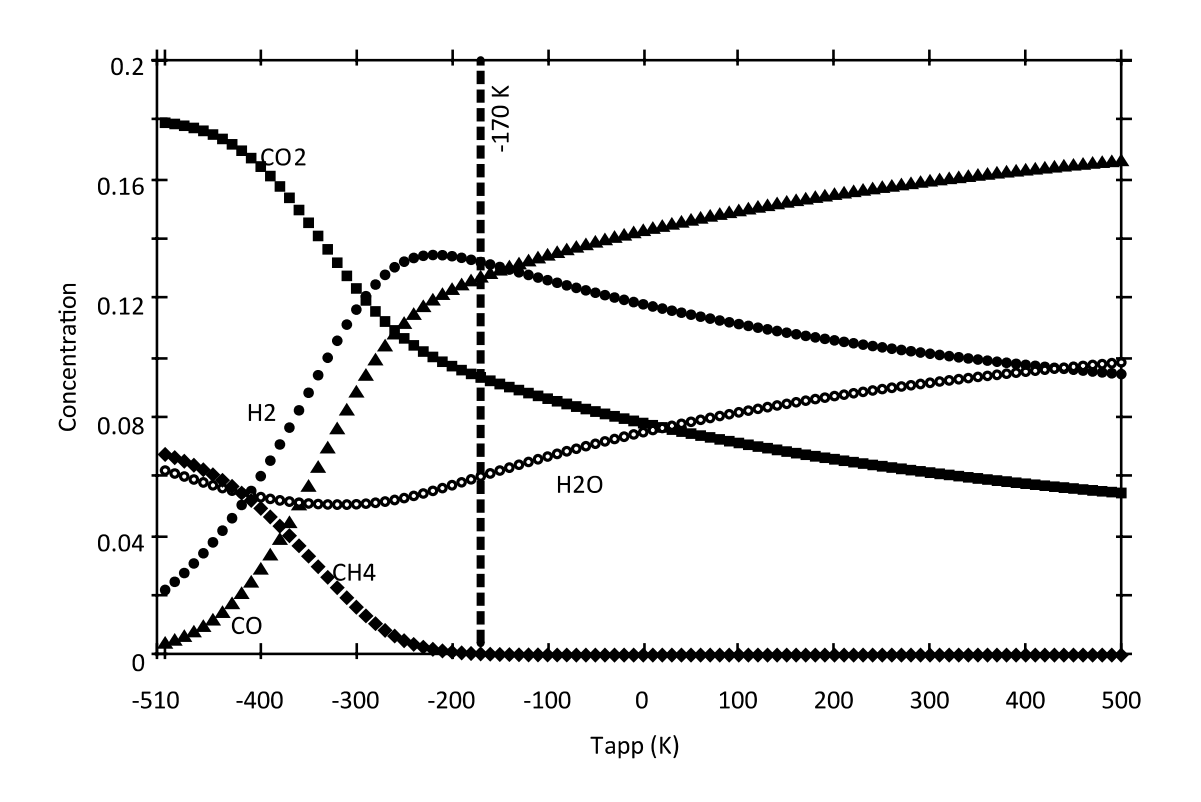


Figure 7.2: Temperature approach sensitivity analysis of Nonstoichiometric equilibrium model of Experiment A and B.

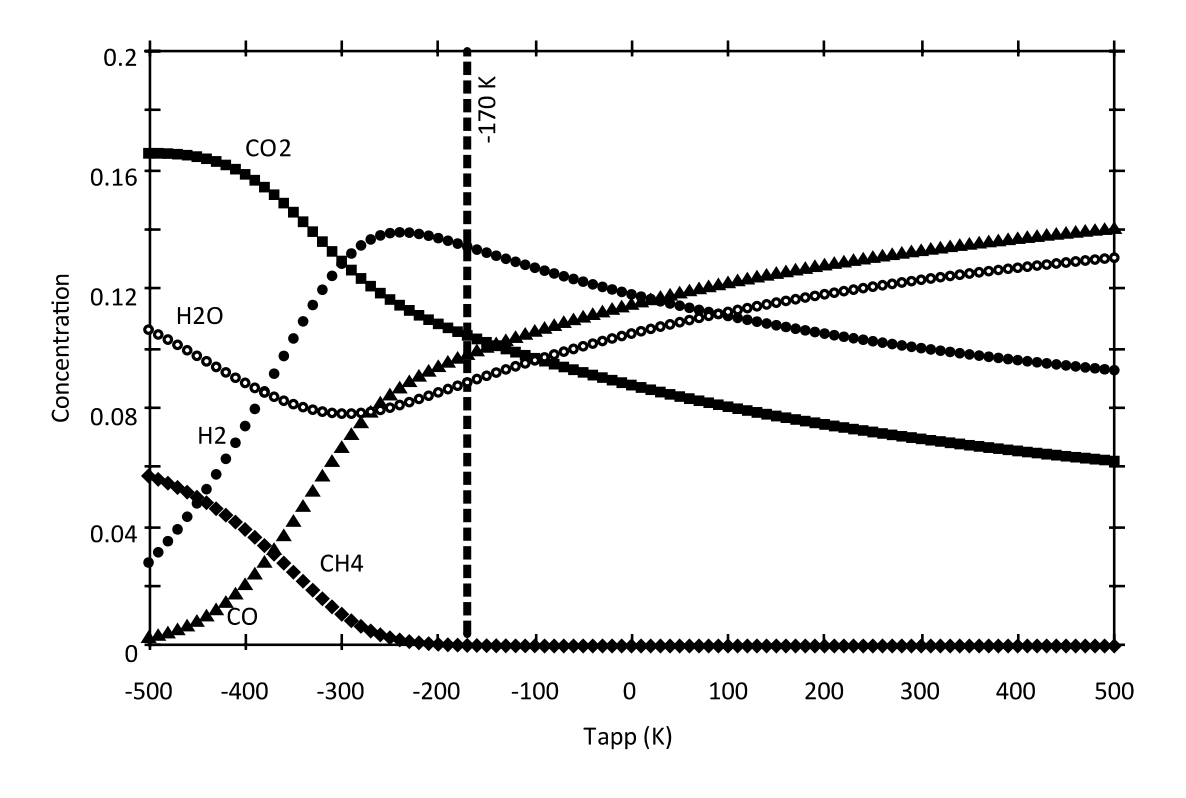


Figure 7.3: Temperature approach sensitivity analysis of Nonstoichiometric equilibrium model of Experiment C.

It was found that a temperature approach of -170K presents better agreement with the experimental results according to root means square error, when compared to the previous simulation (see Table 7.7 and Table 7.8). Nevertheless, carbon monoxide and carbon dioxide still present a difference of over two points.

Table 7.7: Experimental results versus model predictions by Nonstoichiometric equilibrium with temperature approach for Experiment A.

	ASPEN	Experiment	Difference
O2	3.00E-22	0.00%	0.00
N2	58.74%	60.67%	1.93
H2O	6.04%	6.35%	0.31
H2	13.19%	13.52%	0.33
СО	12.63%	10.99%	-1.64
CH4	3.99E-04	0.10%	0.06
CO2	9.36%	8.37%	-0.99
Total Mole	100.00%	100.0%	

Table 7.8: Experimental results versus model predictions by Nonstoichiometric equilibrium with temperature approach for Experiment C.

	ASPEN	Experiment	Difference
O2	0.00%	0.00%	0.00
N2	57.47%	56.80%	-0.67
H2O	8.86%	8.99%	0.13
H2	13.43%	13.96%	0.53
CO	9.77%	7.30%	-2.48
CH4	0.02%	0.18%	0.16
CO2	10.44%	12.77%	2.33
Total Mole	100.00%	100.00%	

7.2.3 Stoichiometric method (reactions enabled)

The use of the stoichiometric method requires the specification of the reactions, such that the number of products is equal to the sum of the number of reactions and elements. Furthermore, the equations must be linearly independent (Schefflan, 2011).

$$C + 2H_2 \rightarrow CH_4 \qquad 7.17$$

$$CH_4 + H_2O \rightarrow CO + 3H_2$$
 7.18

$$CO + H_2O \rightarrow CO_2 + H_2$$
 7.19

$$C + O_2 \rightarrow CO_2 \qquad 7.20$$

$$N_2 + 2O_2 \rightarrow 2NO_2$$
 7.21

Sensitive analysis was applied to every equation, except Eq. 7.21 that has no influence on the results, as N_2 is considered inert. This equation was used only to satisfy solution process restriction. A variation of ± 500 degrees was applied to each reaction in turn, while the remaining reactions were kept with no temperature approach.

7.2.3.1 Sensitivity analysis – Reaction 7.17

Figure 7.4 and Figure 7.5 show the results for the sensitivity analysis of temperature approach in Eq. 7.17. The result shows that this reaction only gives a variation in the product mole fractions under -350 degrees of temperature approach.

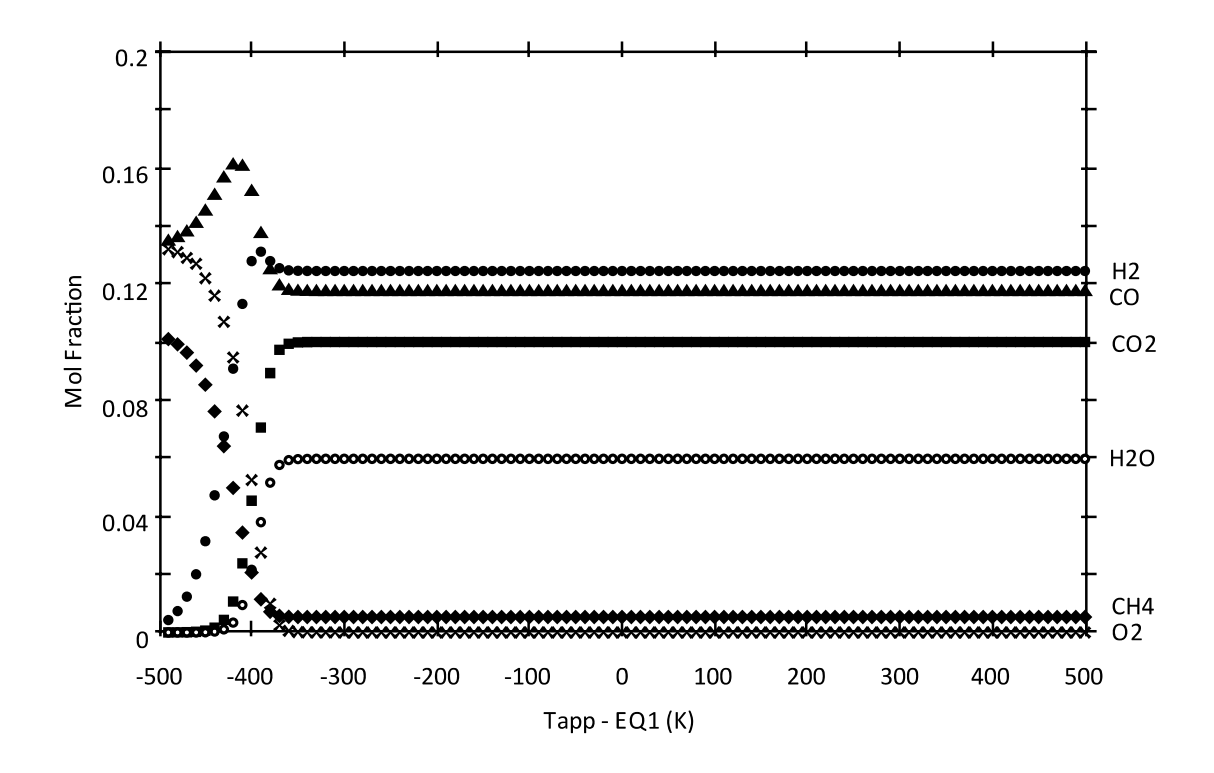


Figure 7.4: Temperature approach sensitivity analysis of Eq. 5.6 for Experiment A and B.

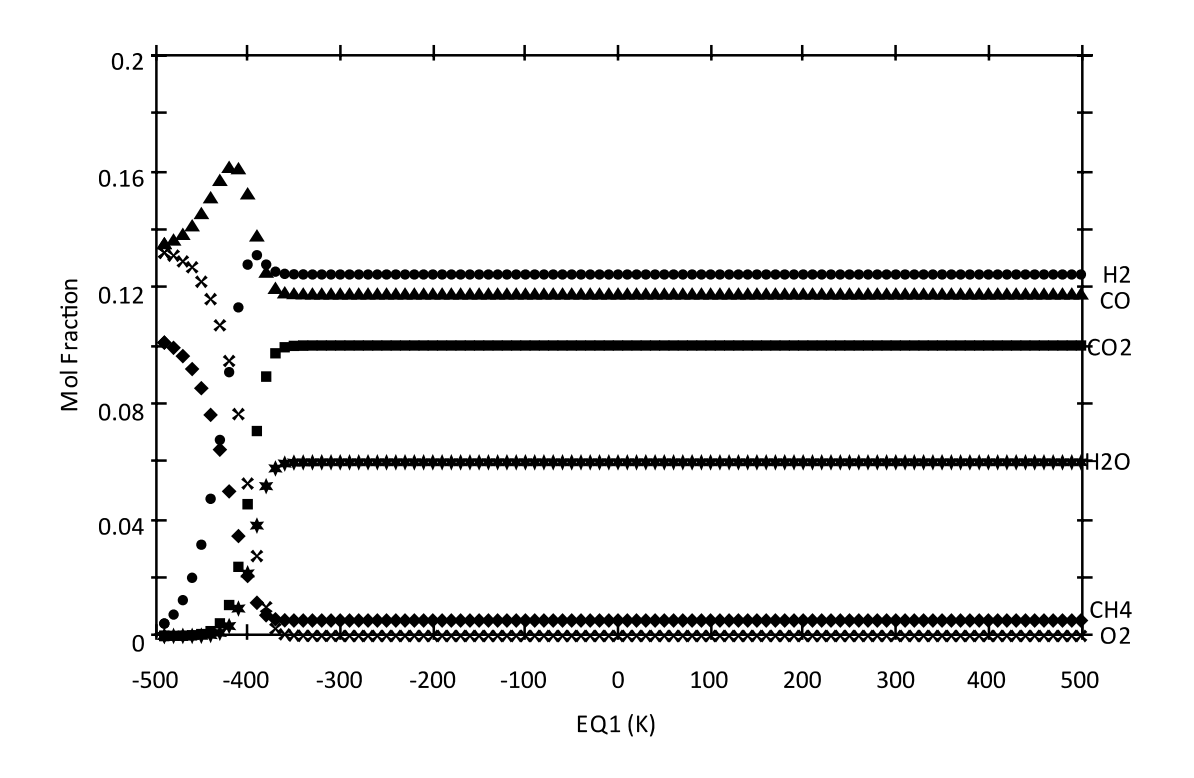


Figure 7.5: Temperature approach sensitivity analysis of Eq. 5.6 for Experiment C.

7.2.3.2 Sensitivity analysis – Reaction 7.18

The results for the sensitivity analysis of temperature approach in Eq. 7.18 can be observed in Figure 7.6 and Figure 7.7. In this reaction, hydrogen, and carbon monoxide mole fractions increase rapidly until a temperature approach of -250 degrees is reached, while methane and carbon dioxide decrease at the same pace.

Over a temperature approach of -250 degrees, the products mole fraction stabilises.

Water mole fraction variation is negligible.

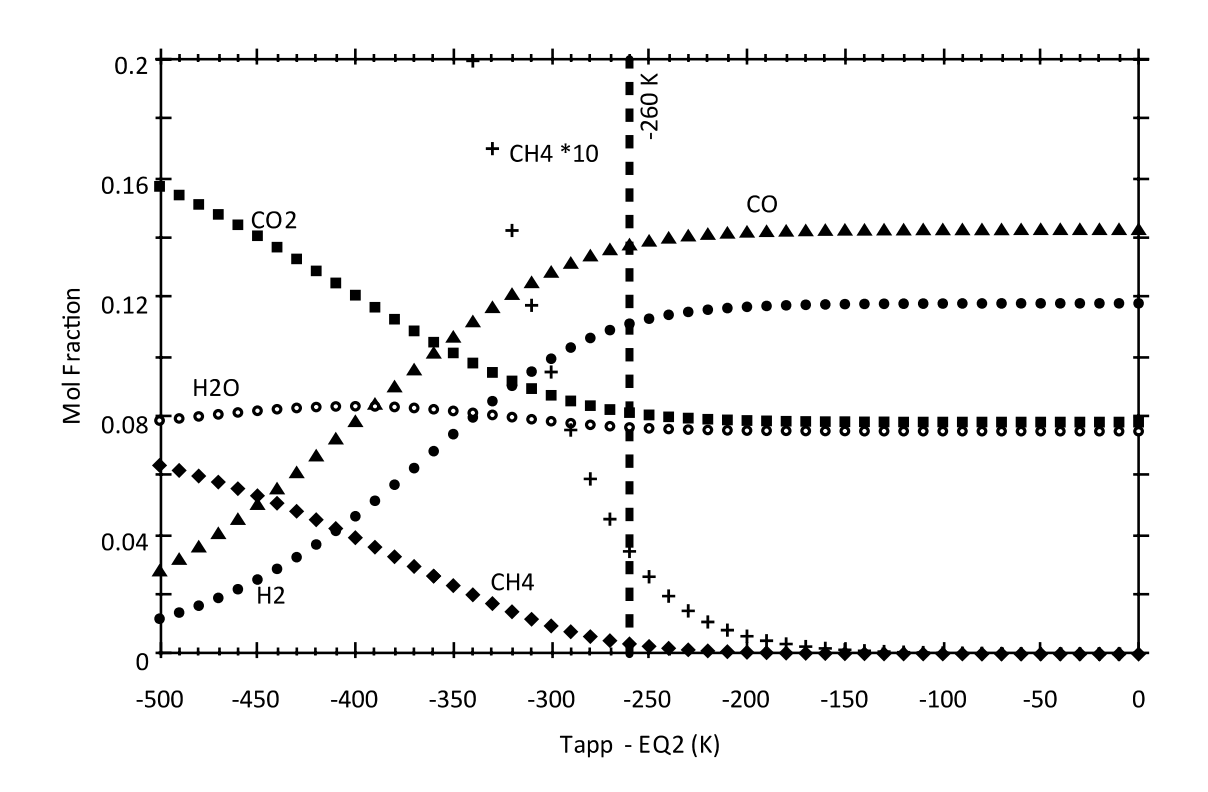


Figure 7.6: Temperature approach sensitivity analysis of Eq. 5.4 for Experiment A and B.

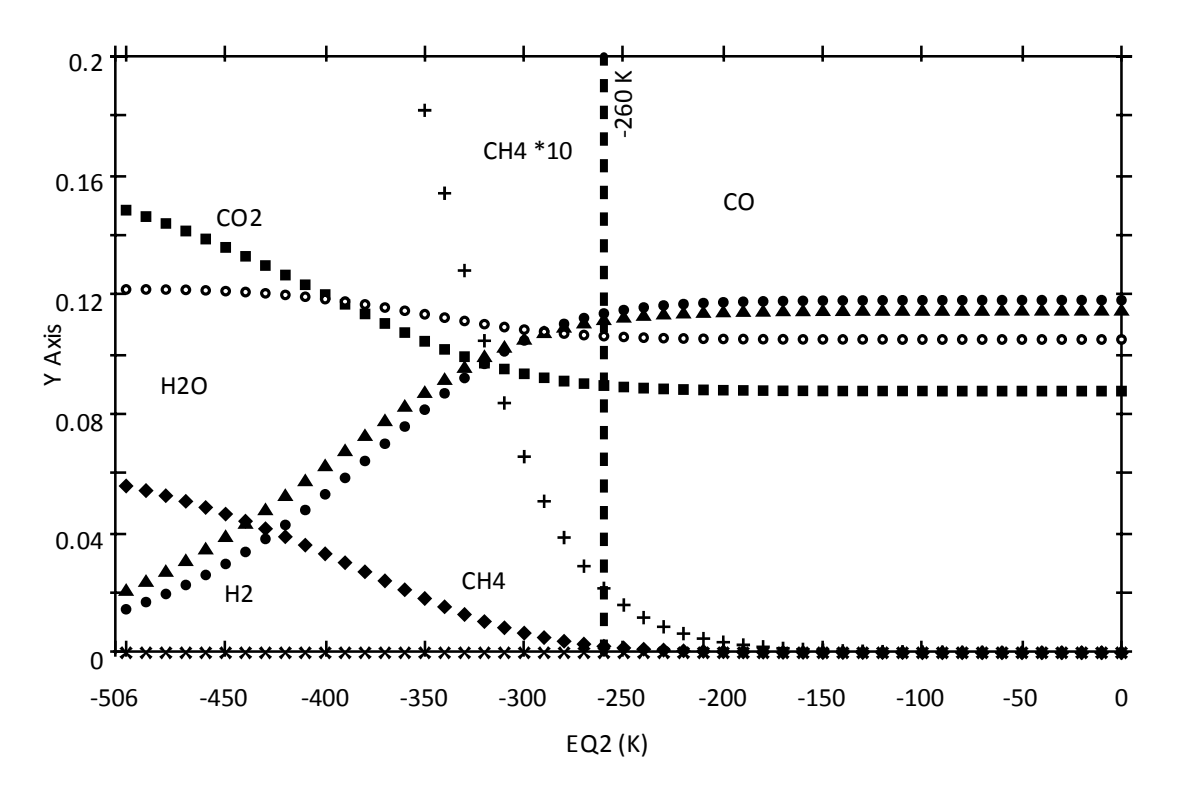


Figure 7.7: Temperature approach sensitivity analysis of Eq. 5.4 for Experiment C.

7.2.3.3 Sensitivity analysis – Reaction 7.19

Figure 7.8 and Figure 7.9 show the results for the sensitivity analysis of temperature approach in Eq. 7.19. In this reaction, the mole fraction of carbon monoxide and carbon dioxide increases, while hydrogen and water decreases. The changes in mole fraction are smooth. Methane and oxygen are not presented in the graph, as they do not appear in significant quantity.

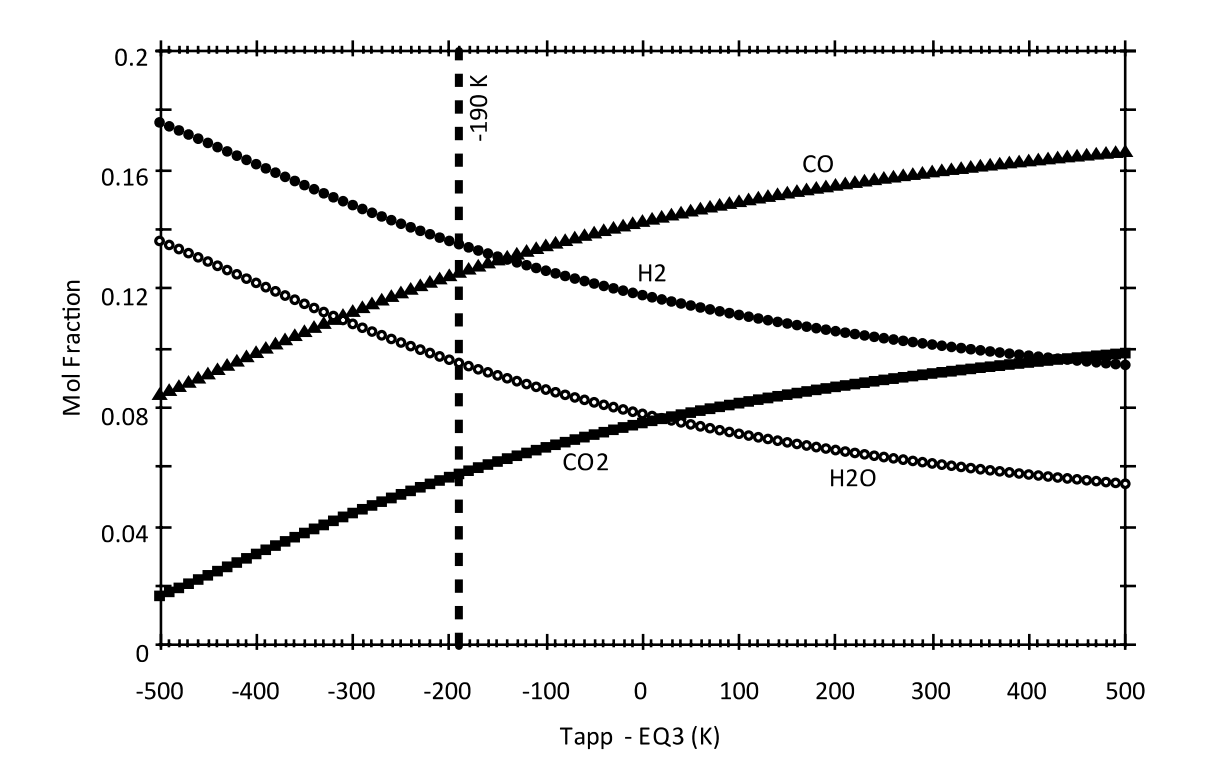


Figure 7.8: Temperature approach sensitivity analysis of Eq. 7.19 for Experiment A.

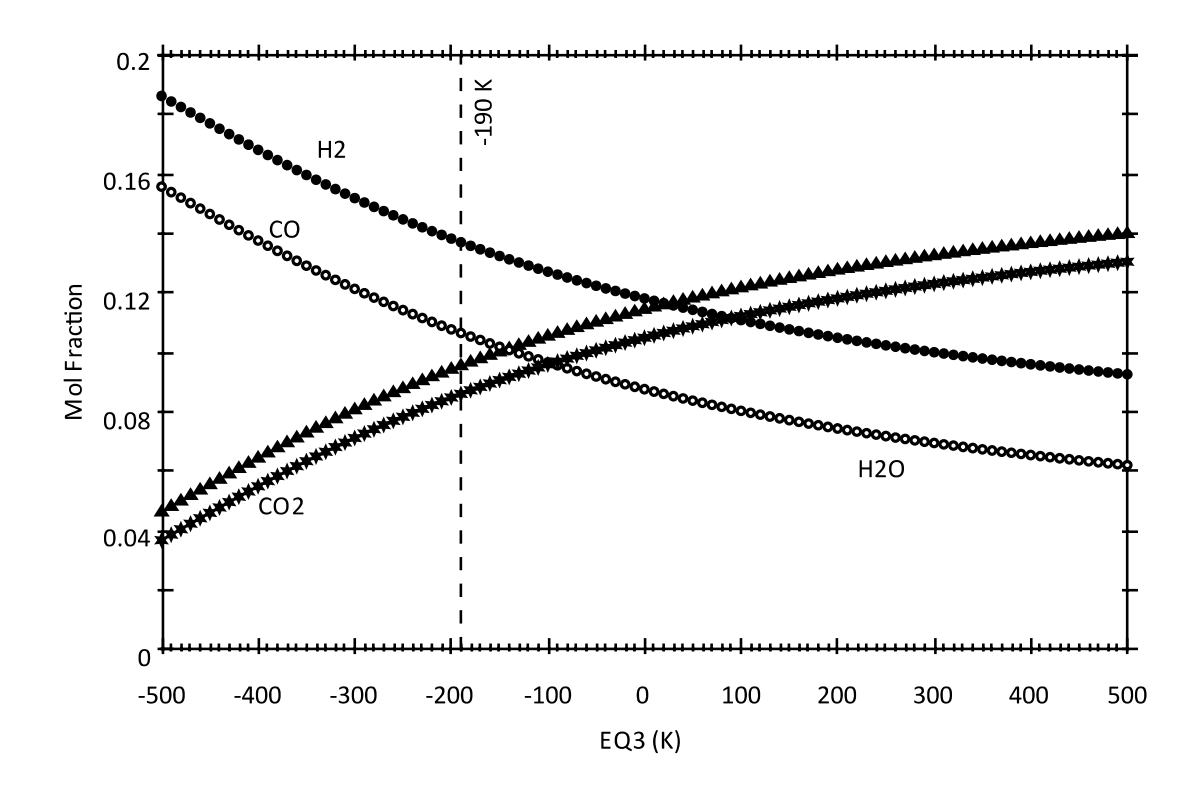


Figure 7.9: Temperature approach sensitivity analysis of Eq. 7.19 for Experiment C.

7.2.3.4 Sensitivity analysis – Reaction 7.20

Figure 7.10 and Figure 7.11 show the results for the sensitivity analysis of temperature approach in Eq. 7.20. No change in mole fraction is presented within the range of temperature approach studied. As presented in previous studies, this reaction has little influence on the biomass gasification process (Van de Steene et al., 2010; Higman & Van Der Burgt, 2003; Zainal, 1996).

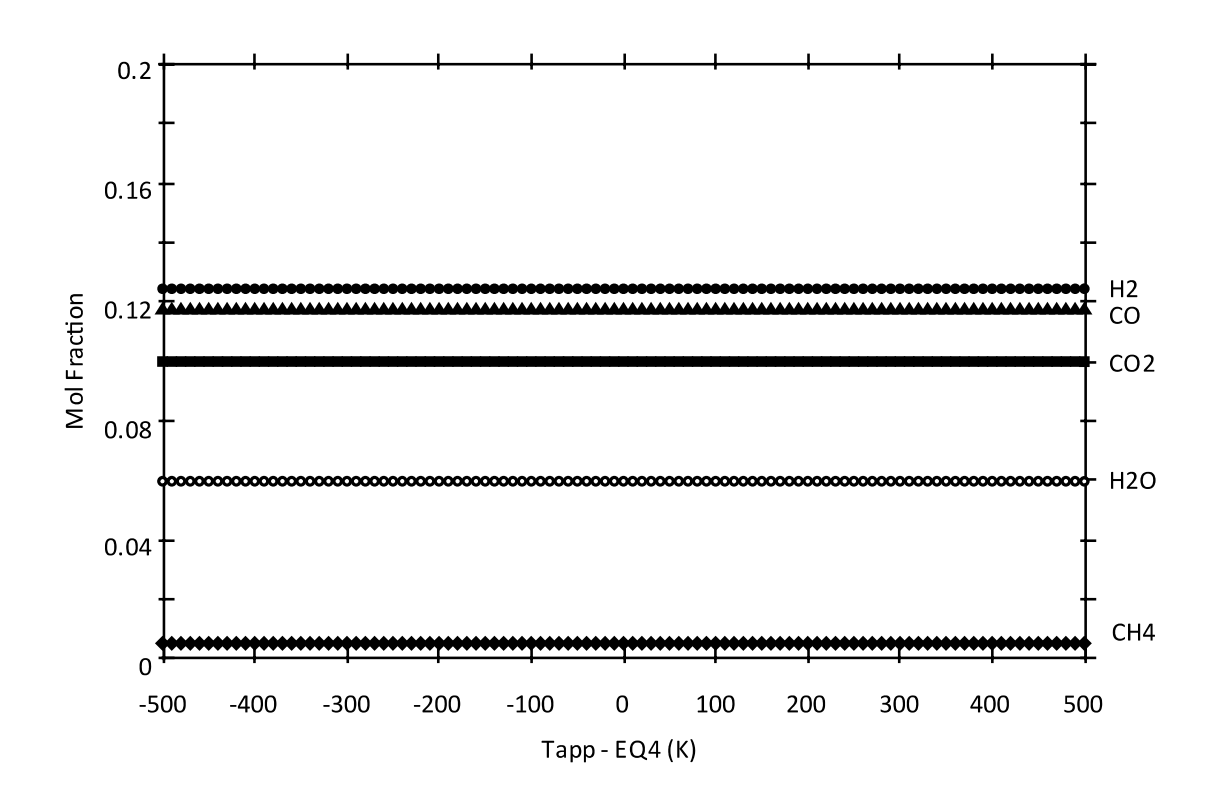


Figure 7.10: Temperature approach sensitivity analysis of Eq. 7.20 for Experiment A.

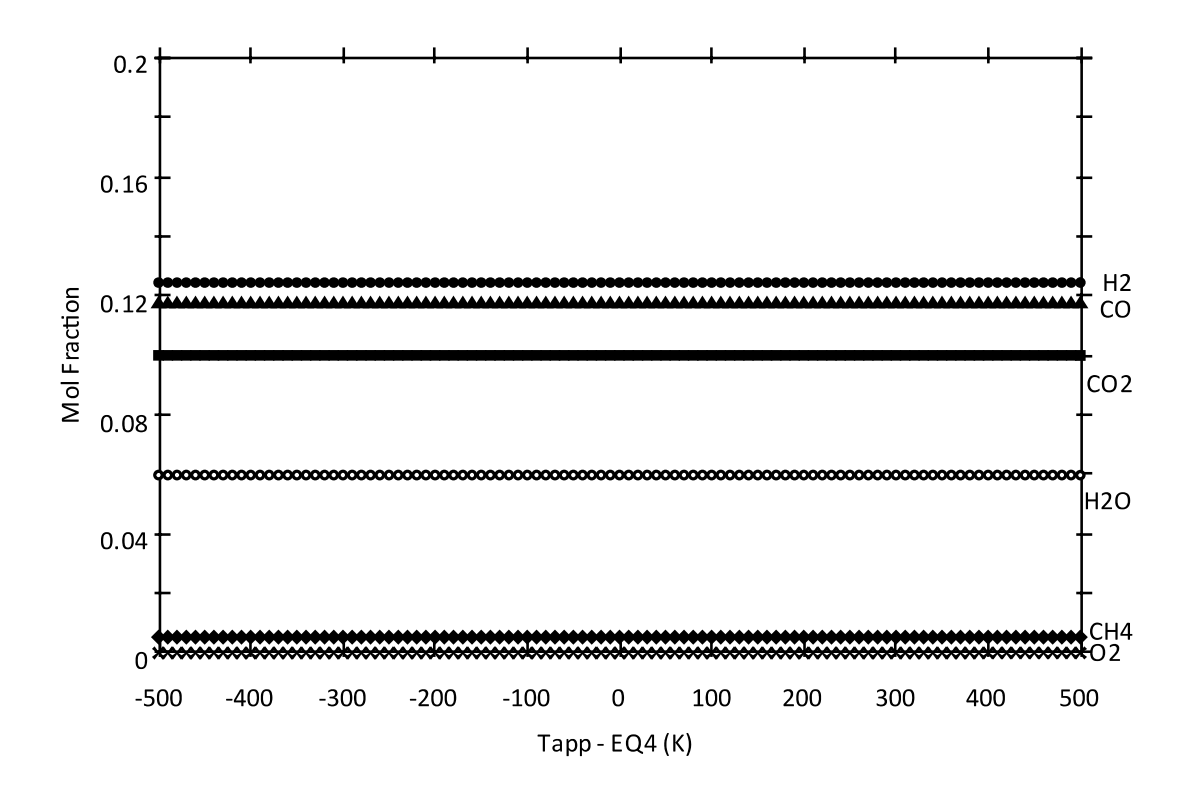


Figure 7.11: Temperature approach sensitivity analysis of Eq. 7.20 for Experiment C.

7.2.3.5 Optimized method

EQ1 and EQ4 presented insignificant influence on the mole fraction of the producer gas. Hence for the optimised method, only EQ2 and EQ3 will be taken into account, with temperature approach applied to both reactions simultaneously. Temperature approach is applied to EQ2 with the aim of finding the optimum mole fraction of CO₂ and CH₄. Once this optimum point is found, temperature approach is applied to EQ3 to get the optimum mole fraction of CO and H₂. The optimum temperature approaches for the reactions are -260 for EQ2 and -170 for EQ3.

The results of the optimized method are shown in Table 7.9 and Table 7.10. It can be seen that this method presents better agreement with the experimental results, when compared to the previous simulation. All the products present difference of less than 2 points.

Table 7.9: Experimental results versus model predictions by Stoichiometric method for Experiment A.

	ASPEN	Experiment	Difference
02	0.00%	0.00%	0.00
N2	59.30%	60.67%	1.37
H2O	5.98%	6.35%	0.37
H2	12.45%	13.52%	1.07
СО	11.74%	10.99%	-0.75
CH4	0.53%	0.10%	-0.43
CO2	10.00%	8.37%	-1.63
Total Mole	100.00%	100.00%	

Table 7.10: Experimental results versus model predictions by Stoichiometric method for Experiment C.

	ASPEN	Experiment	Difference
02	0.00%	0.00%	0.00
N2	57.81%	56.80%	-1.01
H2O	8.80%	8.99%	0.19
H2	13.03%	13.96%	0.93

CHAPTER 7 – SIMULATION OF CHAR GASIFICATION PROCESS IN A CONTINUOUS FIXED BED REACTOR USING ASPEN PLUS

CO	9.12%	7.30%	-1.82
CH4	0.32%	0.18%	-0.14
CO2	10.92%	12.77%	1.85
Total Mole	100.00%	100.00%	

All the results show good agreement with the experimental data for the attack gasses (GAS-ATM). This is easily comprehended, as the process simulated comprises of the combustion of a well-stirred mixture of gasses, with enough time to reach equilibrium.

7.3 Validation of the simulation results

The model presented in this thesis has been compared to experimental work developed by (Van de Steene et al., 2010). The input parameters introduced in the model are presented in Table 7.11.

Table 7.11: Summary of input data of the validation experiment.

	Van de Steene (2010)
Reactants flow (g/min)	
Char feeding rate	25
Air	231.01
Propane	11.78
Added water vapour	35
Unreacted carbon removed via UC	3.1
Block temperature (°C)	
PROP-AIR	25
STEAM	1000
BIOMASS	25
GAS-ATM	1020
GASIFIER	850
Total Pressure (atm)	1.01

The results for validation of the model are presented in the Table 7.12, Table 7.13, and Table 7.14. All the methods presented fair agreement, and with the stoichiometric method the highest difference in mole fraction was -0.67 points.

Table 7.12: Experimental results versus model predictions by Non-stoichiometric equilibrium for Van de Steene (2010)

	ASPEN	Experiment	Difference
02	0.00%	0.00%	0.00
N2	51.50%	52.12%	0.63
H2O	12.62%	10.09%	-2.53
H2	14.26%	16.37%	2.11
СО	12.74%	10.09%	-2.65
CH4	0.0002%	0.21%	0.21
CO2	8.88%	11.12%	2.23
Total Mole	100.00%	100.00%	

Table 7.13: Experimental results versus model predictions by Non-stoichiometric equilibrium with temperature approach for Van de Steene (2010)

	ASPEN	Experiment	Difference
02	0.00%	0.00%	0.00
N2	51.52%	52.12%	0.60
H2O	10.88%	10.09%	-0.79
H2	15.97%	16.37%	0.40
СО	10.97%	10.09%	-0.88
CH4	0.01%	0.21%	0.20
CO2	10.64%	11.12%	0.48
Total Mole	100.00%	100.00%	

Table 7.14: Experimental results versus model predictions by Stoichiometric method for Van de Steene (2010)

	ASPEN	Experiment	Difference
02	0.00%	0.00%	0.00
N2	51.71%	52.12%	0.42
H2O	10.76%	10.09%	-0.67
H2	15.83%	16.37%	0.54
CO	10.48%	10.09%	-0.39
CH4	0.20%	0.21%	0.01
CO2	11.03%	11.12%	0.09
Total Mole	100.00%	100.00%	

7.4 Conclusions

The main objective in this chapter was to develop and validate a numerical method in ASPEN Plus to simulate charcoal gasification in a continuous fixed bed reactor.

The principles of ASPEN Plus simulation were described, as well as, the theory behind the RGibbs reactor model, and the physical property methods available. The necessity of breaking down the gasification process into steps was described, together with the itemization of all the blocks and streams used.

The understanding of charcoal gasification in a continuous fixed bed reactor, thoroughly explained in the previous chapter, allowed the development of an isothermal steady state equilibrium model. This model has three variations as described below:

- Non-stoichiometric equilibrium method: applies the minimization of the Gibbs free energy to model the equilibrium of charcoal gasification;
- Non-stoichiometric equilibrium method with temperature approach: same as above, but allows better results by an overall temperature approach;

• Stoichiometric method: uses chemical reactions to calculate the equilibrium of charcoal gasification. It allows simulation of quasi-equilibrium by temperature approach in different reactions.

Results from all the three approaches were compared to the experimental data and to data from literature. The best agreement was obtained for the stoichiometric method, where the highest difference in mole fraction was -0.67 points. The possibility of calculating the gas creation/destruction contribution, from every reaction, allows a more precise control of the producer gas concentration. The stoichiometric method developed here is able to calculate methane concentration at the same order of magnitude of experimental values, while previous papers are unable to calculate methane with the same accuracy.

As a conclusion, it can be stated that all the methods showed reasonable agreement with the experiments in the previous chapter. However the stoichiometric method provides better results than non-stoichiometric methods and the previous methods presented by other authors. For simulations where the reactions are unknown, it is recommended to use the non-stoichiometric method with overall temperature approach, because it does not require reactions and still provides fair results.

The sensitivity analysis of the reactions effect on producer gas concentration has shown that precise corrections can be made. Therefore, there is still margin for improvement, and reaction able to control unconverted char could be researched and implemented.

CHAPTER 8

GENERAL CONCLUSIONS

There is a vast amount of publish work on the many types of gasification, numerical and experimental. The experimental work on downdraft gasification, mainly focus on tests of several types of biomasses to research whether they are suitable or not. Experimental work that explores the interior of the gasifier, explores the behaviour of the gasifier and measures temperature and gas longitudinal profiles within the reactor is scarce.

Numerical modelling of gasification studies two main fronts: thermodynamic equilibrium models, and kinetic-based and computational fluid dynamics (CFD) models. The first is the most usual and focuses on two techniques; equilibrium constant and Gibbs free energy minimization. Overall, these models present reasonable results. Hydrogen, carbon monoxide, carbon dioxide, water, and nitrogen concentrations agree to the experimental results reasonably well. However, methane is underestimated by most of the models.

Kinetic based models of downdraft gasification, modelling dynamic and steady state process are less common; even less explored are CFD ones. In general, those models require a large set of information to be developed, such as, biomass physicochemical properties, kinetic parameters, as well as a large set of gasification experimental data to validate the model. Therefore, they are more difficult to developed in addition to require larger computational power. Most of the models focus on 1D process; the models covering 2D and 3D are rare. Results produced are far

from being accurate, but they already present fair agreement with the thermal behaviour and composition of gas and temperature profiles.

The scope of this project was to investigate the reduction zone of a downdraft gasifier, to provide the necessary data for development and validation of 2D CFD codes to simulate the behaviour of the gasification zone of a downdraft gasifier, and to develop an Aspen Plus model for char gasification. Overall the main objectives of this work have been accomplished according to the following points.

8.1 Char gasification in a continuous fixed bed reactor - CFiBR

Over a hundred hours of experiments were performed to study two different gasification conditions successfully. It was shown the existence of temperature gradients across the bed, which decreases from the top to the bottom and from the centre to the wall. Gas concentrations changes in the longitudinal direction as expected, but it did not present any relevant change in the radial direction.

The temperature gradient data and the gas longitudinal profile give a clear picture of the gasification of the charcoal and generation of producer gas, as well as showing that most of chemical reactions took place in the first 15 centimetres of bed of the CFiBR where 85% of the char is converted. Three main areas have been identified along the reactor, from top to bottom they are:

- Region 1: Above bed level (T4 = 60 cm from the bottom) a decrease of temperature is observed due to convective heat loss to the wall only, as the reactive atmosphere has not yet encountered the char bed.
- Region 2: Between T4 and T6, once the reactive atmosphere reaches the charcoal bed, the temperature drops rapidly; the radial gradient increases and the temperature in the wall is up to 60 C lower than in the centre.

 Region 3: Under T6, the temperature decrease is less pronounced and the longitudinal gradient reduces. The radial gradient becomes stable, where the maximum radial temperature variation between the centre and the wall is 65 °C for Experiment A/B and 38 °C for Experiment C.

Overall, the results presented a series of data that can be used for numerical model development and validation, which is an effective contribution to the conception, design and development of gasification reactors

8.2 Gasification in a 25kW throated fixed bed biomass gasifier

A commercial available throated biomass gasifier (GEK) was successfully modified to measure axial and longitudinal temperature in the reduction zone. A sampling line developed according to the European tar protocol further complemented this unit, as well as two orifices plates to measure airflow in and producer gas outlet stream, and a specially design set of multipoint thermocouples to measures. This was meant to make the GEK capable of measuring temperature profile in the longitudinal and radial direction, in addition of gas and tar sampling and measurement.

Eleven successful trials were performed with this setup, using six different mixtures of biomass. The data collected under these conditions allowed the analysis and interpretation of the phenomena occurring within the throat of the gasifier bed during gasification. Where of temperature gradients across the bed was confirmed. The temperature decreases from the top to the bottom and from the centre to the wall.

In similar fashion to the experiments with the CFiBR, the data collected from the GEK experiments offers a significant amount of information to support the development of numerical models.

8.3 Simulation of char gasification process in a continuous fixed bed reactor using aspen plus

A numerical method in ASPEN Plus to simulate charcoal gasification in a continuous fixed bed reactor was developed and validated successfully. This model has three variations, non-stoichiometric, non-stoichiometric equilibrium method with temperature approach, stoichiometric method.

Overall, all the three approaches presented fair agreement to experiments. But the stoichiometric method gave better results for producer gas concentration, where the highest difference in mole fraction was -0.67 points.

SUGGESTIONS FOR FURTHER WORK

Numerous studies could be performed to take advantage of the work presented in the thesis and continue the development of the field of gasification. A few examples are:

- 2D/3D CFD modelling of charcoal gasification. This could be validated with the data presented in the chapter 5;
- 2D/3D CFD modelling of biomass gasification. This could be validated with the data presented in the chapter 5;
- Aspen modelling using reaction kinetics to model fixed bed gasification;
- Development of technique to perform longitudinal and radial gas measurements in a GEK;

REFERENCES

- All Power Labs (2008) Gasifier Types « Gasifier Experimenters Kit [Internet]. Available from: http://gekgasifier.com/gasification-basics/gasifier-types/ [Accessed 2010].
- Allaire, S.E. & Parent, L.E. (2003) Size Guide Number and Rosin–Rammler Approaches to describe Particle Size Distribution of Granular Organic-based Fertilisers. *Biosystems Engineering*, 86 (4), pp.503–509. Available from: http://linkinghub.elsevier.com/retrieve/pii/S1537511003001624.
- Allen, T. (1996) *Particle Size Measurement: Surface area and pore size determination*. Springer. Available from: http://books.google.com/books?id=EfLGn1mtLCoC\&pgis=1.
- Altafini, C.R., Wander, P.R. & Barreto, R.M. (2003) Prediction of the working parameters of a wood waste gasifier through an equilibrium model. *Energy Conversion and Management*, 44 (17), pp.2763–2777. Available from: http://linkinghub.elsevier.com/retrieve/pii/S0196890403000256.
- Antonopoulos, I.S., Karagiannidis, A., Gkouletsos, A. & Perkoulidis, G. (2012) Modelling of a downdraft gasifier fed by agricultural residues. *Waste Management*, 32 (4), pp.710–718. Available from: http://linkinghub.elsevier.com/retrieve/pii/S0956053X1100585X.
- AspenTech (2010) Aspen Physical Property System. 7 ed. Burlington, MA, Aspen Technology, Inc.
- ASTM Standard E203 (2008) *Standard Test Method for Water Using Volumetric Karl Fischer Titration*. West Conshohocken, PA, ASTM International.
- Babu, B.V. & Chaurasia, A.S. (2003) Modeling, simulation and estimation of optimum parameters in pyrolysis of biomass. *Energy Conversion and Management*, 44 (13), pp.2135–2158. Available from: http://linkinghub.elsevier.com/retrieve/pii/S0196890402002376.
- Babu, S.P. (1995) Thermal gasification of biomass technology developments: End of task report for 1992 to 1994. *Biomass and Bioenergy*, 9 (1-5), pp.271–285. Available from: http://linkinghub.elsevier.com/retrieve/pii/0961953495000968>.
- Basu, P. (2010a) Biomass Gasification and Pyrolysis. Academic Press.
- Basu, P. (2010b) Biomass Gasification and Pyrolysis. Academic Press.
- Basu, P. (2010c) Chapter 6 Design of Biomass Gasifiers. In: *Biomass Gasification and Pyrolysis*. Academic Press.
- Boundy, B., Diegel, S.W., Wright, L. & Davis, S.C. (2011) Biomass Energy Data Book. U.S

- Department of Energy. Available from: http://cta.ornl.gov/bedb/index.shtml.
- Box, G.E.P. & Draper, N.R. (1987) *Empirical Model-Building and Response Surfaces*. E. B. Wiley-InterscienceWiley-Interscience eds. Wiley. Available from: http://psycnet.apa.org/psycinfo/1987-97236-000>.
- Brandt, P., Larsen, E. & Henriksen, U. (2000) High tar reduction in a two-stage gasifier. *Energy & Fuels*, 14 (4), pp.816–819.
- Bridgwater, A.V. (1995) The technical and economic feasibility of biomass gasification for power generation. *Fuel*, 74 (5), pp.631–653.
- Bryden, K.M. & Ragland, K.W. (1996) Numerical Modeling of a Deep, Fixed Bed Combustor. *Energy & Fuels*, 10 (2), pp.269–275. Available from: http://pubs.acs.org/doi/abs/10.1021/ef950193p http://linkinghub.elsevier.com/retrieve/pii/0140670196889016>.
- Cetin, E., Moghtaderi, B., Gupta, R. & Wall, T.F. (2005) Biomass Gasification Kinetics: Influences of Pressure and Char Structure. *Combustion Science and Technology*, 177 (4), pp.765–791. Available from: <a href="http://www.informaworld.com/openurl?genre=article/doi:10.1080/001022005-90917266/doi:10.1080/001022005-90917266/doi:10.1080/001022005-90917266/doi:10.1080/001022005-90917266/doi:10.1080/001022005-90917266/doi:10.1080/001022005-90917266/doi:10.1080/001022005-90917266/doi:10.1080/001022005-90917266/doi:10.1080/001022005-90917266/doi:10.1080/001022005-90917266/doi:10.1080/001022005-90917266/doi:10.1080/001022005-90917266/doi:10.1080/001022005-90917266/doi:10.1080/001022005-90917266/doi:10.1080/001022005-90917266/doi:10.1080/001022005-90917266/doi:10.1080/do
- Cuiping, L., Chuangzhi, W. & Haitao, H. (2004) Chemical elemental characteristics of biomass fuels in China. *Biomass and Bioenergy*, 27 (2), pp.119–130. Available from: http://linkinghub.elsevier.com/retrieve/pii/S096195340400011X.
- de Souza-Santos, M.L. (2004) Solid fuels combustion and gasification: modeling, simulation, and equipment operation. New York, Marcel Dekker.
- Devi, L., Ptasinski, K.J. & Janssen, F.J.J.G. (2003) A review of the primary measures for tar elimination in biomass gasication processes. *Biomass and Bioenergy*, 24 (2), pp.125–140. Available from: http://linkinghub.elsevier.com/retrieve/pii/S0961953402001022.
- Di Blasi, C. (2000) Dynamic behaviour of stratified downdraft gasifiers. *Chemical Engineering Science*, 55 (15), pp.2931–2944. Available from: http://linkinghub.elsevier.com/retrieve/pii/S000925099900562X.
- Di Blasi, C. (2008) Modeling chemical and physical processes of wood and biomass pyrolysis. *Progress in Energy and Combustion Science*, 34 (1), pp.47–90. Available from: http://linkinghub.elsevier.com/retrieve/pii/S0360128507000214.
- ECN (2011) Phyllis, database for biomass and waste. *Energy Research Centre of the Netherlands (ECN)*. Available from: http://www.ecn.nl/phyllis/>.
- EG G Technical Services Inc (2006) Fuel Cell Handbook. 7 ed.
- Elliott, D.C. (1988) Relation of Reaction Time and Temperature to Chemical Composition of Pyrolysis Oils. In: E. B. Soltes, E. J. Soltes, T. A. Milne, & E. B. Soltes

eds.

- Evans, R.J. & Milne, T.A. (1987) Molecular characterization of the pyrolysis of biomass. *Energy & Fuels*, 1 (2), pp.123–137. Available from: http://pubs.acs.org/doi/abs/10.1021/ef00002a001>.
- Faaij, A., van Doorn, J., Curvers, T., Waldheim, L., Olsson, E., van Wijk, A. & Daey-Ouwens, C. (1997) Characteristics and availability of biomass waste and residues in the Netherlands for gasification. *Biomass and Bioenergy*, 12 (4), pp.225–240.
- Francescato, V., Antonini, E. & Bergomi, L.Z. (2009) Wood fuels handbook.
- Franco, C., Pinto, F., Gulyurtlu, I. & Cabrita, I. (2003) The study of reactions influencing the biomass steam gasification process. *Fuel*, 82 (7), pp.835–842. Available from: http://linkinghub.elsevier.com/retrieve/pii/S0016236102003137.
- Glassman, I. & Yetter, R. (2008) Combustion. 4 ed. Academic press.
- Good, J., Ventress, C., Knoef, H.A.M., Zielke, U., Lyck, H., van de Kamp, W., de Wild, P., Coda, B., van Paasen, S.V.B., Kiel, J., Suomalainen, M. & Simell, P. (2005) *Sampling and analysis of tar and particles in biomass producer gases*. CEN. Available from: http://www.tarweb.net/results/pdf/Technical-Report-version-3_8-final.pdf>.
- Goswami, D.Y. (1986) Alternative energy in agriculture. Boca Raton, FL, CRC Press Inc.
- Groeneveld, M.J. & van Swaaij, W.P.M. (1980) 39 Gasification of char particles with CO2 AND H2O. *Chemical Engineering Science*, 35 (1-2), pp.307–313. Available from: http://linkinghub.elsevier.com/retrieve/pii/0009250980801011>.
- Hairui, Y., Wirsum, M., Junfu, L., Xianbin, X. & Guangxi, Y. (2004) Semi-empirical technique for predicting ash size distribution in CFB boilers. *Fuel Processing Technology*, 85 (12), pp.1403–1414. Available from: http://www.sciencedirect.com/science/article/pii/S0378382003002261 http://linkinghub.elsevier.com/retrieve/pii/S0378382003002261>.
- Henriksen, U., Ahrenfeldt, J., Jensen, T.K., Gobel, B., Bentzen, J.D., Hindsgaul, C. & Sorensen, L.H. (2006) The design, construction and operation of a 75kW two-stage gasifier. *Energy*, 31 (10-11), pp.1542–1553. Available from: http://linkinghub.elsevier.com/retrieve/pii/S0360544205001246.
- Higman, C. & Van Der Burgt, M. (2003) *Gasification*. Gulf Professional Publishing. Available from: http://www.amazon.com/dp/075068528X.
- Higman, C. & Van Der Burgt, M. (2008) *Gasification*. 2nd ed. Gulf Professional Publishing. Available from: http://www.sciencedirect.com/science/book/9780750685283.
- Hobbs, M.L., Radulovic, P.T. & Smoot, L.D. (1993) Combustion and gasification of coals in fixed-beds. *Progress in Energy and Combustion Science*, 19 (6), pp.505–586. Available from:

- .
- Institute of Gas Technology (1978) Coal Conversion Systems.
- Jarungthammachote, S. & Dutta, A. (2007) Thermodynamic equilibrium model and second law analysis of a downdraft waste gasifier. *Energy*, 32 (9), pp.1660–1669. Available from:
 - http://linkinghub.elsevier.com/retrieve/pii/S0360544207000199.
- Jayah, T.H., Aye, L., Fuller, R.J. & Stewart, D.F. (2003) Computer simulation of a downdraft wood gasifier for tea drying. *Biomass and Bioenergy*, 25 (4), pp.459–469. Available from:
 - http://linkinghub.elsevier.com/retrieve/pii/S0961953403000370.
- K G Mansaray A E Ghaly A M (2000) Mathematical Modeling of a Fluidized Bed Rice Husk Gasifier: Part III Model Verification. *Energy Sources*, 22 (3), pp.281–296. Available from:
 - http://www.tandfonline.com/doi/abs/10.1080/00908310050014063.
- Kirubakaran, V., Sivaramakrishnan, V., Nalini, R., Sekar, T., Premalatha, M. & Subramanian, P. (2009) A review on gasification of biomass. *Renewable and Sustainable Energy Reviews*, 13 (1), pp.179–186. Available from: http://linkinghub.elsevier.com/retrieve/pii/S1364032107001141.
- Klautau, J.V.P. (2008) Análise experimental de uma fornalha a lenha de fluxo cocorrente para secagem de grãos. Universidade Federal do Paran\'a. Available from: http://dspace.c3sl.ufpr.br:8080//dspace/handle/1884/17778.
- Knoef, H.A.M. (2005) *Handbook biomass gasification*. E. B. Knoef, H. A. M. Knoef, & E. B. Knoef eds. BTG Biomass Technology Group. Available from: http://books.google.com/books?id=qSSKQAAACAAJ\&pgis=1.
- Kumabe, K., Hanaoka, T., Fujimoto, S., Minowa, T. & Sakanishi, K. (2007) Cogasification of woody biomass and coal with air and steam. *Fuel*, 86 (5-6), pp.684–689. Available from: http://linkinghub.elsevier.com/retrieve/pii/S0016236106003401.
- Kurkela, E. & Ståhlberg, P. (1992) Air gasification of peat, wood and brown coal in a pressurized fluidized-bed reactor. I. Carbon conversion, gas yields and tar formation. *Fuel Processing Technology*, 31 (1), pp.1–21. Available from: http://www.sciencedirect.com/science/article/pii/037838209290038R.
- Lee, S. (2005) Encyclopedia of chemical processing. CRC. Available from: .">http://scholar.google.com/scholar?hl=en\&btnG=Search\&q=intitle:Encyclopedia+of+chemical+processing+volume+1\#0>.
- Lienhard IV, J.H. & Lienhard V, J.H. (2011) A heat transfer textbook. 3rd ed. Cambridge Massachusetts, Phlogiston Press. Available from: heat+tran

- sfer+textbook\#0>.
- Luque, R., Campelo, J.M. & Clark, J.H. (2011) *Handbook of Biofuels Production*. Woodhead Pub Limited.
- Mahishi, M. & Goswami, D.Y. (2007) Thermodynamic optimization of biomass gasifier for hydrogen production. *International Journal of Hydrogen Energy*, 32 (16), pp.3831–3840. Available from: http://linkinghub.elsevier.com/retrieve/pii/S0360319907002911.
- Mansaray, K.G., Ghaly, A.E., Al-Taweel, A.M., Handullahpur, F. & Ugursal, V.I. (2000)

 Mathematical Modeling of a Fluidized Bed Rice Husk Gasifier: Part I-Model

 Development. Energy Sources, 22 (1), pp.83–98. Available from:

 http://www.informaworld.com/openurl?genre=article/&doi=10.1080/009083100

 50014243\&magic=crossref||D404A21C5BB053405B1A640AFFD44AE3

 http://cat.inist.fr/?aModele=afficheN/&cpsidt=1295167

 http://www.tandfonline.com/doi/abs/10.1080/00908310050014243.
- Martinez, J.D., Mahkamov, K., Andrade, R.V. & Silva Lora, E.E. (2012) Syngas production in downdraft biomass gasifiers and its application using internal combustion engines. *Renewable Energy*, 38 (1), pp.1–9. Available from: http://www.sciencedirect.com/science/article/pii/S0960148111004186>.
- Mathieu, P. & Dubuisson, R. (2002) Performance analysis of a biomass gasifier. *Energy Conversion and Management*, 43 (9-12), pp.1291–1299. Available from: http://linkinghub.elsevier.com/retrieve/pii/S0196890402000158>.
- Matsumura, Y., Minowa, T., Potic, B., Kersten, S., Prins, W., Vanswaaij, W., Vandebeld, B., Elliott, D.C., NEUENSCHWANDER, G. & Kruse, A. (2005) Biomass gasification in near- and super-critical water: Status and prospects. *Biomass and Bioenergy*, 29 (4), pp.269–292. Available from: http://linkinghub.elsevier.com/retrieve/pii/S0961953405000735.
- McKendry, P. (2002a) Energy production from biomass (Part 1): Overview of biomass. Bioresource Technology, 83 (1), pp.55–63. Available from: http://www.ncbi.nlm.nih.gov/pubmed/12058829 http://www.ncbi.nlm.nih.gov/pubmed/12058831>.
- McKendry, P. (2002b) Energy production from biomass (part 2): conversion technologies. *Bioresource Technology*, 83 (1), pp.47–54.
- Melgar, A., Pérez, J.F., Laget, H. & Horrillo, A. (2007) Thermochemical equilibrium modelling of a gasifying process. *Energy Conversion and Management*, 48 (1), pp.59–67. Available from: http://linkinghub.elsevier.com/retrieve/pii/S0196890406001646>.
- Mermoud, F. (2006) Gazéification de charbon de bois à la vapeur d'eau : de la particule isolée au lit fixe continu. Institut Polytechnique de Toulouse. Available from:

- http://ethesis.inp-toulouse.fr/archive/00000353/>.
- Mermoud, F., Golfier, F., Salvador, S., Van de Steene, L. & Dirion, J.L. (2006) Experimental and numerical study of steam gasification of a single charcoal particle. *Combustion and Flame*, 145 (1-2), pp.59–79. Available from: http://linkinghub.elsevier.com/retrieve/pii/S0010218006000022.
- Milne, T.A., Evans, R.J. & Abatzoglou, N. (1998) *Biomass Gasifier 'Tars': Their Nature , Formation , and Conversion*. Golden, NREL.
- Neeft, J.P.A. (2005) Rationale for setup of impinger train as used in the Technical Specification of Sampling and Analysis of Tar and Particles in the Product Gases of Biomass Gasification. Technical background document. SenterNovem. Available from: http://www.tarweb.net/>.
- Netto, G.B.F., de Paula Oliveira, A.G., Coutinho, H.W.M., Nogueira, M.F.M. & Rendeiro, G. (2006) Caracterização energética de biomassas amazônicas. In: Campinas. Available from:

 .">http://www.google.com.br/search?client=safari&rls=10_7_4&q=Caracteriza+cc+ao+energ+etica+de+biomassas+amaz+onicas&ie=UTF-8&oe=UTF-8&redir_esc=&ei=jFI5UbWmPJOc8QTPsYD4DA>.
- Nordin, A. (1994) Chemical elemental characteristics of biomass fuels. *Biomass and Bioenergy*, 6 (5), pp.339–347. Available from: http://linkinghub.elsevier.com/retrieve/pii/0961953494E0031M>.
- Paviet, F., Chazarenc, F. & Tazerout, M. (2009) Thermo chemical equilibrium modelling of a biomass gasifying process using ASPEN PLUS. *International Journal of Chemical Reactor Engineering*, 7 (7), p.40. Available from: http://www.bepress.com/cgi/viewcontent.cgi?article=2089\&context=ijcre.
- Perkins, G. & Sahajwalla, V. (2008) Steady-State Model for Estimating Gas Production from Underground Coal Gasification. *Energy & Fuels*, 22 (6), pp.3902–3914. Available from: http://pubs.acs.org/doi/abs/10.1021/ef8001444>.
- Plis, P. & Wilk, R.K. (2010) Theoretical and experimental investigation of biomass gasification process in a fixed bed gasifier. *Energy*, pp.9–18. Available from: http://linkinghub.elsevier.com/retrieve/pii/S0360544210004755.
- Priyadarsan, S., Annamalai, K., Sweeten, J.M., Holtzapple, M.T. & Mukhtar, S. (2005) Co-gasification of blended coal with feedlot and chicken litter biomass. Proceedings of the Combustion Institute, 30 (2), pp.2973–2980. Available from: http://linkinghub.elsevier.com/retrieve/pii/S0082078404001894.
- Puig-Arnavat, M., Bruno, J.C. & Coronas, A. (2010) Review and analysis of biomass gasification models. *Renewable and Sustainable Energy Reviews*, 14 (9), pp.2841–2851. Available from: http://linkinghub.elsevier.com/retrieve/pii/S1364032110002108>.

- Purnomo, D., Aerts, D.J. & Ragland, K. (1990) Pressurized downdraft combustion of woodchips.
- Quaak, P. (1999) Energy from biomass A review of combustion and gasification technologies. E. B. Knoef, H. A. M. Knoef, & H. E. Stassen eds. World Bank. Available from: http://www.worldbank.icebox.ingenta.com/content/wb/324.
- Quaak, P., Harrie, K. & Stassen, H.E. (1999) *Energy from Biomass*. The World Bank. Available from: http://www.cabdirect.org/abstracts/19851826094.html>.
- Rajvanshi, A.K. (1986) Biomass Gasification. In: E. B. Goswami & D. Y. Goswami eds. Alternative energy in agriculture. Boca Raton, FL, CRC Press Inc., pp.83–102. Available from: http://njveg.rutgers.edu/assets/pdfs/2010-55thAtlanticCoastAgConvention-Proceedings.pdf #page=186>.
- Ramzan, N., Ashraf, A., Naveed, S. & Malik, A. (2011) Simulation of hybrid biomass gasification using Aspen plus: A comparative performance analysis for food, municipal solid and poultry waste. *Biomass and Bioenergy*, 35 (9), pp.3962–3969. Available from: http://linkinghub.elsevier.com/retrieve/pii/S0961953411003291.
- Reed, T.B. (1985) *Biomass gasification: principles and technology*. Park Ridge, Noyes Data Corp.
- Reed, T.B. & Das, A. (1988) Handbook of Biomass Downdraft Gasifier Engines Systems.

 Golden, CO, SERI. Available from:

 <taylor.ifas.ufl.edu/.../Handbook_of_Biomass_Downdraft_Gasifier_Engine_S ystems.pd>.
- Rezaiyan, J. & Cheremisinoff, N.P. (2005) *Gasification technologies : a primer for engineers and scientists*. Taylor \& Francis. Available from: http://marc.crcnetbase.com/ISBN/9781420028140>.
- Rogel, A. & Aguillon, J. (2006) The 2D Eulerian Approach of Entrained Flow and Temperature in a Biomass Stratified Downdraft Gasifier. *American Journal of Applied Sciences*, 3 (10), pp.2068–2075. Available from: http://scipub.org/fulltext/ajas/ajas3102068-2075.pdf.
- Sander, B. (1997) Properties of Danish biofuels and the requirements for power production. *Biomass and Bioenergy*, 12 (3), pp.177–183. Available from: http://linkinghub.elsevier.com/retrieve/pii/S0961953496000724>.
- Scala, F. (2013) Fluidized Bed Technologies for Near-Zero Emission Combustion and Gasification. Elsevier.
- Schefflan, R. (2011) Teach Yourself the Basics of Aspen Plus. Wiley-AIChE.
- Sharma, A.K. (2008) Equilibrium and kinetic modeling of char reduction reactions in a downdraft biomass gasifier: A comparison. *Solar Energy*, 82 (10), pp.918–928.

- Available from: http://linkinghub.elsevier.com/retrieve/pii/S0038092X08000649.
- Sharma, A.K. (2011) Experimental investigations on a 20 kWe, solid biomass gasification system. *Biomass and Bioenergy*, 35 (1), pp.421–428. Available from: http://linkinghub.elsevier.com/retrieve/pii/S096195341000317X.
- Sharma, A.K. (2009) Experimental study on 75kWth downdraft (biomass) gasifier system. *Renewable Energy*, 34 (7), pp.1726–1733. Available from: http://linkinghub.elsevier.com/retrieve/pii/S0960148109000068>.
- Susanto, H. & Beenackers, A.A.C.M. (1996) A moving-bed gasifier with internal recycle of pyrolysis gas. *Fuel*, 75 (11), pp.1339–1347.
- Tagutchou, J.P. (2008) Gazeification du Charbon de Plaquettes Forestieres: Particule Isolee et Lit Fixe Continu. Universite de Perpingnan.
- The German Solar Energy SocietyEcofys 2005 (2005) *Planning and Installing Bioenergy Systems: A guide for installers, architects and engineers*. London, James & James.
- Van de Steene, L., Tagutchou, J.P., Mermoud, F., Martin, E. & Salvador, S. (2010) A new experimental Continuous Fixed Bed Reactor to characterise wood char gasification. *Fuel*, 89 (11), pp.3320–3329. Available from: http://linkinghub.elsevier.com/retrieve/pii/S0016236110001407>.
- Walawender, W.P., Chern, S.M. & Fan, L.T. (1985) Wood chip gasification in a commercial downdraft gasifier. *Fundamentals of thermochemical*
- Warnatz, J., Maas, U. & Dibble, R.W. (2006) *Combustion: physical and chemical fundamentals, modeling and simulation, experiments, pollutant formation.*Springer.
- Yamazaki, T., Kozu, H., Yamagata, S., Murao, N., Ohta, S., Shiya, S. & Ohba, T. (2005) Effect of Superficial Velocity on Tar from Downdraft Gasification of Biomass. *Energy & Fuels*, 19 (3), pp.1186–1191. Available from: http://pubs.acs.org/doi/abs/10.1021/ef0497210.
- Yang, W., Ponzio, A., Lucas, C. & Blasiak, W. (2006) Performance analysis of a fixed-bed biomass gasifier using high-temperature air. *Fuel Processing Technology*, 87 (3), pp.235–245. Available from: http://linkinghub.elsevier.com/retrieve/pii/S037838200500130X.
- Yang, Y.B., Goh, Y.R., Zakaria, R., Nasserzadeh, V. & Swithenbank, J. (2002) Mathematical modelling of MSW incineration on a travelling bed. *Waste management (New York, NY)*, 22 (4), pp.369–380. Available from: http://www.ncbi.nlm.nih.gov/pubmed/12099494.
- Zainal, Z.A. (1996) Performance and characteristics of a biomass gasifier system. University of Wales. Available from:

- ."
- Zainal, Z.A., Ali, R., Lean, C.H. & Seetharamu, K.N. (2001) Prediction of performance of a downdraft gasifier using equilibrium modeling for different biomass materials. Energy conversion and
- Zainal, Z.A., Rifau, A., Quadir, G.A. & Seetharamu, K.N. (2002) Experimental investigation of a downdraft biomass gasifier. *Biomass and Bioenergy*, 23 (4), pp.283–289. Available from: http://linkinghub.elsevier.com/retrieve/pii/S0961953402000594>.
- Zeleznik, F.J. & Gordon, S. (1968) CALCULATION OF COMPLEX CHEMICAL EQUILIBRIA. *Industrial & Engineering Chemistry*, 60 (6), pp.27–57. Available from: http://dx.doi.org/10.1021/ie50702a006>.

LIST OF PUBLICATIONS

 de Paula-Oliveira, A. G.; Brammer, J. G. . Experimental Study of a Throated Downdraft Biomass Gasifier: Part I. Instrumentation for Measurements of Temperature and Gas Concentration in the Radial and Longitudinal Directions.. In: Bioten Conference, 2010, Birmingham. Bioten Conference, 2010

de Paula-Oliveira, A. G.; Brammer, J. G. . Experimental Study of a Downdraft Char Gasifier: Variation of Temperature and Gas Concentration in the Radial and Longitudinal Directions. In: 18th European Biomass Conference and Exhibition, 2010, Lyon. Proceedings of the 18th European Biomass Conference and Exhibition, 2010